PEROXYMONOCARBONATE AS A NEW REACTIVE OXYGEN SPECIES AND ITS REACTIVITY WITH BIOMOLECULES

By

CELESTE AIDA SERVANDO REGINO

A DISSERTATION PRESENTED TO THE GRADUATE SCHOOL
OF THE UNIVERSITY OF FLORIDA IN PARTIAL FULFILLMENT
OF THE REQUIREMENTS FOR THE DEGREE OF
DOCTOR OF PHILOSOPHY

UNIVERSITY OF FLORIDA

Copyright 2002

by

Celeste Aida Servando Regino

ACKNOWLEDGEMENTS

None of these projects would have been possible without a great deal of help from a lot of people. I would like to thank these wonderful people who have contributed into making these endeavors achievable.

My deepest gratitude goes to my research advisor, Dr. David E. Richardson, for his support, his patience and his guidance all throughout my stay here in UF. He has given me the opportunity to grow not only as a person but also as a scientist. The diverse projects I have worked on have given me an opportunity to dabble in a lot of interesting areas of science. I have enjoyed working on these projects so that it does not seem to have been work at all. Dr. Richardson has also helped me improve my writing and presentation skills, which will be important in my future professional career.

I wish to thank the Richardson group, past and present, for making the lab a pleasure to work in 24-7. The diverse characters of the group have contributed to a lively and happy environment. I thank them immensely for their friendship and support. I especially want to thank Ken Weakley for the helpful discussions on the synthesis part and for laughing in my face when I am frustrated which then results in making me laugh. I am grateful to Dr. Linda Nichols for teaching and helping me in the ESI-FTICR-MS of the RNase A. I also would like to thank Dr. Joy Méndez for her guidance in the RNase A purification and assay. I thank Dr. Huirong Yao for her help in the methionine oxidation, and for her friendship and advice. I thank Andy Burke for relieving me of my duties in the lab and Dan Denevan and Deon Bennett for keeping me posted.

The antimicrobial studies reported herein have been done in collaboration with Dr. Jeffrey Hillman. I wish to thank him for taking the time from his busy schedule to teach me techniques in microbiology and for his generosity in sharing his lab equipment and supplies. His guidance and helpful suggestions about the project enabled me to gather preliminary information on the enhancement of the antimicrobial properties of hydrogen peroxide. I only wish I had time to pursue the studies more completely. I also wish to thank his group for welcoming me into their group. I especially want to thank Karen Byer for showing me how to make the agar plates, to grow cultures, and to properly dispose of the plates.

The HPLC/ESI/QIT-MS data presented herein have been obtained by Dr. Jodie Johnson of the Department's Spectroscopic Services Facility. I am ever grateful to Jodie for the acquisition of the data and for his help in deciphering the vast amounts of spectra taken. I also would like to thank Dr. David Powell for obtaining the MALDI/TOF-MS of the crude α1-proteinase inhibitor. Their helpful suggestions and discussions have helped me in the analysis of the MS data.

I thank Scott McClung of the ICBR Protein Core Lab for the amino acid analysis of α1-proteinase inhibitor. He accommodated the quirks in the not so usual amino acid analysis of my sample without complaints and was enough to bump his schedules even on weekends.

The oxidation of RNase A has been investigated using the ESI/FTICR-MS. I thank Dr. John Eyler and his group for allowing me to run the experiments in their lab. I thank Stan Stevens for his patience in teaching me techniques on the use the FTICR-MS. I also would like to thank Dr. Lisa Lang for her earlier help in the copper(II) samples.

The SDS-PAGE experiments were done in Dr. Ben Horenstein's lab. I thank Dr. Horenstein for the generous use their lab equipment and supplies. I would also like to thank Jingsong Yang for teaching me how to make a good gel.

The crystal structure of the butylated dipyridylamine copper complex was obtained by Dr. Khalil Abboud. I would like to thank Dr. Abboud, Matt Peters and Ana Ison for the help in the structure of Cudpa and other related complexes.

My stay at UF has been filled with remarkable memories due to the people in the inorganic division. The faculty, postdocs, and fellow graduate students established an atmosphere that was pleasurable and at the same time challenging.

Our lives as graduate students have been easier with the help of the people from the inorganic division office (Amanda Garrigues, Maribel Lisk, and Kay Lewis), the business office (Marie Zombory, Beverly Lisk, and Wendy McCleskey) and the graduate coordinator's office (Donna Balkom and Lori Clark).

Generous financial support has been provided by the Department of Chemistry of the University of Florida, and the Army Research Office. I am grateful for their financial support in the tuition fee waivers, stipends and travel funds.

Diversions from chemistry have fostered many friendships and have made graduate school more enjoyable. I would like to thank my friends for the tremendous support they have given me over the past years; their love and friendship have been a great source of strength. I would especially like to thank Ruby Tapec-Dytioco who has been there for me since high school. I wish to thank Camille and Gino Ables, Janina Gutierrez, the Cariños (Stephen, Czar and little A.D.), the Kemeraits (Bob, Pam and little Mia), Karina Kerns, Mary Ann Endoma, Suzy and Ed Pabit, and Danilo Ortillo for

activities and trips outside the lab. And I wish to thank Aimee Liz Malingan, Cherry Jane Rios, Jennifer Miguel, Sherill Ann Mercado, and Karen Abella for their cheers and words of encouragement even if they are thousands of miles away.

I am indebted to my parents and family for their love and encouragement all through my life. They have trusted and supported me in pursuit of this degree instead of medicine and have been patient that I will eventually finish school. Their ever-present love and support keeps me going. I would especially like to thank my mom for listening and for encouraging me and giving me that little push when I really needed it. She has also kept me abreast of things happening back home. I wish to thank my brother, Joel, for visiting me here in Gainesville with his family, for allowing me to get to know my little niece, and for sending pictures of the whole family.

Most importantly I thank God for all His blessings throughout my life.

Enter into his gates with thanksgiving,
And into his courts with praise;
Be thankful unto him and bless his name.
Psalm 100:4

TABLE OF CONTENTS

page

ACKNOWLEDGMENTS iii

LIST OF TABLES x

LIST OF FIGURES xi

ABSTRACT xvi

CHAPTERS

1 INTRODUCTION 1

Reactive Oxygen Species 1
Hydrogen Peroxide 4
Carbon Dioxide 8
Peroxymonocarbonate 9

2 THIOL AND DISULFIDE OXIDATIONS 14

Introduction 14
Materials and Methods 18
    Materials and Instrumentation 18
    Catalase Decomposition of Peroxymonocarbonate 19
    Apparent Molar Absorptivity of 2-Nitro-5-thiobenzoate 19
    Thiol Oxidation Reactions 20
    Disulfide Oxidation Reactions 20
Results and Discussions 21
    Catalase Activity on Peroxymonocarbonate 21
    Apparent Molar Absorptivity of TNB 21
    Thiol Oxidations by Hydrogen Peroxide 23
    Thiol Oxidations by Peroxymonocarbonate 28
    Disulfide Oxidation by Hydrogen Peroxide 31
Conclusions 37

3 METHIONINE OXIDATION TO METHIONINE SULFOXIDE 39
Introduction 39
Materials and Methods 45

Materials and Instrumentation..45
Apparent Molar Absorptivity of Hydrogen Peroxide and Other Oxidants 46
Free Methionine Oxidation...47
Oxidation of α1-Proteinase Inhibitor 48
Synthesis of Sepharose Blue Dextran (SBD) Affinity Chromatography..........48
Purification of α1-PI 49
Elastase-Inhibitor Complex Formation using SDS-PAGE 50
CNBr Cleavage and Methionine Sulfoxide Analysis 50
Peptide Mapping of Oxidized α1-PI using HPLC/ESI/QIT-MS...................51
RNase A Oxidation 51
Results and Discussions...52
Free Methionine Oxidation...52
Purification of α1-PI 61
Oxidation of Methionines in α1-PI...66
Methionine Sulfoxide Analysis 70
Peptide Mapping of the Oxidized α1-PI. 76
RNase A Oxidation...86
Conclusions..86

4 OXIDATION OF GUANOSINE MONOPHOSPHATE 91
Introduction 91
Materials and Methods...95
Materials and Instrumentation 95
Oxidation of Guanosine-5'-monophosphate (GMP) 99
Results and Discussions 100

5 ANTIMICROBIAL ACTIVITY OF PEROXYMONOCARBONATE 108
Introduction 108
Materials and Methods 112
Materials and Instrumentation 112
Turbidity Measurements 115
Microbicidal Assay 115
Hydrogen Peroxide Determination by CuDMP Method 117
Results and Discussions 119
Cell Growth 119
Hydrogen Peroxide Toxicity 119
Kinetics 122
Conclusions 126

6 GENERAL CONCLUSIONS...131

7 SYNTHESIS AND REACTIVITY OF BIOCONJUGATABLE COPPER (II) COMPLEXES...138
Introduction..138
Experimental Section..145
General Methods..145

Synthesis of *N*-Hydroxysuccinimidyl *N,N*-(2',2'-dipyridyl)aminoacetate....146
  Synthesis of ethyl *N,N*-(2',2'-dipyridyl)aminoacetate........................146
  Synthesis of *N,N*—(2'2'-dipyridyl)aminoacetic acid........................147
  Synthesis of *N*-hydroxysuccinimidyl *N,N*-(2',2'-dipyridyl)aminoacetate.147
Synthesis of 4-Mercapto-*N,N*-(2',2'-dipyridyl)butanamine.....................147
  Synthesis of *N*-(4-chloro)butyl-2',2'-dipyridylamine.........................147
  Synthesis of *O*-ethyl *S*-4(*N,N*-dipyridyl)aminobutylxanthate...............148
  Synthesis of 4-mercapto-*N,N*-(2',2'-dipyridyl)butanamine.................148
Synthesis of Disulfide Model Ligands..149
  Synthesis of 4-*N,N*-(2',2'-dipyridyl)aminobutyl phenyl disulfide.........149
  Synthesis of 4-*N,N*-(2',2'-dipyridyl)aminobutyl pyridyl disulfide.........150
Synthesis of alkylated 2',2'-dipyridylamine.....................................150
Syntheses of Dichloro Copper (II) Complexes..................................150
Synthesis of Ethyl *p*-nitrophenylphosphoric acid...............................152
  Synthesis of sodium *p*-nitrophenoxide...152
  Synthesis of diethyl *p*-nitrophenylphosphate.................................152
  Synthesis of ethyl *p*-nitrophenyl phosphoric acid............................153
Potentiometric Titrations...153
Molar Absorptivity of *p*-Nitrophenolate...154
Apparent Acid Dissociation Constant of *p*-Nitrophenolate....................154
Hydrolysis of *p*-Nitrophenyl Acetate (pNPA)...................................154
Hydrolysis of Bis-(*p*-nitrophenyl)phosphate (BNPP)...........................155
Results and Discussions...156
  Synthesis...156
  Kinetics...163
Conclusions 175

APPENDICES

APPENDIX A PROTEOLYTIC DIGEST OF α1-PI 176

APPENDIX B ^{1}H NMR SPECTRA OF DIPYRIDYLAMINE LIGANDS 191

APPENDIX C CRYSTAL DATA FOR Cu(dpab)Cl_2 (**19**) 202

LIST OF REFERENCES...209

BIOGRAPHICAL SKETCH 225

LIST OF TABLES

Table page

1-1 Some common reactive oxygen species 2

2-1 Second-order rate constants for thiol oxidation 26

3-1 Comparative amino acid composition of the native and oxidized α1-PI 75

3-2 Predicted fragments for the native α1-PI digest by Endo Lys-C 79

4-1 One-electron reduction potentials for nucleobases 94

4-2 Some m/z ions obtained from the HPLC/ESI/QIT-MS of the reaction mixture 106

5-1 Rate constants for the different oxidants used in the microbicidal assay 129

7-1 Acid dissociation constants obtained using potentiometric titration and FORTRAN –77 program by Martell and Motekaitis 167

7-2 Catalyzed hydrolysis of *p*-nitrophenyl acetate 169

7-3 Summary of the catalyzed hydrolysis of bis(*p*-nitrophenyl)phosphate...........171

7-4 Selected bond angles and bond distance for copper (II) complexes 174

LIST OF FIGURES

Figure page

1-1 Schematic diagram of the effect and fate of reactive oxygen species in a normal cell 5

1-2 Fenton chemistry and removal by antioxidants of hydrogen peroxide 25

1-3 ^{13}C NMR spectra for the equilibration reaction between bicarbonate ($NaH^{13}CO_3$) in hydrogen peroxide at 25 °C 10

1-4 Schematic diagram showing the intermediacy of carbon dioxide in the peroxymonocarbonate formation 11

2-1 Some of the different oxidation intermediates of thiol oxidation to sulfonic acid 16

2-2 Carbon-13 NMR spectra of the equilibration reaction with catalase..........22

2-3 pH dependence of k_{obs} for the uncatalyzed cysteine oxidation 24

2-4 Reactivities of the different thiol substrates 25

2-5 First-order dependence of k_{obs} on [HCO_3^-] for cysteine oxidation at pH 8.0 29

2-6 Proton NMR spectra of the oxidation of methyl disulfide (30 mM) with hydrogen peroxide (30 mM) in 0.10 M H_3PO_4 32

2-7 Proton NMR spectra of the oxidation of methyl disulfide (30 mM) with hydrogen peroxide (30 mM) in 0.10 M HPO_4^{2-} 34

2-8 Proton NMR spectra of the oxidation of methyl disulfide (30 mM) with hydrogen peroxide (30 mM) in 0.10 M HCO_3^- 35

2-9 Product distribution for the hydrogen peroxide oxidation of methyl disulfide in the three conditions used 36

3-1 The oxidation of methionine to methionine sulfoxide and methionine sulfone.....40

3-2 Schematic diagram for the assay of α1-PI before and after oxidation 44

3-3 Dependence of the rate of oxidation on (a) $[H_2O_2]$ and (b) [RSMe] 53

3-4 Plot of the reciprocal of $[H_2O_2]$ versus time for methionine oxidition when $[H_2O_2]$ = [RSMe] = 0.10 M as a fit to eq 3-4 55

3-5 Proton NMR of the methionine oxidation to methionine sulfoxide 56

3-6 Profile of methionine oxidation showing the loss of absorbance of H_2O_2 at λ= 275 nm for the uncatalyzed and catalyzed reactions 57

3-7 Dependence of the rate of oxidation to $[HCO_3^-]$ 58

3-8 Methionine oxidation by hydrogen peroxide obtained from ^{1}H NMR 60

3-9 Plot of the reciprocal of [*t*-BuOOH] versus time for the oxidation of methionine to methionine sulfoxide by *tert*-butylhydroperoxide 62

3-10 Dependence of the oxidation rate on pH 63

3-11 SDS-PAGE of α1-proteinase inhibitor in 12% gel and 0.1 % SDS 65

3-12 3D plot summarizing the loss of inhibitory activity of α1-PI on elastase in the course of oxidation 67

3-13 Plot of the dependence of k_{obs} on the $[HCO_3^-]$ indicating a first-order dependence 69

3-14 First-order plot of the elastase activity as a function of oxidation time from eq 3-19 69

3-15 Amino acid analysis chromatograms of the native and oxidized α1-PI 72

3-16 Schematic diagram for the simultaneous analysis of methionine and methionine sulfoxide 73

3-17 Full mass chromatograms of the native and oxidized α1-PI 77

3-18 Primary sequence of α1-PI 78

3-19 Relative abundance of the monooxidized fragment 28-31 and dioxidized fragment 30 of the reactive center loop 80

3-20 Mass spectra of m/z = 1146 which corresponds to the +2 charge state of the dioxidized species of fragment 30 81

3-21 A space-filled model of α1-PI showing the exposed methionines and cysteine 83

3-22 Relative abundance of the monooxidized fragment 18-19 and dioxidized fragment 18 84

3-23 Mass spectra m/z = 748 which corresponds to the +2 charge state of the monooxidized species of fragment 18-19 85

3-24 Profile for RNase oxidation by ESI/FTICR-MS 86

3-25 Assay of the hydrolytic activity of RNase A towards cytidine 2',3'-cyclic monophosphate (2',3'-cCMP) to yield cytidine 3'-monophosphate 88

3-26 A space-filled model of ribonuclease A showing solvent-exposed Met29 89

4-1 Numbering scheme in nucleobases and nucleosides 92

4-2 Schematic diagram of strand scission via deglycosylation of the nucleobase 93

4-3 Reaction of hydroxyl radical to guanine 96

4-4 Electrochemical oxidation of 8-oxoG 97

4-5 Oxidation pathway for 8-oxoG 98

4-6 Proton NMR spectra of GMP and GMP reaction mixtures 101

4-7 HPLC chromatograms of GMP and the bicarbonate-containing oxidation reaction mixture using an anion exchange column 102

4-8 HPLC/ESI/QIT-MS of the oxidation reaction mixture 103

4-9 Mass spectra of GMP (m/z = 364) and MS/MS of GMP showing the intact nucleobase and sugar moieties 104

4-10 MS/MS of the m/z = 380 showing the modified guanine base, 8-oxoG species and the intact sugar moiety 105

5-1 Schematic diagram of the phagocytic response of neutrophils 109

5-2 Various neutrophil-generated oxidative toxins that have been proposed their pathways for formation 110

5-3 Carbon-13 NMR of pH shock experiments showing sub-burst formation of HCO_4^- 113

5-4 Schematic diagram of the procedure for the microbicidal assay 116

5-5 Calibration curve for $Cu(DMP)_2^+$ for H_2O_2 determination 118

5-6 Hydrogen peroxide toxicity 120

5-7 Hydrogen peroxide toxicity 121

5-8 Monitoring the $[H_2O_2]$ in the microbicidal assay for aerobically-grown *Samonella* 123

5-9 Viable cell count using spread plate method 124

5-10 Viabilities of aerobically-grown *Streptococcus mutans* following exposure to 500 µM hydrogen peroxide 125

5-11 Plot of the ln [*f*] versus exposure time 127

5-12 Comparison of the toxicities of hypochlorous acid, peroxymonocarbonate and hydrogen peroxide to anaerobically-grown *E.coli* 128

7-1 Diaquo-2,2'-dipyridylaminecopper (II), hydrolysis catalyst ($Cudpa^{2+}$)..............140

7-2 Proposed scheme for the catalyzed hydrolysis of methyl acetate by diaqua-2,2'-dipyridylaminecopper (II)..141

7-3 Preparation of the semi-synthetic catalyst using an amide group as the linking group 143

7-4 Preparation of the semi-synthetic catalyst using a disulfide as the linking group 144

7-5 Preparation of the *N*-hydroxysuccinimidyl ester derivative of dipyridylamine ligand 158

7-6 Proposed mechanism for the formation of **4** 159

7-7 Other synthetic routes used to synthesize **4** 160

7-8 Preparation of the thiol derivative of 2,2'-dipyridylamine ligand 161

7-9 Preparation of a disulfide model 162

7-10 Preparation of ethyl *p*-nitrophenyl phosphoric acid (**15**) 164

7-11 Structures of the different copper (II) complexes synthesized and used 165

7-12 Hydrolysis of *p*-nitrophenyl acetate 167

7-13 Catalyzed hydrolysis of *p*-nitrophenyl acetate 168

7-14 Dependence of the k_{obs} on the concentration of the catalyst 169

7-15 Hydrolysis of bis-(*p*-nitrophenyl)phosphate 171

7-16 Crystal structure of butylated copper (II) dipyridylamine chloride 173

Abstract of Dissertation Presented to the Graduate School
of the University of Florida in Partial Fulfillment of the
Requirements for the Degree of Doctor of Philosophy

PEROXYMONOCARBONATE AS A NEW REACTIVE OXYGEN SPECIES AND ITS REACTIVITY WITH BIOMOLECULES

By

Celeste Aida Servando Regino

May 2002

Chairman: Professor David E. Richardson
Major Department: Chemistry

Reactive oxygen species have been implicated in the process of aging, in diseases, and in the immune response. In this study, we proposed that peroxymonocarbonate (HCO_4^-) be considered as a reactive oxygen species formed from the equilibrium reaction of bicarbonate and hydrogen peroxide, both of which are ubiquitous in extracellular fluids. The effect of the presence of bicarbonate on the oxidation rates of biologically important molecules such as cysteine, gluthathione, methionine (both free and in proteins), and nucleic acids such as guanosine-5'-monophosphate are presented. In the hydrogen peroxide oxidations of thiols and methionines, the rate of oxidation is at least doubled in the presence of bicarbonate. For the guanosine-5' monophosphate oxidation, the reaction occurs only in the presence of bicarbonate at pH 8.0 and room temperature. Kinetic and spectroscopic results support the formation of peroxymonocarbonate as the oxidant in the catalytic pathway. We have also shown that peroxymonocarbonate may be a substrate for catalase. The presence of bicarbonate has also been shown to enhance the antimicrobial properties of hydrogen peroxide. The proposed oxidant, HCO_4^-, substantially increases the oxidizing ability of hydrogen peroxide.

A semi-synthetic enzyme with novel properties can be formed from the incorporation of a synthetic catalyst into a protein or enzyme. This strategy takes advantage of the inherent specificity and binding capabilities of the native protein or enzyme and gives the native protein or enzyme additional reactivity provided for by the conjugated synthetic catalyst. Syntheses of ligands based on dipyridylamine for use in such bioconjugates and the hydrolytic activities of the copper (II) complexes of the dipyridylamine-derivatized ligands are presented.

CHAPTER 1
INTRODUCTION

Reactive Oxygen Species

Anaerobes are believed to have been the first forms of life on earth when there was little free oxygen in the atmosphere. What little oxygen produced in the atmosphere was most probably from the photosynthetic breakdown of water by cyanobacteria (blue green algae). As the level of oxygen increased, it led to the formation of the ozone layer that helped screen out the deleterious effects of ultraviolet radiation and facilitated life on land. However, the increased oxygen levels either killed the primitive anaerobes, forced them to retreat to low-oxygen conditions or totally anaerobic environments, or forced them to evolve, utilize the oxygen and develop defense mechanisms to cope with the oxidizing environments. The toxicity of oxygen to anaerobes is believed to be due to the oxidation of essential metabolic intermediates in cellular components such as iron-sulfur active sites and pteridine cofactors and thiols, thereby removing the reducing equivalents needed for biosynthetic reactions [1].

Today, except for a few species of anaerobic bacteria and aero-tolerant bacteria, all life forms require oxygen for efficient production of energy through oxygen-dependent electron transport chains. Aerobes only survive due to the presence of antioxidants, repair systems, and the highly evolved complex systems that control the delivery of oxygen and its oxidizing equivalents to areas where they are needed. However, despite the need for oxygen, oxygen still causes damage to cellular components of aerobes. Exposure to oxygen concentration greater than the normal 21% gradually damages the lungs in adult rats and humans [1]. Even plant tissues are damaged at above normal concentration of oxygen, as observed by inhibition of chloroplast development, decrease in seed viability and root growth, damage in membranes, and shriveling and shedding of leaves [2]. These deleterious effects of oxygen are proposed to be caused by the production of free radicals [3] or reactive oxygen species (ROS) during oxygen metabolism. Table 1.1 lists some of the commonly encountered reactive oxygen species. The reactive oxygen species include not only free radicals but also nonradical species such as hydrogen peroxide (H_2O_2), hypochlorous acid (HOCl), and peroxynitrite ($ONOO^-$).

Table 1-1. Some common reactive oxygen species.

Radicals	Non-radicals
Superoxide, $O_2^{-\bullet}$	Hydrogen peroxide, H_2O_2
Hydroxyl, OH•	Hypochlorous acid, HOCl
Peroxyl, ROO•	Peroxynitrite, $ONOO^{-}$[a]
Alkoxyl, RO•	Alkyl hydroperoxide, ROOH
Hydroperoxyl, HOO•	
Thiyl, RS•[b]	

[a]Considered also as reactive nitrogen species.
[b]Considered as reactive sulfur species.

Because of the potential damage of the reactive oxygen species produced from oxygen metabolism, antioxidants and repair systems have been developed by aerobes to enable their survival. Primary antioxidants [4,5] are those involved in directly removing the reactive oxygen species either by catalytically inactivating the ROS or by non-enzymatic reaction with the ROS to produce a less toxic product. Examples of primary antioxidants are superoxide dismutases (SOD), catalases, peroxidases, ascorbate and thiols. Secondary antioxidants [4,5] are those proteins that avoid the production of ROS by either minimizing the availability of pro-oxidants such as iron and copper ions (i.e. ferritin, ceruloplasmin) [4,6] or by catalyzing the direct reduction of substrate quinones to quinols to avoid formation of semiquinone radical intermediates (i.e. DT diaphorase)[4-6].

However, antioxidants alone are not enough to stop the damaging effects of ROS. Another defense mechanism is the removal and repair system. One important repair process is the re-reduction of the disulfide bond on proteins or peptides by disulfide reductases. Another important repair mechanism for oxidized proteins is the reduction of methionine sulfoxide to methionine by methionine sulfoxide reductase (MsrA). A more commonly known repair mechanisms in protein oxidation is the recognition and removal or degradation of oxidized protein. A replacement of the entire or the excised portion of the oxidized protein is synthesized and inserted. Extensive studies have revealed that oxidized proteins are recognized by proteases and completely degraded to amino acids to be reused for protein synthesis [7-12].

Another response to the presence of ROS utilized by mitotic cells is transient growth-arrest, in which DNA is largely supercoiled, replication is halted, and only a few shock or stress genes are transcribed and translated [13,14]. Once the stress of the ROS is over or lowered, after about 3 hours of transient growth-arrest, the cells re-enter the growth cycle wherein the DNA is in an uncoiled state with no histone protein coating.

Despite the protective mechanisms against ROS and ROS damage repair systems, oxidative damage still occurs and accumulates with age. It has been estimated that the number of oxidative hits to DNA per cell per day is 10^6 in rats and 10^4 in humans [15,16], and the mutations accumulate with age [17,18]. Increased levels of oxidized proteins have also been shown to accumulate with age [19]. This constant barrage of reactive oxygen species has been implicated in the process of aging [20] as well as numerous degenerative diseases such as cardiovascular diseases [21,22], cancer [15], and neurodegenerative diseases [23,24]. Figure 1-1 summarizes the effect of ROS generated in a normal cell.

Hydrogen Peroxide

Mitochondria and phagocytic cells are the two main sources of ROS. Out of 85-90% of the oxygen taken up by animals to be utilized by the mitochondria for metabolic energy production, 1-3% of it is converted to superoxide [1]. The superoxide produced can be damaging by itself or it can dismutate to produce hydrogen peroxide. This dismutation of superoxide to hydrogen peroxide is rapid ($k_{\text{uncat}} = 5 \times 10^5\ M^{-1}s^{-1}$ and $k_{\text{SOD}} = 2 \times 10^9\ M^{-1}s^{-1}$) [6] at physiological pH and any molecule that reacts with the superoxide competes with the dismutation reaction. Thus, any biological system that produces superoxide inevitably generates hydrogen peroxide. Other sources of hydrogen peroxide generated *in vivo* are enzymes such as xanthine, urate, D-amino acid, and monoamine oxidases [25,26].

Hydrogen peroxide readily mixes with water and is very diffusible within and between cells *in vivo*, with a permeability constant of 0.2 cm/min for peroxisomal membranes [27] and 0.04 cm/min for erythrocyte plasma membrane [28], comparable to water with a permeability ranging from 0.02 to 0.42 cm/min [29]. Though hydrogen peroxide is generally considered a weakly nonspecific oxidizing agent ($E^\circ = 1.77$ vs. NHE) [30] in organic oxidation reactions, it is still a potent one under physiological conditions. Under relatively mild conditions, hydrogen peroxide is highly specific for thioethers, thiols, disulfides, indoles, phenols, and imidazoles [31]. It can oxidize

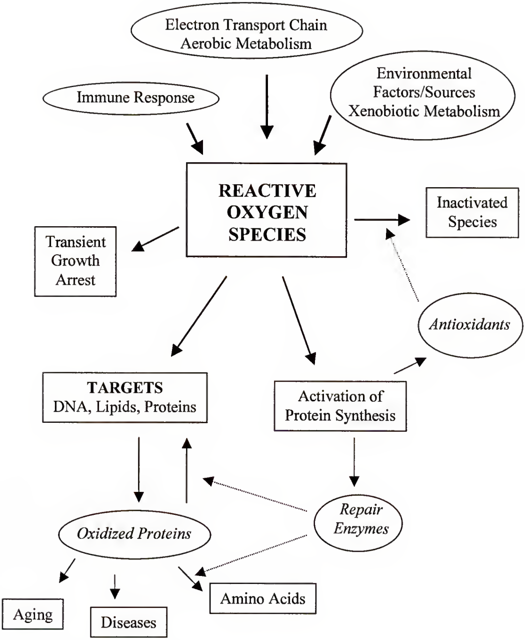

Figure 1-1. Schematic diagram of effect and fate of reactive oxygen species in a normal cell.

important cysteine residues in the proteins that can lead to loss in enzymatic activity [32,33], change in protein hydrophobicity [34], and change in protein structure. Peroxide can also lead to the activation of antioxidant genes [35,36]. Several enzymes, such as gluthathione peroxidase and catalase actively remove hydrogen peroxide by reducing it to water (Figure 1-2). Hydrogen peroxide is also reactive toward transition metals to produce hydroxyl radicals (Fenton chemistry) [37] (Figure 1-2). Thus, proteins involved in sequestering these transition metals have antioxidant properties.

Besides transition metals, other inorganic and organic compounds have been used as activators for hydrogen peroxide. These include carboxylic acids to form peroxyacids, nitriles to form imidoperoxic acid, and urea to form peroxyisourea [30]. The mechanism for activation usually involves substitution of the hydrogen atom in hydrogen peroxide with another atom or group of atoms (X) where OX is a better leaving group than OH (eq 1-1) [30].

$$\mathrm{XY + HOO\text{-}H \xrightarrow{-HY} HOO\text{-}X \xrightarrow{S} SO + XOH} \qquad (1\text{-}1)$$

For example, in activation by carboxylic acids to form peracids, X = R(C=O) and Y = OH. The leaving group OX is the carboxylate ion, a weaker base and a better leaving group than OH. Another method for activating of hydrogen peroxide using bicarbonate was first described by Drago and co-workers [38] and further studied by Richardson and co-workers [39,40] for sulfide oxidations in mixed alcohol/water solvents. The active oxidant was assigned as peroxymonocarbonate ion (HCO_4^-) formed from the perhydration of carbon dioxide with hydrogen peroxide [41]. Both carbon dioxide and hydrogen peroxide are ubiquitous in extracellular fluids and therefore expected to form the peroxymonocarbonate *in vivo*.

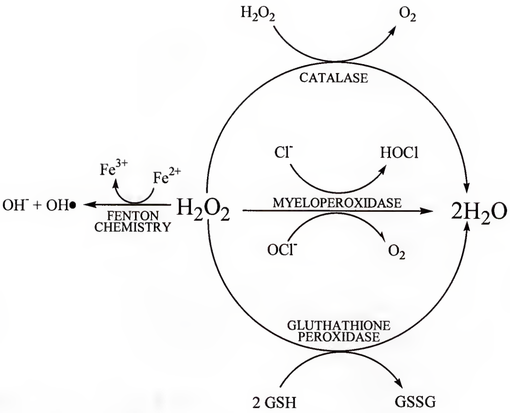

Figure 1-2. Fenton chemistry and removal by antioxidants of hydrogen peroxide.

Carbon Dioxide

Carbon dioxide exists in three forms in the blood: as dissolved gas (~30%) with a solubility that is 20 times greater than oxygen; as a carbamate adduct (~10%) ($RNHCO_2^-$) to non-ionized available amino groups in hemoglobin (carbamino hemoglobin) [42,43]; and as bicarbonate ion (~60%) from the perhydration of carbon dioxide in the presence of carbonic anhydrase (CA) (eq 1-2). This perhydration process (eq 1-2) is very slow under physiological conditions in the absence of carbonic anhydrase and about 99% of the carbon dioxide in solution stays as dissolved gas and only about 1% is converted to carbonic acid (H_2CO_3) ($pK_{a1} = 3.9$ and $pK_{a2} = 10.3$) (eq 1-3) [44].

$$CO_2 + H_2O \rightleftharpoons H_2CO_3 \qquad (1\text{-}2)$$

$$H_2CO_3 \rightleftharpoons H^+ + HCO_3^- \qquad (1\text{-}3)$$

This slow hydration of CO_2 (eq 1-2) is strongly pH-dependent and cannot be influenced by a conventional acid or base catalysis but requires a combination of Lewis acid attack on the carbonyl oxygen and Lewis base attack on the carbonyl carbon otherwise known as the "push-pull" effect [45]. In CA, a zinc-bound hydroxide from the deprotonation of coordinated water serves as the nucleophile that attacks the carbonyl carbon while the metal center itself serves to attract, orient and polarize the CO_2 molecule [46]. The rate-determining step in this catalysis is the autoprotolysis of the coordinated water [47].

Carbon dioxide produced from aerobic metabolism diffuses into the red blood cells where carbonic anhydrase hydrates it to HCO_3^-. The resulting decrease in the pH inside the red blood cell facilitates the release of O_2 to the tissue. The bicarbonate diffuses out into the plasma. Dehydration of bicarbonate by carbonic anhydrase facilitates the reverse process of releasing the CO_2 out of the lungs. A normal rested individual will have a total dissolved CO_2 of 25 to 28 mM, pCO_2 of 40 to 43 mm Hg, and $[HCO_3^-]$ of 24 to 27 mM in the arterial blood plasma at pH 7.4 [48].

Peroxymonocarbonate

Recent studies have shown the rapid equilibrium formation of peroxymonocarbonate ion (HCO_4^-) from bicarbonate ion and hydrogen peroxide at 25° C and near neutral pH in both aqueous and alcohol/water mixtures (eq 1-3) (Figure 1-3) [49].

$$HCO_3^- + H_2O_2 = HCO_4^- + H_2O \quad K_{eq} = \frac{[HCO_4^-]}{[HCO_3^-][H_2O_2]} = 0.32 \qquad (1\text{-}3)$$

This equilibration reaction is believed to occur via the perhydration of CO_2 formed in equilibrium with bicarbonate (Figure 1-4) [41]. The presence of carbonic anhydrase or carbonic anhydrase model 1,4,7,10-tetraazacyclododecanezinc (II) complex accelerates the equilibrium reaction through catalysis of the dehydration of bicarbonate and possibly catalysis of the perhydration step (Figure 1-4) [41]. Thermodynamic results estimate the redox potential of peroxymonocarbonate to be E° (HCO_4^-/HCO_3^-) = 1.8 V (vs. NHE), and so it is therefore a potent oxidant in aqueous solution [49]. The structure of peroxymonocarbonate anion is that of a true peroxide, i.e., $HOOCO_2^-$, as characterized by X-ray crystallography of $KHCO_4 \bullet H_2O_2$ [50] and by vibrational spectroscopy [51,52].

Previous studies on the bicarbonate-catalyzed oxidation of organic sulfides [49,53] strongly supported the role of peroxymonocarbonate as the oxidant. The kinetic and spectroscopic results obtained were consistent with the equilibrium formation of peroxymonocarbonate. The reactivity of peroxymonocarbonate toward sulfides at moderate temperature and its stability at near neutral pH suggested possible significance as a reactive oxygen species. To our knowledge, peroxymonocarbonate has only been

$$H_2O_2 + HCO_3^- \rightleftharpoons H_2O + HCO_4^-$$

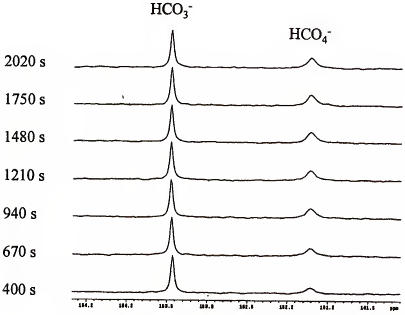

Figure 1-3. ^{13}C NMR spectra for the equilibration reaction between bicarbonate (0.10 M $NaH^{13}CO_3$) in hydrogen peroxide (2.0 M) at 25°C. Times on the left are for the completion of acquisition from the time of mixing [49].

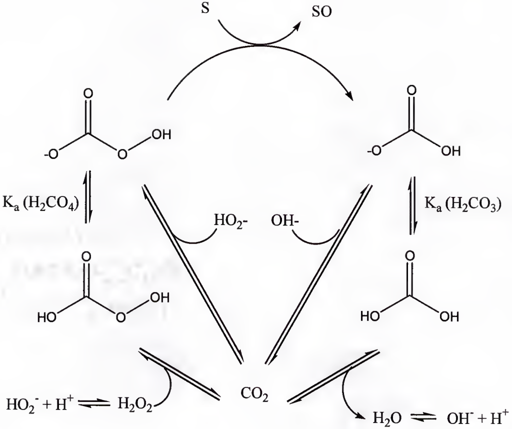

Figure 1-4. Schematic diagram showing the intermediacy of CO_2 in HCO_4^- formation [41]. The right side of the figure is the CO_2/HCO_3^- equilibrium and known to be catalyzed by carbonic anhydrase and various model complexes. The left side is the proposed perhydration of CO_2 to form the percarbonic acid in equilibrium with its conjugate base, peroxymonocarbonate. Reaction of HCO_4^- with a substrate, S (via O-transfer) results in the recovery of HCO_3^- (top portion).

mentioned briefly as a possible reactive oxygen species [54] and no supporting data were provided.

The research herein describes our investigations of peroxymonocarbonate as a possible reactive oxygen species. Both hydrogen peroxide and bicarbonate are ubiquitous in extracellular fluids, and the rapid equilibrium formation of peroxymonocarbonate in aqueous solutions at near neutral pH makes it a possible oxidant of biological targets. *In vitro* oxidations of possible biological targets *in vivo* are investigated in this work.

Thiols represent one of the most reactive nucleophiles in biological systems and are readily oxidized by a wide variety of oxidants. In Chapter 2, kinetic parameters for the hydrogen peroxide oxidation of cysteine, gluthathione and *N*-acetylcysteine to the corresponding disulfide in the absence and presence of bicarbonate are presented. Oxidation of methyl disulfide, a model for biologically relevant disulfide oxidation, is also described.

Another biologically active nucleophile is methionine. Methionine is also susceptible to oxidation and has been proposed to be an endogenous antioxidant. Oxidation of free amino acid methionine to methionine sulfoxide is presented in Chapter 3. As an example of methionine oxidation in proteins, oxidations of α1-proteinase inhibitor and ribonuclease A are investigated.

Nucleic acids are also potential substrates for oxidation. Oxidation of guanosine-5'-monophosphate is presented in Chapter 4 as a model for nucleic acid oxidation. As a model of *in vivo* oxidative stress, the antimicrobial activities of the hydrogen peroxide in the absence and presence of bicarbonate are compared and are presented in Chapter 5.

The role of peroxymonocarbonate as the oxidant in the oxidation reactions is supported by kinetic and spectroscopic results.

CHAPTER 2
THIOL AND DISULFIDE OXIDATIONS

Introduction

Thiols and thiol derivatives are important and versatile functional groups in biological systems. Much of the unique biochemistry of thiols is associated with the relative ease with which thiols react with oxidants, bases and metal ions even at moderate temperature and neutral pH. Thiols are weakly acidic and able to participate in hydrogen bonding. The conjugate base thiolate anion (RS^-) appears to be one of the strongest biological nucleophiles and also a good ligand for metal ions. Thiols are also easily oxidized by a number of oxidants such as dioxygen, superoxide, hydrogen peroxide, disulfides, various nitrogen oxides (peroxynitrite, nitric oxide), and transition metals. The oxidation of a thiol can be a reversible one- or two-electron process. It is then not surprising that a wide spectrum of biological phenomena such as protein folding, enzyme activity, cell signaling and even redox homeostasis are dependent on thiols and its derivatives.

Cysteines, other low molecular weight thiols and protein thiols are crucial targets for oxidative stress and are excellent antioxidants *in vivo.* Oxidation of protein thiols can lead to loss in enzymatic activity [32,33,55-57] and can also lead to the activation of the expression of antioxidant genes [9,36,58,59]. While protein thiols are believed to scavenge 50-75% of reactive oxygen species (ROS) or reactive nitrogen species (RNS), non-protein thiols such as gluthathione (GSH) can also protect against oxidative injury [60,61], regulate gene expression, and inhibit signal transduction [62,63].

Disulfides, on the other hand, are less reactive and are more resistant to oxidation than thiols. Disulfide oxidation usually requires large excess of the oxidant, higher temperature, or a catalyst [64,65]. They are however easily reduced back to thiols under physiological conditions. A thiolate ion is capable of reducing the disulfide bond by nucleophilic displacement or interchange reaction (eq 2-1).

$$\text{R'SH} + \text{RSSR} \rightarrow \text{R'SSR} + \text{RSH} \qquad \text{(eq 2-1)}$$

This reaction has been widely used in structural studies of proteins wherein the protein disulfide is reduced by an excess amount of a simple thiol such as dithiothreitol (DTT) into two protein –SH groups. This reaction is also the basis of the sulfhydryl-disulfide equilibrium involved in the redox homeostasis [66].

Further oxidation of thiols to sulfonic acids involves several intermediates shown in figure 2-1, most of which are irreversible under physiological conditions and are important in the metabolism of thiols and disulfides to sulfates [67]. Thiosulfinates (**4**), the initial oxidized product, occur naturally in plants such as alliciin in garlic and onions (*Allium cepa*) [68,69]. Thiosulfinates are easily reduced to disulfides by thiols (eq 2-2) and are slowly hydrolyzed to sulfinic acids (**8**) by water (eq 2-3) [68].

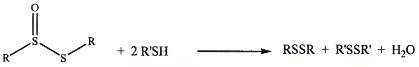

(2-2)

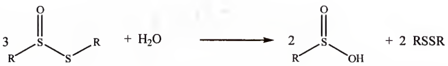

(2-3)

The next step in the disulfide oxidation is controversial. Studies by Freeman and co-workers [70,71] and Folkins and Harpp [75] suggested that the α-disulfoxide (**5**) is

$R{-}SH$

thiol

1

$RS{-}OH$

sulfenic acid

2

$RS{-}SR$

disulfide

3

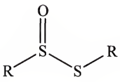

thiosulfinate

4

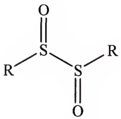

α-disulfoxide

5

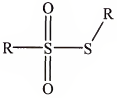

thiosulfonate

6

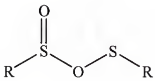

O,S-sulfenyl sulfinate

7

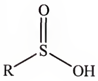

sulfinic acid

8

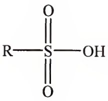

sulfonic acid

9

Figure 2-1. Some of the different oxidation intermediates of thiol oxidation to sulfonic acid.

initially formed and then rearranged into thiosulfonates (**6**) via *O,S*-sulfenyl sulfinate intermediate (**7**) (eq 2-4).

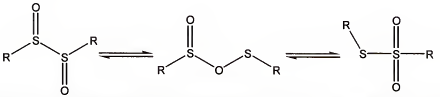

(2-4)

Both species are unstable, and thiosulfonates derived from cysteine and gluthathione have been obtained only by oxidation under anhydrous conditions [68]. In aqueous solution, thiosulfonates and α-disulfoxides are hydrolyzed to sulfinic acids (**8**) (eq 2-5) and reaction with thiols yield the same products as thiosulfinates (eq 2-6) [68].

$$2\ RS_2O_2R + 2\ H_2O \rightarrow 3\ RSO_2H + RSH \qquad (2\text{-}5)$$

$$RS_2O_2R + RSH \rightarrow RSO_2H + RSSR \qquad (2\text{-}6)$$

Sulfinic acids are stable oxidation products that can be obtained from the oxidation of the disulfide or the thiol [68]. A widely distributed enzyme, cysteamine oxygenase, catalyzes the direct oxidation of thiol cysteamine to sulfinic acid hypotaurine (eq 2-7) [72,73].

$$H_2NCH_2CH_2SH + O_2 \xrightarrow[\text{oxygenase}]{\text{cysteamine}} H_2NCH_2CH_2SO_2H \qquad (2\text{-}7)$$

Sulfonic acids are easily obtained from the oxidation of sulfinic acids or from the oxidation of thiols or disulfides using strong oxidizing agents [68]. Some examples of naturally occurring sulfonic acids are taurine [74], isethionic acid [75] and methane sulfonic acid [76].

In this chapter, catalysis of hydrogen peroxide oxidation of thiols by bicarbonate ion is demonstrated. Kinetic evidence also shows that the oxidation by peroxymonocarbonate is consistent with the equilibrium reaction for the formation of peroxymonocarbonate. Catalysis of the hydrogen peroxide disulfide oxidation to sulfonic acid has also been investigated.

Materials and Methods

Materials and Instrumentation

Bovine liver catalase (EC 1.11.1.6), L-cystine, and gluthathione (both reduced and oxidized forms) were obtained from Sigma Chemical Co. (St. Louis, MO). Ellman's reagent (5,5'-dithiobis-2-nitrobenzoic acid) was obtained from Pierce (Rockford, IL). *N*-acetylcysteine and L-cysteine hydrochloride were obtained from Acros (Atlanta, GA). Cysteine hydrochloride was recrystallized from 20% HCl [77]. Purity was confirmed by using elemental analysis performed by the University of Florida Department of Chemistry Spectroscopic Services. Methyl disulfide and 2-mercaptoethanol were obtained from Acros (Atlanta, GA). 2-Hydroxyethyl disulfide was obtained from Aldrich (St. Louis, MO). Hydrogen peroxide (70%) was obtained from Solvay Interox (Houston, TX) and standardized iodometrically. Sodium hydrogen phosphate, sodium dihydrogen phosphate, sodium phosphate, phosphoric acid, sodium bicarbonate, sodium carbonate and hydrochloric acid were all analytical grade and obtained from Fisher (Atlanta, GA). Water was purified using Barnstead E-Pure 3-Module Deionization System (water resistance $\geq$ 17 megohm-cm). Dinitrogen was bubbled through all buffer solutions for at least 30 minutes before use.

Proton and ^{13}C NMR spectra were obtained on a Gemini 300 spectrometer. Chemical shifts are reported in parts per million. The residual solvent peak was used as an internal standard. Deuterated water (99.9%) and ^{13}C-enriched sodium bicarbonate (99%) used for the NMR experiments were obtained from Cambridge Isotope

Laboratory, Inc (Andover, MA). Carbon-13 NMR were generally obtained with *d1* = 10 s and 10 acquisitions.

Spectral measurements were obtained on a Hewlett-Packard 8453 spectrophotometer using 0.5 and 1.0 cm quartz cells from Starna Cells, Inc. Temperature was maintained at 25 ($\pm$ 0.1) °C using a Fisher Scientific Isotemp 1600S water bath circulator.

Catalase Decomposition of Peroxymonocarbonate

A peroxymonocarbonate solution was prepared from a ^{13}C-enriched bicarbonate solution (1.0 M) with hydrogen peroxide (0.10 M) and equilibrated for at least one hour. A ^{13}C NMR was obtained to confirm formation of HCO_4^- before addition of catalase to the solution. After catalase addition, a ^{13}C NMR spectrum was then obtained to determine the amount of peroxymonocarbonate in solution.

Apparent Molar Absorptivity of 2-Nitro-5-thiobenzoate (TNB)

Solutions of thiols, with concentrations ranging from 3-70 uM, and of 5,5'-dithiobis(2-nitrobenzoic acid) (DTNB) (Ellman's Reagent) (2.0 mg/mL) in sodium phosphate buffer at pH 8.0 and $\mu = 0.30$ were prepared. An aliquot of 36 uL of the DTNB solution was then added to the thiol solutions (final volume of 1 mL). The mixture was left standing for 20 minutes before the absorbance at 412 nm in a 1.0 cm path cell were taken. The apparent molar extinction coefficient of 5-thio-2-nitrobenzoate dianion (TNB) was then determined from the plot of the absorbance against the thiol concentration.

The same procedure was used to determine if addition of catalase (0.1 nm) and bicarbonate have any effect on the apparent molar absorptivity of TNB.

Thiol Oxidation Reactions

All reactions were performed at room temperature at an ionic strength of 0.30 M at pH 8.0 unless otherwise stated. For uncatalyzed reactions, solutions of thiol substrate and hydrogen peroxide, both in sodium phosphate buffer at pH 8.0, were mixed. Aliquots of the reaction mixture were then taken at different time intervals and added to a solution of catalase (1 nM) to quench the reaction. The concentration of the unreacted thiol was then determined by using DTNB (Ellman's reagent) [77,78]. The rate of oxidation reaction was measured by following the loss of thiol as a function of time. Thiol concentrations were calculated using Beer's Law from the absorbance of TNB at 412 nm and the calculated molar absorptivity of the given thiol-DTNB combination.

Similar experiments were performed for the catalyzed reaction where the hydrogen peroxide was in sodium bicarbonate solution (0.025 to 0.25 M). Spontaneous oxidation by air, wherein no oxidant was added, was measured under the same conditions and time frame. The rate of spontaneous oxidation under the same conditions was negligible due to the low concentration of thiol and low oxygen content in the nitrogen-flushed solution.

Dependence of the rate of oxidation on pH was investigated in sodium phosphate buffer solutions at constant ionic strength of 0.30 M. The pH of the buffer solutions ranges from 6.4 to 10.5 and were checked by using an Orion Research Digital pH/Millivolt Meter Model 611.

Disulfide Oxidation Reactions

A solution of hydrogen peroxide (0.030 M) in 0.10 M sodium dihydrogen phosphate for the uncatalyzed reaction or 0.10 M sodium bicarbonate for the catalyzed reaction, was pre-equilibrated for two hours before the addition of the substrate disulfide

(0.030 M). Proton NMR was then obtained, and the disappearance of the methyl peak for methyl disulfide was monitored to follow the reaction.

Similar experiments were performed using 0.10 M phosphoric acid instead of sodium phosphate in the oxidation reaction.

Results and Discussions

Catalase Activity on Peroxymonocarbonate

The decomposition of peroxymonocarbonate by catalase was investigated by ^{13}C NMR using a pre-equilibrated solution of ^{13}C-enriched bicarbonate (1.0 M) with hydrogen peroxide (0.10 M) (eq 1-3). A peak for peroxymonocarbonate was observed before addition of catalase solution (0.1 nM), which then disappeared after the addition of catalase and within the time required to obtain the initial ^{13}C NMR spectrum ($t < 60$ s) (Figure 2-2). With an estimated half-life of 10 s, the minimum second-order rate constant for catalase decomposition of peroxymonocarbonate, k_{HCO4}, was ~ 10^9 $M^{-1}s^{-1}$ vs. k_{H2O2} = 4×10^7 $M^{-1}s^{-1}$ [79]. There was an apparent increase in the reactivity for the decomposition of the peroxymonocarbonate compared to hydrogen peroxide. However, care must be taken into interpreting such results since the effect of the high salt concentration (1.0 M $NaHCO_3$), the binding and dissociation constants, and the presence of another substrate (hydrogen peroxide) have not been taken into consideration.

Apparent Molar Absorptivity of TNB

Molar absorptivities of TNB obtained from the different thiols were as follows: $\varepsilon_{cys} = 13671 \pm 127$, $\varepsilon_{gsh} = 13799 \pm 70$, and $\varepsilon_{nac} = 14101 \pm 106$ $M^{-1}cm^{-1}$. Slight differences in the values may be due to the purity of the starting thiol.

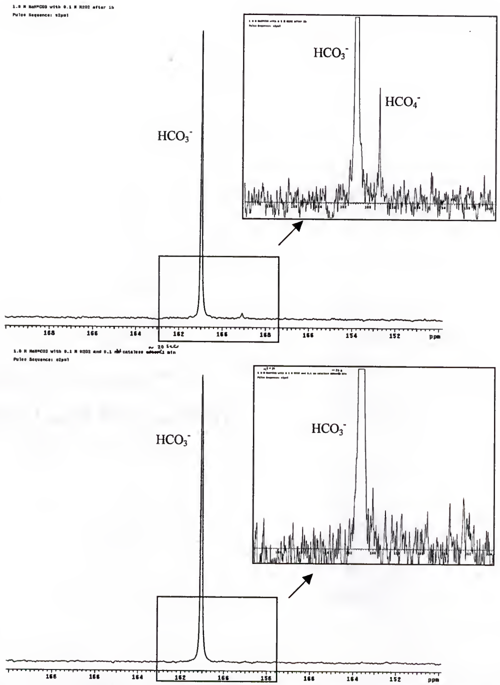

Figure 2-2. Carbon-13 NMR spectra of the equilibration reaction between ^{13}C-enriched bicarbonate (1.0 M) and H_2O_2 (0.10 M) after one hour in (a) the absence and (b) the presence of catalase (0.10 nM).

Thiol Oxidations by Hydrogen Peroxide

Oxidation of the thiols was followed by measuring the decrease in thiol concentration as a function of time. Loss of thiol was monitored by measuring the decrease in the absorbance, at 412 nm, of the released 5-thio-2-nitrobenzoate dianion (TNB) upon disulfide exchange (eq 2-8). The starting symmetric aryl disulfide, 5,5'-dithiobis-2-nitrobenzoic acid and the resulting mixed alkyl aryl disulfide and symmetric alkyl disulfide products do not absorb significantly in this region.

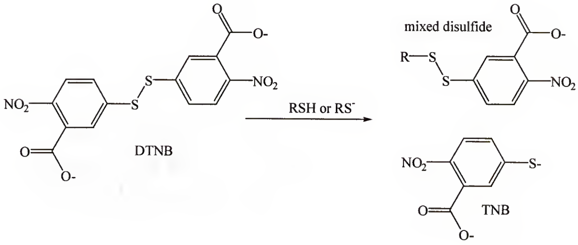

(2-8)

Variations in [H_2O_2] and in [RSH] indicated that the rate of reaction to be first order with respect to the hydrogen peroxide and first order with respect to the thiol substrate (eq 2-9).

$$-\frac{d[\mathrm{RSH}]}{dt} = k_{\mathrm{obs}}[\mathrm{RSH}][\mathrm{H_2O_2}] \qquad (2\text{-}9)$$

Variation in pH showed a dependence of the second-order rate constant k_{obs} on [H_3O^+] suggesting the thiolate anion to be the reactive species [80] (eq 2-10) in the rate-controlling step (Figure 2-3). Cysteine, which has the lowest pK_a among the thiols investigated, showed the greatest reactivity at pH 8 (Figure 2-4) (Table 2-1).

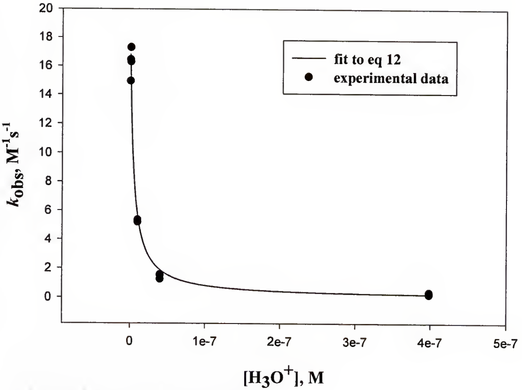

Figure 2-3. pH dependence of k_{obs} for the uncatalyzed cysteine oxidation. In all reactions, [Cys] = $[H_2O_2]$= 0.50 mM and pH adjusted using phosphate buffers, $\mu = 0.30$. (●) Experimental data and lines are fits from eq 2-18 in the text.

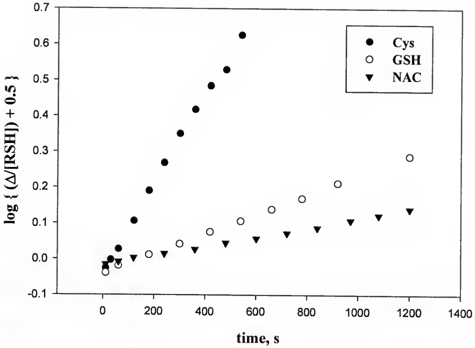

Figure 2-4. Reactivities of the different thiol substrates. A plot of the log {(Δ/[RSH]) + 0.5} vs. time, the slope of which gives the $k_{obs}\Delta$ from eq 9 in the text. In all reactions, [RSH] = [H_2O_2] = 0.50 mM at pH 8.0 and 25°C. Plots of (●) cysteine, (○) gluthathione, and (▼) *N*-acetylcysteine reactivities.

Table 2-1. Second Order Rate Constants for Thiol Oxidation

		pH 8.0[b]	RS$^-$ rate constant[c]	
Substrate	p*K*a of –SH[a]	k_{obs} ($M^{-1}s^{-1}$)	k_{01} ($M^{-1}s^{-1}$)	k_c ($M^{-1}s^{-1}$)
cysteine	8.3	5.6 ± 0.1	17 ± 2	990 ± 80
gluthathione	9.1	1.3 ± 0.1	18 ± 2	1920 ± 70
N-acetylcysteine	9.5	0.5 ± 0.1	17 ± 1	1490 ± 10

Errors are reported as standard errors.

[a] p*K*a values from Merck Index. New Jersey: Chapman & Hall; 1996.

[b] Values reported are the observed rate constants for uncatalyzed thiol oxidation.

[c] Values reported are second-order rate constants for the thiolate anion

$$RSH + H_2O = RS^- + H_3O^+ \qquad K_a = \frac{[RS^-][H_3O^+]}{[RSH]} \tag{2-10}$$

This pH dependence was consistent with a proposed mechanism for thiol oxidation [84] wherein the reactive species, thiolate anion, acts as a nucleophile to the oxidant hydrogen peroxide to form initially sulfenic acid, RSOH (eq 2-11). Once formed, the sulfenic acid would presumably reacts rapidly with a thiol or thiolate anion to form the disulfide (eq 2-12).

$$RS^- + H_2O_2 \rightarrow RSOH + OH^- \qquad k_{01} \tag{2-11}$$

$$RSOH + RSH \rightarrow RSSR + H_2O \qquad \textit{fast} \tag{2-12}$$

The rate of thiol loss can then be rewritten as eq 2-13, where $[RS^-]$ is the concentration of the thiolate ion at equilibrium.

$$-\frac{d[\mathrm{RSH}]}{dt} = k_{\mathrm{obs}}[\mathrm{RS}^-][\mathrm{H_2O_2}] \tag{2-13}$$

The $[RS^-]$ is related to the total thiol concentration by $[RSH]_T = [RS^-] + [RSH]$. Using this relationship and eq 2-10, the rate law can be expressed as eq 2-14.

$$-\frac{d[\mathrm{RSH}]}{dt} = \frac{k_{01}K_a}{[\mathrm{H_3O^+}] + K_a}[\mathrm{RSH}]_T[\mathrm{H_2O_2}] = k_{\mathrm{obs}}[\mathrm{RSH}]_T[\mathrm{H_2O_2}] \tag{2-14}$$

Previous studies have established the stoichiometry of the reaction [80] and at all times it was found that $\delta[RSH] = 2\delta[H_2O_2]$ consistent with the overall oxidation reaction (eq 2-15). The disulfide product was confirmed through ^{1}H NMR and no further oxidation was observed under the time frame of the reaction (~2h).

$$2\,RSH + H_2O_2 \rightarrow RSSR + 2\,H_2O \tag{2-15}$$

Given the stoichiometry of the reaction and expressing $[H_2O_2]$ at any time *t* in terms of $[RSH]_t$, we can then rewrite the eq 2-14 as eq 2-16.

$$-\frac{d[\mathrm{RSH}]}{dt}=\frac{k_{01}K_\mathrm{a}}{[\mathrm{H_3O^+}]+K_\mathrm{a}}[\mathrm{RSH}]_\mathrm{T}=k_\mathrm{obs}[\mathrm{RSH}]_\mathrm{T}\left(\Delta+\frac{1}{2}[\mathrm{RSH}]_\mathrm{T}\right)\quad(2\text{-}16)$$

In eq 2-16, $\Delta = [H_2O_2]_o - ½\ [RSH]_o$, $[H_2O_2]_o$ and $[RSH]_o$ are the initial concentrations, and $[H_2O_2]_o > ½\ [RSH]_o$. Integrating the rate law of eq 2-16 gives eq 2-17.

$$\log\left(\frac{\Delta}{[\mathrm{RSH}]_\mathrm{T}}+\frac{1}{2}\right)=k_\mathrm{obs}\Delta \mathrm{t}\qquad(2\text{-}17)$$

where k_{obs} is given by eq 2-18.

$$k_\mathrm{obs}=\frac{k_{01}K_\mathrm{a}}{[\mathrm{H_3O^+}]+K_\mathrm{a}}\qquad(2\text{-}18)$$

From the plots of $\log\{(\Delta/[RSH]_t) + ½\}$ vs time t (eq 2-17), we obtained the experimental k_{obs} from the slope(= $k_{obs}\Delta$). The resulting second-order rate constant for the thiolate anion was obtained by using a nonlinear regression fit to eq 2-18 from the plots of experimental k_{obs} values vs $[H_3O^+]$ (Figure 2-3). All kinetic data were consistent with the rate expression, and the calculated second order rate constants, k_{01}, for the different thiolate ions were within experimental error of each other, and, allowing for temperature differences, were in agreement with previous studies (Table 2-1) [80,81].

Thiol Oxidations by Peroxymonocarbonate

The kinetics of the bicarbonate-catalyzed oxidation of thiols by hydrogen peroxide were investigated by using the same method as the above uncatalyzed reaction. Rates of peroxide oxidation were accelerated in the presence of bicarbonate. Variation in $[HCO_3^-]$ indicated the catalytic reactions were first order in bicarbonate (Figure 2-5).

Previous studies have treated the kinetics of peroxymonocarbonate sulfide oxidations [49] to be a pre-equilibrium rate law wherein the equilibration rate for eq 1-3 is rapid compared to the oxidation rate. In this study, the rates of thiol oxidation are much faster than the rates of sulfide oxidations (k_{01} for RSR $\approx 10^{-4}\ M^{-1}s^{-1}$ vs. RSH $\approx 17\ M^{-1}s^{-1}$).

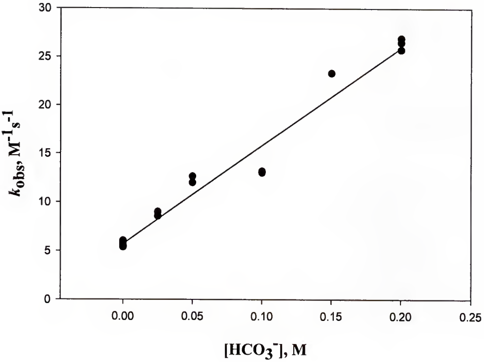

Figure 2-5. First-order dependence of k_{obs} on $[HCO_3^-]$ for cysteine oxidation at pH 8.0. In all reactions, [RSH] = $[H_2O_2]$ = 0.50 mM, $[HCO_3^-]$ = 0 to 0.25 M and pH adjusted using phosphate buffers, $\mu = 0.30$ and 25°C.

Assuming that the equilibration rate for eq 1-3 to be unchanged as found in sulfide oxidations, then the rate of formation for HCO_4^- becomes rate-limiting. However, numerical simulation of the loss of thiol as a function of time suggested catalysis of the equilibrium formation of peroxymonocarbonate (eq 1-3), presumably due to nucleophilic catalysis by the thiol [82]. As a result, the equilibration reaction (eq 1-3) was rapid compared to the oxidation reaction (eq 2-19) and the pre-equilibrium rate law was applied.

$$RS^- + HCO_4^- \rightarrow RSOH + CO_3^{2-} \qquad k_c \qquad (2\text{-}19)$$

The rate of thiol loss is the sum of the rates due to the uncatalyzed (eq 2-11) and to the catalyzed (eq 2-19) oxidation and is given by eq 2-20, where $[HCO_4^-]$ is the concentration of peroxymonocarbonate at equilibrium.

$$-\frac{d[\mathrm{RSH}]}{dt} = k_c[\mathrm{HCO_4^-}][\mathrm{RSH}] + k_{01}[\mathrm{H_2O_2}][\mathrm{RSH}] \qquad (2\text{-}20)$$

The $[HCO_4^-]$ is related to the initial concentration of bicarbonate by $[HCO_3^-]_o = [HCO_4^-] + [HCO_3^-]$. Using this relationship, we can then express $[HCO_4^-]$ as eq 2-21.

$$[\mathrm{HCO_4^-}] = \frac{K_{\mathrm{eq}}[\mathrm{HCO_3^-}]_o[\mathrm{H_2O_2}]}{1 + K_{\mathrm{eq}}[\mathrm{H_2O_2}]} \qquad (2\text{-}21)$$

At low $[H_2O_2]$, $[HCO_4^-] \approx K_{eq}[HCO_3^-]_o[H_2O_2]$. The overall rate law can then be expressed as eq 2-22.

$$-\frac{d[\mathrm{RSH}]}{dt} = \left(\frac{k_c K_a K_{\mathrm{eq}}[\mathrm{HCO_3^-}]_o + k_{01}K_a}{[\mathrm{H_3O^+}] + K_a}\right)[\mathrm{RSH}]_T\left(\Delta + \frac{1}{2}[\mathrm{RSH}]_T\right) \qquad (2\text{-}22)$$

The integrated form of eq 2-22 is simplified to eq 2-17 where k_{obs} is given by eq 2-23.

$$k_{\mathrm{obs}} = \frac{k_c K_a K_{eq}[\mathrm{HCO_3^-}]_o + k_{01}K_a}{[\mathrm{H_3O^+}] + K_a} \qquad (2\text{-}23)$$

The second-order rate constants for both the uncatalyzed, k_{01}, (eq 2-11) and catalyzed, k_c, (eq 2-19) pathways was obtained by using a nonlinear regression to fit eq 2-23 from the plot of experimental k_{obs} vs $[H_3O^+]$ with increasing amounts of $[HCO_3^-]$ (Figure 2-5). As, expected, the resulting k_{01} values were unchanged from the values obtained by fitting eq 2-18. The calculated second-order rate constants, k_c, were approximately 100-fold greater than the second order rate constant for the background reaction, k_{01} (Table 2-1). This enhancement was consistent with expectations based on a Brønsted analysis of the kinetics for heterolytic oxidation by peroxymonocarbonate [49,53,83].

Disulfide Oxidation by Hydrogen Peroxide

The products of oxidation of methyl disulfide were identified by comparison with the known ^{1}H NMR of the possible intermediates. From the ^{1}H NMR results of the hydrogen peroxide oxidation of methyl disulfide in 0.10 M phosphoric acid, the main product was the thiosulfonate even after 48 h (Figure 2-6). The thiosulfinate, being the first expected oxidation product before thiosulfonate, was not observed but may be a transient intermediate to thiosulfonate ($k_2 >> k_1$) (eqs 2-24 and 2-25).

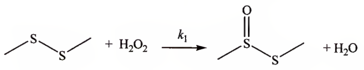

(2-24)

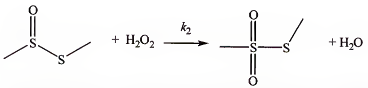

(2-25)

The estimated second-order rate constant for the oxidation of the disulfide to thiosulfinate (eq 2-24), k_1 was 10^{-5} $M^{-1}s^{-1}$. Some further oxidation products (<3%) that did not correspond to the final oxidation product, sulfonic acid, started to appear after 24 h (Figure 2-6). From the given chemical shifts of the new products, the proposed

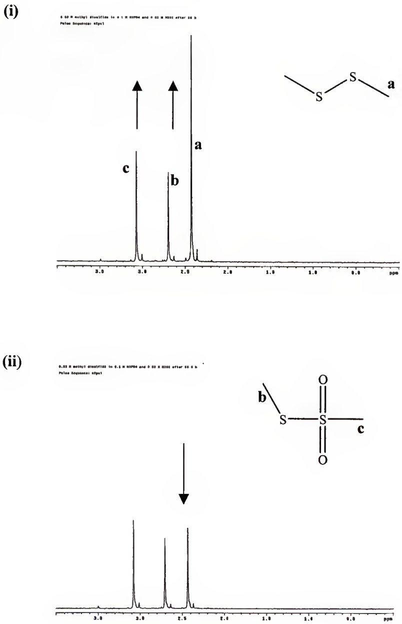

Figure 2-6. Proton NMR spectra of the oxidation of methyl disulfide (30 mM) with hydrogen peroxide (30 mM) in 0.10 M H_3PO_4. The major product of oxidation is thiosulfonate and no sulfonic acid appears even after (i) 26 h and (ii) 36 h of reaction.

structures were the next oxidation step products, sulfoxide sulfonate and *O,S*-sulfenyl sulfonate (eqs 2-26 to 2-27), and the hydrolysis product sulfinic and sulfonic acids (eqs 2-5 and 2-28).

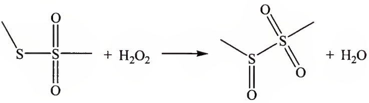

(2-26)

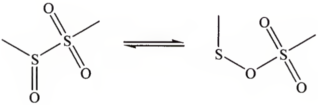

(2-27)

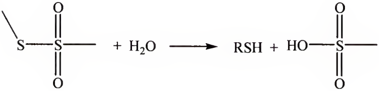

(2-28)

In contrast to the previous disulfide oxidation in phosphoric acid, oxidation at near neutral pH (~8.0) with 0.10 M Na_2HPO_4 gave a different product distribution. After 24 h, the main oxidation product was the sulfonate (sulfonic acid), and thiosulfonate was less than 5% of the total products (Figure 2-7). This result was what we would have expect at higher pH if the thiosulfonate was unstable in the presence of nucleophiles (OH^- becomes more available at higher pH). Consequently, hydrolysis reactions producing the sulfonic acid would be expected to be faster than under acidic conditions.

In the presence of bicarbonate, the product distribution was yet again different from the other two conditions (Figures 2-8 to 2-9). Both the thiosulfonate and the sulfonate were the major oxidation products. Other unidentifiable oxidation products

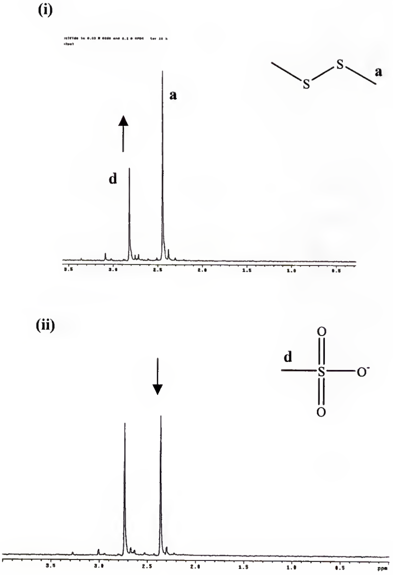

Figure 2-7. Proton NMR spectra of the oxidation of methyl disulfide (30 mM) with hydrogen peroxide (30 mM) in 0.10 M HPO_4^{2-} after (i) 26 h and (ii) 36 h. The major product of oxidation is sulfonate (from sulfonic acid) and thiosulfonate appears to be a minor product (<5%).

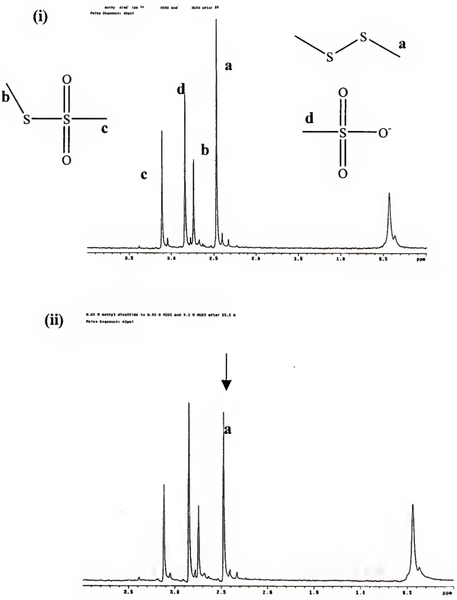

Figure 2-8. Proton NMR spectra of the oxidation of methyl disulfide (30 mM) with hydrogen peroxide (30 mM) in 0.10 M HCO_3^- after (i) 26 h and (ii) 36 h of reaction.. The major products of oxidation are thiosulfonate and sulfonic acid.

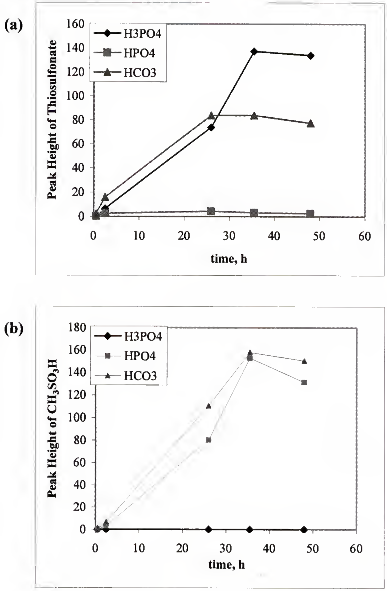

Figure 2-9. Product distribution for the hydrogen peroxide oxidation of methyl disulfide in the three conditions used. The top graph (a) illustrates the amount of thiosulfonate produced during the oxidation reaction while the bottom graph (b) illustrates the sulfonate (sulfonic acid) production.

were also visible at less than 5%. We would expect this distribution if catalysis by bicarbonate was occurring in the formation of thiosulfinate (eq 2-24). Comparison of the thiosulfonate product (Figure 2-9a) in all three conditions also supported the catalysis for thiosulfinate formation (eq 2-24). Catalysis in the subsequent steps may be occurring but further investigation is needed.

Conclusions

Although it is known that thiols react rapidly with hydrogen peroxide, their relative reactivities with hydrogen peroxide in the presence of bicarbonate have not been previously studied. In the absence of bicarbonate, the thiols are oxidized directly by hydrogen peroxide to disulfides. The relative rates of reaction for the different thiols are inversely related to the p*K*a of the thiol group, such that at pH 8.0 cysteine ($pK_a = 8.3$, $k_{obs} = 5.6 \pm 0.1\ M^{-1}s^{-1}$) is most reactive while *N*-acetylcysteine ($pK_a = 9.5$, $k_{obs} = 0.5 \pm 0.1\ M^{-1}\ s^{-1}$) was least reactive. The calculated second-order rate constant for the reaction of the thiolate anion with hydrogen peroxide is $17 \pm 2\ M^{-1}\ s^{-1}$ for all three substrates. In the presence of bicarbonate, the reaction rate for thiolate oxidation is increased by a factor of two to four. The calculated second-order rate constants for the direct reaction of the different thiolate anions with peroxymonocarbonate fell within the range of 950 - 1970 $M^{-1}s^{-1}$. Kinetic and spectroscopic results strongly support the formation of peroxymonocarbonate as the oxidant in the catalytic pathway.

Disulfide oxidation is about six orders of magnitude slower than the thiol oxidation to disulfide. Product distributions are dependent upon the conditions used. Under acidic conditions, the major product of oxidation is the thiosulfonate. At near neutral pH, hydrogen peroxide oxidation produces the sulfonate as the major product of the oxidation reaction. In the presence of bicarbonate, both the thiosulfonate and the sulfonate are the major products of the oxidation reaction. Catalysis of the disulfide oxidation by bicarbonate may be occurring at the first step of the disulfide oxidation.

Catalases, along with peroxidases, have been known to be responsible for the elimination of hydrogen peroxide before any cell damage can occur. Results have shown the direct decomposition of peroxymonocarbonate by catalase indicating that catalase is a possible defense mechanism against any peroxymonocarbonate that is formed.

CHAPTER 3
METHIONINE OXIDATION TO METHIONINE SULFOXIDE

Introduction

The thioether group of methionine is a moderately strong nucleophile comparable to amines, however, in contrast to other biological nucleophiles, methionines resist protonation at low pH and are nucleophilic even under acidic conditions. Previous studies have shown that under acidic conditions, methionine is much more susceptible to hydrogen peroxide oxidation than cysteine or cystine [84,85]. Other residues such as tryptophan, tyrosine, and histidine are generally more resistant to attack. Histidine in a polypeptide chain appears to be resistant [86] while *N*-acetyl-L-tryptophan oxidation occurs optimally at pH range of 8 to 10 [87].

In addition to hydrogen peroxide, a number of reagents have been used to oxidize methionine residues in proteins to methionine sulfoxide (Figure 3-1). Periodate has been shown to oxidize cysteine, cystine, methionine, tryptophan, tyrosine, histidine, and *N*-terminal serine and threonine [88]. Periodate has also been used to selectively oxidize methionine residues in α-chymotrypsin [89] and in apomyoglobin [90] at pH 5.0 and 0° C. Other oxidizing reagents used include iodine, dimethyl sulfoxide (DMSO), *N*-bromosuccinimide (NBS), *N*-chlorosuccinimide (NCS), and chloramine-T [91,92]. Of these reagents, chloramine-T has been shown to be specific for cysteine and methionine oxidation at pH 7.0-8.5 [91].

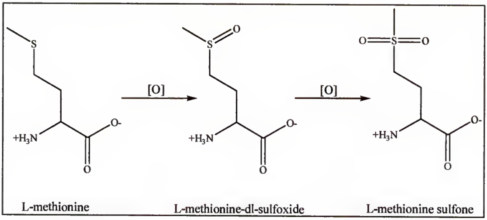

Figure 3-1. The oxidation of methionine to methionine sulfoxide and methionine sulfone.

Non-enzymatic reduction of methionine sulfoxide to methionine can be achieved by using excessive amounts sulfhydryl agents or thioethers [93]. However, further oxidation of methionine sulfoxide to methionine sulfone is essentially irreversible (Figure3-1) [91,92]. Enzymatic reduction of methionine sulfoxide is accomplished by endogenous reductases. In various organisms and tissues, methionine sulfoxide reductase (MsrA) has been identified and, in conjunction with thioredoxin, reduces free or protein bound methionine sulfoxide back to methionine [92]. Thus, as with cysteine and other related thiols, a repair mechanism exists for reducing oxidized methionine residues in proteins.

Proteolytic digestion and ligation are other ways by which oxidized methionines are repaired. Oxidation of methionine to methionine sulfoxide decreases the side chain flexibility [94] and increases the hydrophobicity of the protein surface by perturbing the native structure and exposing the hydrophobic residues [34,95]. This increase in hydrophobicity is recognized by proteasome for proteolytic digestion [96]. Methionine oxidation has also been reported to increase the protein susceptibility of proteins to ligation by the ubiquitin-ligase system [97].

The reversible oxidation process and the existence of repair mechanisms for methionine oxidation have led to the hypotheses by Levine and co-workers that methionine can act as an endogenous antioxidant [98], protecting vital residues from oxidation, and can regulate intracellular functions [92,94,96,99-102]. As endogenous antioxidants, only solvent-exposed methionine residues of the native proteins are oxidized effectively scavenging oxidants before they can attack residues that are critical to the structure or function. An example of this type of methionine is the oxidative inactivation of α2-macroglobulin, a proteinase inhibitor often acting at the sites of inflammation where ROS or RNS are at relatively high concentrations. Initially, no loss of inhibitory activity was noted while ROS are consumed and the consumption of the oxidant was stoichiometric with methionine oxidation [103]. However at higher concentration of ROS, a single tryptophan residue is oxidized and loss of inhibitory activity is observed [104]. Due to the lack of crystallographic data for this protein, the protecting methionines are presumed to be solvent-exposed.

Another example of solvent-exposed methionine oxidation, is the oxidation of glutamine synthetase wherein the loss of the Mg^{2+}-dependent but not the Mn^{2+}-dependent γ-glutamyl transferase activity of enzyme is accredited to the oxidation of eight out of sixteen methionines with no other covalent modifications detected [98]. Studies also show that the methionine sulfoxide residues are clustered at the entrance to the active site and are referred to as "guardian" methionines [96,98,105].

In many proteins, the oxidation of methionine causes loss of biological activity. The synthetic chemotactic factor peptide f-Met-Leu-Phe, related to the bacterial chemotaxin and human C5a, a complement-derived peptide, are inactivated by methionine oxidation [106-110]. The ribosomal protein of *E. coli* L12 involved in protein synthesis loses its binding affinity for ribosome upon oxidation of the three methionines with hydrogen peroxide and regains the activity upon reduction of the oxidized methionines [92,111].

Accumulation of methionine sulfoxide residues in the tissue has been also been associated with aging. The human juvenile lens protein for example contains little methionine sulfoxide [112]. However with age, the methionine sulfoxide content rises. In cataractous lenses, about 45% of the total methionine residues and 60% of the total cysteine residues are oxidized [112-114]. The methionine sulfoxide content of collagenous proteins contained in the trabecular meshwork of the human eyes also increases with age. Up to 35% of the total methionine residues are oxidized at the age of 20 and 40% at the age of 80 [115]. In calmodulin, a mediator for calcium-regulated activities, six out of nine methionines are found to be methionine sulfoxides in the brains of aged Fischer rats but not in the brains of young rats [100]. The oxidation of the methionines corresponds to the age-dependent reduction of the ability of calmodulin to activate the plasma membrane Ca-ATPase [100] that can be restored by methionine sulfoxide reductase [101].

In the oxidative inactivation of α1-proteinase inhibitor (α1-PI) (formerly named α1-antitrypsin), a protein present in blood plasma and in other body fluids which inhibits a wide spectrum of serine proteases, oxidation of two out of nine methionines, particularly of Met358 in the reactive center, results in the decrease in the binding affinity for the protease resulting in the decrease in its inhibitory activity [107,121-124] (Figure 3-2). The inactivation of α1-PI shifts the equilibrium between the elastase and the inhibitor favoring the elastase. Uncontrolled activity of the elastase can lead to adult respiratory distress syndrome [125,126], chronic obstructive pulmonary disease (COPD) [127-129], emphysema [128-133], and rheumatoid arthritis [98,127,129,134].

In this chapter, we investigate the rate of hydrogen peroxide oxidation of free methionine and methionine in proteins such as α1-PI and ribonuclease A (RNase A) in the absence and presence of bicarbonate. The effect of oxidation of methionine to methionine sulfoxide on the activity of the protein is investigated. The rate of oxidative inactivation of human α1-PI to porcine pancreatic elastase by hydrogen peroxide in the presence of increasing amounts of bicarbonate is measured by assaying the hydrolytic activity of elastase-inhibitor solution towards the synthetic elastase substrate Suc-$(Ala)_3$-Nan in accordance to previously established procedure [135-138]. Cyanogen bromide treatment prior to acid hydrolysis in the amino acid analysis is used to determine the methionine sulfoxide content of the oxidized α1-PI. An HPLC/ESI/QIT-MS analysis of the endoproteinase Lys-C digest of the oxidized α1-PI is also investigated to determine the sites of oxidation.

For the oxidation of RNase A, the hydrolytic activity of RNase A is measured by using the synthetic substrate cytidine 2',3'-cyclic monophosphate. Oxidation of RNase A is followed by directly following the signal intensities of the native and oxidized protein using ESI/FTICR-MS.

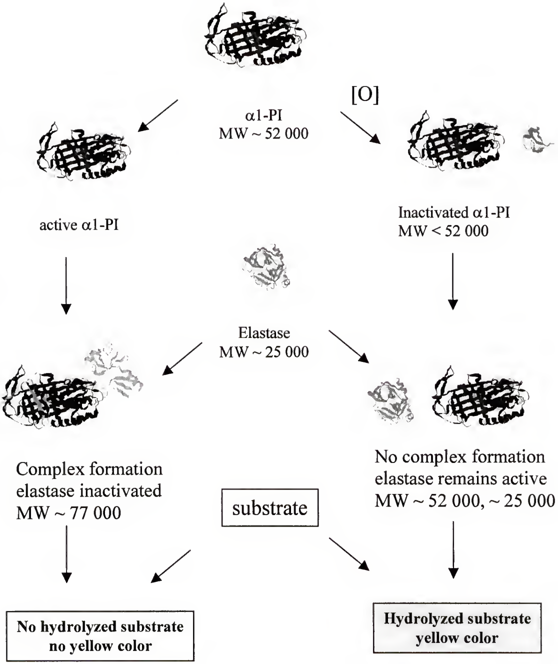

Figure 3-2. Schematic diagram for the assay of α1-PI before and after oxidation. The native α1-PI is active to form a complex with the protease elastase (left side). Bound elastase is then unable to hydrolyze the substrate and no yellow color of the hydrolysis product *p*-nitroaniline is observed. However, if the α1-PI is oxidized (right side), the inhibitor cannot bind to the protease elastase and elastase is free to hydrolyze the substrate. A yellow color of the hydrolysis product *p*-nitroaniline is observed at $\lambda = 410$ nm.

Materials and Methods

Materials and Instrumentation

Human α1-proteinase inhibitor, bovine pancreatic ribonuclease A (EC 3.1.27.5) type I-AS, porcine pancreatic elastase (EC 3.4.21.36) type IV, endoproteinase Lys C (EC 3.4.21.50) from *Lysobacter* enzymogenes, and bovine liver catalase (EC 1.11.1.6) were obtained from Sigma (St. Louis, MO) and used as received unless otherwise specified. Human α1-proteinase inhibitor was purified according to Travis and co-workers [116,117]. Ribonuclease A was purified according to reported procedures [118,119]. *N*-Succinyl-L-trialanyl-*p*-nitroanilide (Suc-(Ala)$_3$-Nan), and cytidine cyclic 2',3'-phosphate (cCMP), were obtained from Sigma (St. Louis, MO) and used as received. DL-Methionine was obtained from Eastman Chemical Company (Kingsport, TN) and used as received. Hydrogen peroxide (70%) was obtained from Solvay Interox (Houston, TX) and standardized iodometrically. Oxone (potassium persulfate) and *tert*-butylhydroperoxide T-HYDRO solution at 70% by weight in water were obtained from Sigma (St. Louis, MO) and standardized iodometrically. Diethylenetriaminepentaacetic acid (DTPA), trihydroxymethylamine (TRIS), ammonium bicarbonate, and ammonium phosphate (dibasic and monobasic forms) were all analytical grade and obtained from Sigma (St. Louis, MO) and used as received. Acetonitrile, dimethyl sulfoxide (DMSO), *N,N*-dimethylformamide (DMF), hydrochloric acid (36% by wt), sodium hydroxide, sodium chloride, ammonium sulfate, sodium bicarbonate, sodium carbonate, and sodium phosphate (tribasic) were all analytical grade and obtained from Fisher (Atlanta, GA). Formic acid (70%) sequence grade was obtained from Fisher (Atlanta, GA). Sepharose 4B, Sephadex G-25, diethylaminoethyl (DEAE) cellulose fibrous form anion exchange resin, and blue dextran were obtained from Sigma (St. Louis, MO). Bio-Rex 70 cation exchange resin (200-400 mesh) was obtained from Biorad (Hercules, CA). Water was purified using a Barnstead E-Pure 3-Module Deionization System (water resistance $\geq$ 17 megohm-cm).

Proton and ^{13}C NMR spectra were obtained on a Gemini 300 spectrometer. Chemical shifts are reported in parts per million. The residual solvent peak was used as an internal standard. Deuterated water (99.9%) and ^{13}C-enriched sodium bicarbonate (99%) used for the NMR experiments were obtained from Cambridge Isotope Laboratory, Inc (Andover, MA).

Spectral measurements were obtained on a Hewlett-Packer 8453 spectrophotometer using 0.5 and 1.0 cm quartz cells from Starna Cells, Inc. Temperature was maintained at 25 ($\pm$ 0.1) °C using a Fisher Scientific Isotemp 1600S water bath circulator.

Amino acid analyses were provided by Scott McClung of the Protein Chemistry Core Facility, Biotechnology Program of the University of Florida. Dr. Jodie Johnson of the Department of Chemistry Spectroscopic Services acquired the HPLC/ESI/QIT-MS data.

Apparent Molar Absorptivities of Hydrogen Peroxide and Other Oxidants

Solutions of hydrogen peroxide with concentrations ranging from 10 to 175 mM, in ammonium phosphate buffer at pH 7.85-8.00 and $\mu = 0.10$ were prepared. The solution was left standing for one hour before measuring the absorbance at 275 nm in a 1.0 cm path cell. The apparent molar extinction of hydrogen peroxide ($\varepsilon = 6.22 \pm 0.15$ M^{-1}cm^{-1}) at 275 nm was then determined from the slope of the plot of absorbance versus hydrogen peroxide concentration. Another batch was prepared in a similar manner, however the buffer contained 0.10 M ammonium bicarbonate. No change in the apparent molar absorptivity was observed.

Similar experiments were performed to obtained the apparent molar absorptivity of *tert*-butylhydroperoxide ($\varepsilon = 6.48 \pm 0.12\ M^{-1}cm^{-1}$) at 260 nm in both phosphate and bicarbonate buffer

Free Methionine Oxidation

All reactions were performed at room temperature (~25°C) at pH 7.85 and $\mu = 0.10$ unless otherwise stated. For the uncatalyzed reactions, solutions of methionine and hydrogen peroxide, both in ammonium phosphate buffers, were mixed. The decrease in absorbance of hydrogen peroxide at 275 nm over time was monitored.

Similar experiments were performed wherein the methionine and hydrogen peroxide were in 0.10 M NH_4HCO_3 solution instead of ammonium phosphate buffer. The hydrogen peroxide in bicarbonate solution was pre-equilibrated for at least one hour before adding to the methionine solution. The rate of reaction was measured by monitoring the decrease in the absorbance of the oxidant at 275 nm over time.

Dependence of the rate of hydrogen peroxide oxidation on pH was investigated for both the uncatalyzed and catalyzed reactions. The pH ranged from 4.5 to 9.5 for the uncatalyzed reactions and from 6.7 to 9.5 for the catalyzed ones. The pH was checked using an Orion Research Digital pH/Millivolt Meter Model 611.

Similar experiments were performed using *tert*-butylhydroperoxide as the oxidant. The rate of oxidation was followed by measuring the decrease in the absorbance of *tert*-butylhydroperoxide at 260 nm over time.

Proton NMR was also used to follow the rate of methionine oxidation. The disappearance of the methyl protons of methionine or the appearance of the methyl protons of methionine sulfoxide was monitored to obtain the rate of oxidation.

Oxidation of α1-Proteinase Inhibitor [120]

Stock solutions of hydrogen peroxide with $(NH_4)_2HPO_4$ or with NH_4HCO_3 in 0.20 M TRIS-HCl at pH 8.00 were pre-equilibrated for one hour. Quantitative amounts of the oxidant solution were then added to a solution of human α1-proteinase inhibitor in 0.20 M TRIS-HCl buffer at pH 8.00. Final conditions for the oxidation reactions were [α1-PI] ~ 13 uM, $[H_2O_2]$ = 10 mM, $[(NH_4)_2HPO_4]$ = 0.10 M or $[NH_4HCO_3]$ = 0.10 to 0.70 M, 0.20 M TRIS-HCl pH 8.00 at 25°C. Aliquots of the reaction mixture were then taken at different time intervals and added to a solution of catalase (2 nM) in 0.20 M TRIS-HCl buffer at pH 8.00 to quench the reaction. Elastase in 0.20 M TRIS-HCl at pH 8.00 was added to the quenched reaction and equilibrated for two hours to allow the elastase-inhibitor complex to form. The inhibitory activity of α1-PI on elastase was monitored by measuring the proteolytic activity of elastase on Suc-$(Ala)_3$-Nan (20 mM stock solution in DMF). Final conditions for the α1-PI inhibitory assay were: [α1-PI] = [elastase] = 0.10 μM, and [substrate] = 0.33 mM all in 0.20 M TRIS-HCl buffer pH 8.0 at 25°C. The release of the product *p*-nitroaniline was monitored by measuring the increase in absorbance at 410 nm.

Synthesis of Sepharose Blue Dextran (SBD) Affinity Column [117] [121]

Cooled Sepharose 4B, 20-25 mL of the settled resin previously rinsed with purified cold water (500 mL), in 0.10 M sodium carbonate buffer at pH 9.5 was activated with 4.1 g cyanogen bromide. The cyanogen bromide was added slowly to the stirred suspension of Sepharose in an ice bath (<10°C). The pH was maintained between 10.8

and 11.2 by addition of cold 4.0 M NaOH. When no further drop in pH was observed (about 4 h), the activated resin was then rinsed with 150 mL of cold 0.10 M sodium carbonate buffer at pH 9.5. Blue dextran (0.34 g), previously dissolved in the same sodium carbonate buffer, was added to the stirred activated Sepharose at 4°C in 0.10 M sodium carbonate buffer at pH 9.50. The suspension was stirred for 36 h at 4°C and was then washed with a liter each of cold 0.10 M sodium carbonate buffer pH 9.50, 6.0 M urea, purified water, and 0.50 M NaCl in 50 mM TRIS-HCl at pH 8.00. The Sepharose-blue dextran (SBD) derivative was stored at 4°C. To regenerate after use, the column was washed with 6M urea followed by a liter each of water and the TRIS-HCl buffer.

Purification of α1-PI [116]

The four-step purification of α1-proteinase inhibitor was based on procedures developed by Travis and coworkers [116] to obtain the protein from human plasma. Crude α1-proteinase inhibitor (8 mg) was first passed through the synthesized Sepharose Blue Dextran (SBD) affinity column (1.0 x 30 cm). The column was eluted at a flow rate of ~1mL/min with 200 mL of 2.0 mM NaCl in 50 mM TRIS-HCl buffer pH 8.00 at 4°C. One peak eluted and was collected and concentrated. The fraction collected from the SBD column was then fractionated with solid ammonium sulfate. The precipitate was collected using a refrigerated centrifuge at 4°C and 4000 rpm. The precipitated protein was then solubilized and dialyzed using 5.0 mM NaCl in 50 mM TRIS-HCl at pH 8.80. The dialyzed fraction was then applied to a DEAE-cellulose column pre-equilibrated with 5.0 mM NaCl in 50 mM TRIS-HCl at pH 8.80. A linear gradient from 5.0 mM to 200 mM NaCl, both in 50 mM TRIS-HCl pH 8.80 (total volume ~ 500 mL), was used to elute α1-PI at 4°C with a flow rate of 0.70 mL/min. The fractions collected in the 9th to 12th-hour were pooled, concentrated and dialyzed with 2.0 mM NaCl in 5.0 mM sodium phosphate buffer at pH 6.50. The dialyzed α1-PI from the first DEAE-cellulose column was applied to a DEAE-cellulose column pre-equilibrated with 2.0 mM NaCl in 5.0 mM sodium phosphate buffer at pH 6.50. A linear gradient from 2.0 mM to 200 mM NaCl, both in 5.0 mM sodium phosphate buffer at pH 6.50 (total volume ~ 500 mL), was used to elute the inhibitor at 4°C with a flow rate of 0.70 mL/min. The fractions from the first peak eluted at the 2nd to 4th-hour were pooled and concentrated. The purified protein was stored at 4°C and used within 3 days. Purified α1-PI was used in the SDS-PAGE, amino acid analysis and peptide mapping experiments.

The purified sample of α1-PI (10 μM) was oxidized for 8 hours using hydrogen peroxide (10 mM) in Na_2HPO_4 (0.10 M) or $NaHCO_3$ (0.10 M). Aliquots of the reaction mixture were then placed in glass vials and quickly frozen using liquid nitrogen. The frozen solutions were then lyophilized overnight and used for methionine sulfoxide analysis and for proteolytic digest using endoproteinase Lys C.

Elastase-Inhibitor Complex Formation using SDS-PAGE

Mixtures of purified α1-PI and elastase equilibrated for at least 2 h were run in 12%T/2.7%C with 0.1% SDS gel electrophoresis. An initial voltage of 70 V was applied for about 10 min and then raised to 135 V to run for about an hour. The gel was then stained using Coomassie brilliant blue G overnight and was then soaked in a destaining solution (30 % methanol in 10% acetic acid in water) for one hour.

CNBr Cleavage and Methionine Sulfoxide Analysis [122]

To the oxidized protein (10 μM) in a glass vial, a 100 μL of 100 mM CNBr was added. The cyanogen bromide solution was freshly prepared as a 10 M stock in acetonitrile and diluted to 100 mM using 70% formic acid [122]. The glass vial was then wrapped in aluminum foil and incubated overnight at room temperature in the hood.

After 18 hours, the solution was lyophilized and then hydrolyzed in 6M HCl at 110°C for 24 hours in the presence of 1.5 mM dithiothreitol (DTT). The samples were then used for amino acid analysis using a pre-column derivatization PITC method on the Applied Biosystem Model 420A instrument.

Peptide Mapping of Oxidized α1-PI using HPLC/ESI/QIT-MS [122]

To the lyophilized oxidized protein (~30 μg) was added 25 μL of 0.20 M TRIS-HCl 2 mM EDTA buffer at pH 8.5 followed by 25 μL of hexafluoroisopropanol as a denaturant. The solution was then lyophilized for 6 hours and 50 μL of water was added. Endoproteinase Lys-C (20 μL) was then added to the lyophilized sample and was then incubated at 37°C overnight. The digest was then cooled and run in an HPLC/ESI/QIT-MS with both spectrophotometric (Applied Biosystems Model 785A Programmable Absorbance Detector at $\lambda = 220$ nm) and mass spectrometric detection. The MS data were acquired using ThermoFinnigan MAT LCQ (San Jose, CA) in electrospray ionization (ESI) mode. An ion spray voltage of 3.5 kV, capillary voltage of 15 V, capillary temperature of 240°C with nitrogen sheath (60) and auxiliary (5) gases were the typical operating parameters. MS data were acquired in the m/z range of 400-2000. The mobile phase was introduced using a Beckman Instruments (Fullerton, CA) System Gold model 126 pump. A binary system with mobile phase A as 0.5 % acetic acid in water and B as 0.5 % acetic acid in methanol is used. A Waters (Milford, MA) Symmetry Shield RP18 (2.1 x 150 mm x 3.5 μm) with no guard column was used for chromatographic separation at a flow rate of 0.2 mL/min.

RNase A Oxidation

A purified sample of RNase A (55 μM) was oxidized in a 1% methanol and 0.1% acetic acid with hydrogen peroxide (55 mM) and directly electrosprayed into the Fourier

Transform Ion Cyclotron Resonance (FTICR) mass spectrometer. Oxidation was monitored by measuring the normalized signal intensities for the native and oxidized RNase.

All ESI/FTICR/MS data were collected using a Bruker BioApex external source shielded 4.7 Tesla FT-ICR mass spectrometer by Bruker Analytical Systems, Inc. (Billerica, MA) equipped with a Bruker Xmass 4.0.3 data system. The electrospray source was a modified Analytica electrospray source (Analytica of Branford, Branford, CT). The stainless steel desolvation capillary was held at ground potential and heated to 120°C. The FTICR cell pressure was maintained at $\sim 10^{-9}$ torr. Samples were sprayed at a rate of 1 µL/min using a microsyringe pump. The electrospray needle with a voltage of ~2950 V was located at 1 cm from the capillary. Capillary and skimmer voltages were adjusted to maximize the signal intensities at m/z =1711 for the +8 charged state for the native RNase. Typical values were ~ 68 V for the capillary and 3-5 V for the skimmer. Mass data were collected in the m/z range of 1450 to 1800.

Another set of oxidation experiments were carried out in either 0.10 M $(NH_4)_2HPO_4$ or 0.10 M NH_4HCO_3. As with α1-PI, reaction was quenched using catalase and the ribonuclease A was assayed for activity at different time intervals during the oxidation. A sample after 2 h of oxidation was used for ESI/HPLC/QIT-MS experiments.

Results and Discussions

Free Methionine Oxidation

The rate of methionine oxidation was followed by measuring the decrease in the absorbance of hydrogen peroxide as a function of time. Variations in $[H_2O_2]$ and in

(a)

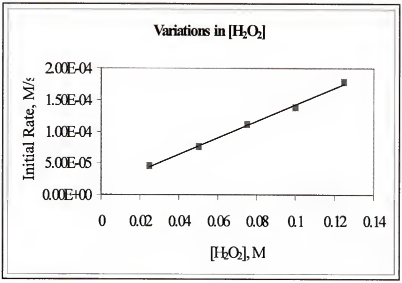

(b)

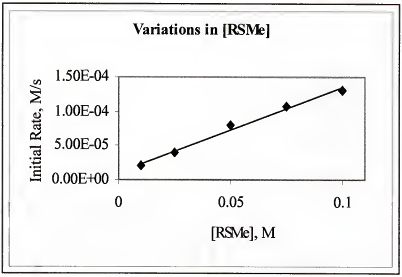

Figure 3-3. Dependence of the rate of oxidation on (a) [H_2O_2] and (b) [RSMe]. The linear fits of the initial rate to the [H_2O_2] and to the [RSMe] indicate the rate of methionine oxidation to be first-order with respect to [H_2O_2] and first-order with respect to [RSMe].

[RSMe] (Figure 3-3) indicated that the rate of oxidation to be first-order with respect to hydrogen peroxide and first-order with respect to methionine (eq 3-1).

$$-\frac{d[H_2O_2]}{dt} = k_{01}[H_2O_2][RSMe] \qquad (3\text{-}1)$$

Results also suggest that the stoichiometry of the reaction to be $\delta[H_2O_2] = \delta[RSMe]$ at all times (eq 3-2) and this was also confirmed by ^{1}H NMR. This was also in accordance with previous studies [123]

$$RSMe + H_2O_2 \rightarrow RSOMe + H_2O \qquad (3\text{-}2)$$

For $[H_2O_2] = [RSMe]$, given the stoichiometry of the reaction, we can rewrite eq 3-1 as eq 3-3.

$$-\frac{d[H_2O_2]}{dt} = k_{01}[H_2O_2]^2 \qquad (3\text{-}3)$$

Integration of the rate law from eq 3-3 gives eq 3-4.

$$\frac{1}{[H_2O_2]_t} = \frac{1}{[H_2O_2]_o} + k_{01}t \qquad (3\text{-}4)$$

The slope of the plot of the reciprocal of $[H_2O_2]$ vs. time (Figure 3-4) gave the second-order rate constant, k_{01} as 7.5 ($\pm$ 0.4) x 10^{-3} $M^{-1}s^{-1}$.

The rate of methionine oxidation was also be measured by monitoring the decrease in the intensity (peak height) of the methyl proton of methionine (Figure 3-5). Under similar conditions as stated above, the calculated second-order rate constant, k_{01} = 6.7 ($\pm$0.2) x 10^{-3} $M^{-1}s^{-1}$ was comparable to the one obtained using spectrophotometric method.

In the presence of bicarbonate, the rate of oxidation of methionine was accelerated (Figure 3-6). Variations in the $[HCO_3^-]$ indicated the rate of oxidation to be first order with respect to the bicarbonate concentration (Figure 3-7). Previous studies

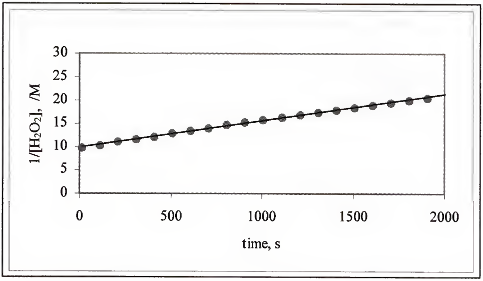

Figure 3-4. Plot of the reciprocal of [H_2O_2] versus time for methionine oxidation when [H_2O_2] = [RSMe] = 0.10 M as a fit to eq 3-4.

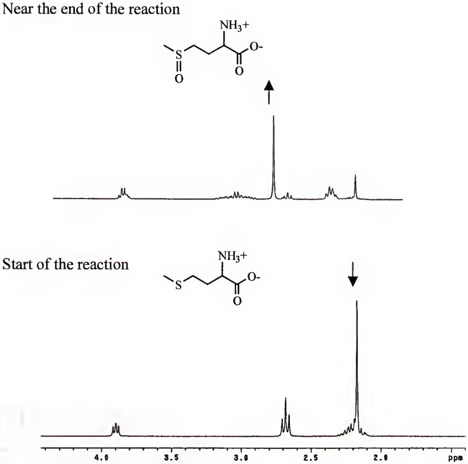

Near the end of the reaction

Start of the reaction

Figure 3-5. Proton NMR of the methionine oxidation to methionine sulfoxide. The reaction can be followed by monitoring the disappearance of the methyl protons (indicated by the arrows) for methionine (bottom) or the appearance of the methyl protons for methionine sulfoxide (top).

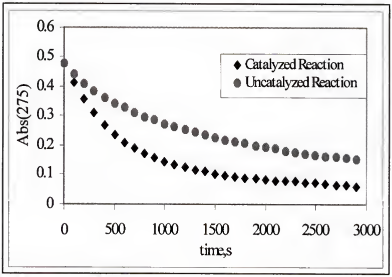

Figure 3-6. Profile of methionine oxidation showing the loss of absorbance of H_2O_2 at $\lambda = 275$nm for the uncatalyzed (•) and the catalyzed (♦) reactions. Reaction conditions are: [RSMe] = [H_2O_2]=0.10 M, 0.10 M HPO_4 for the uncatalyzed reaction and 0.10 M for the catalyzed reaction both at 25°C.

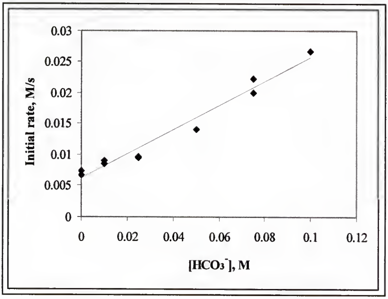

Figure 3-7. Dependence of the rate of oxidation on $[HCO_3^-]$. The linear fit indicates a first-order dependence of the oxidation reaction to $[HCO_3^-]$.

have treated the kinetics of aryl sulfide oxidation by peroxymonocarbonate to follow a pre-equilibrium rate law wherein the equilibration rate for eq 1-3 is rapid compared to the oxidation rate (eq 3-5).

$$\mathrm{RSMe} + \mathrm{HCO_4^-} \rightarrow \mathrm{RSOMe} + \mathrm{HCO_3^-} \qquad k_c \qquad (3\text{-}5)$$

In the case of alkyl sulfides, assuming that the equilibration rate for eq 1-3 to be unchanged as that found in sulfide oxidation, the rate of bicarbonate-catalyzed oxidation was comparable to the equilibration rate. Numerical simulations have been used to fit the kinetic data from ^{1}H NMR for the bicarbonate-catalyzed methionine oxidation. From the numerical simulation, a fit for $k_c = 1.0\ \mathrm{M^{-1}s^{-1}}$ [41] and $k_{01} = 6.6 \times 10^{-3}\ \mathrm{M^{-1}s^{-1}}$ have been obtained.

Previous studies on the catalysis of the formation of $\mathrm{HCO_4^-}$ (eq 1-3) by 1,4,7,10-tetraazacyclododecanezinc (II) in the methionine oxidation (Figure 3-8) indicated the experimental data to fit the pre-equilibrium rate law and the derived second-order rate constant, $k_c = 0.9\ \mathrm{M^{-1}s^{-1}}$, to be the same as that obtained in the earlier numerical simulation of the data in the absence of the zinc catalyst [41]. These results indicated that the equilibration rate for eq 1-3 has been accelerated by the presence of methionine presumably due to nucleophilic catalysis [82] and the pre-equilibrium rate law can be applied as with thiol oxidation.

The rate of bicarbonate-catalyzed methionine oxidation is the sum of the rates due to the uncatalyzed (eq 3-2) and to the catalyzed (eq 3-5) oxidation and is given by the pre-equilibrium rate eq 3-6.

$$-\frac{d[\mathrm{RSMe}]}{dt} = \frac{k_c K_{eq}[\mathrm{HCO_3^-}]_o[\mathrm{H_2O_2}][\mathrm{RSMe}]}{1 + K_{eq}[\mathrm{H_2O_2}]} + k_{01}[\mathrm{H_2O_2}][\mathrm{RSMe}] \qquad (3\text{-}6)$$

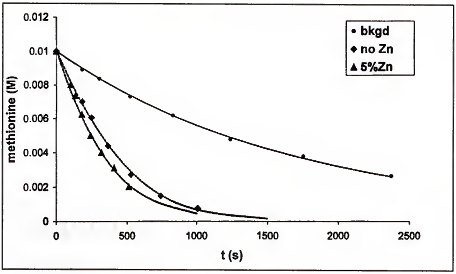

Figure 3-8. Methionine oxidation by hydrogen peroxide obtained from ^{1}H NMR [41]. In all reactions, $[H_2O_2] = 0.10$ M and [RSMe] = 10 mM at pH 8.0. (●) Uncatalyzed reaction 0.10 M $(NH_4)_2HPO_4$; (▲) catalyzed reaction 0.10 M NH_4HCO_3; and (♦) zinc-catalyzed reaction [ZnL] = 5.0 mM in 0.10 M NH_4HCO_3. The lines are nonlinear fits from the numerical simulations. Second-order rate constants obtained from the numerical fits are: $k_{01} = 0.0066\ M^{-1}s^{-1}$, $k_c = 1.0\ M^{-1}s^{-1}$, and $k_{ZnL} = 0.90\ M^{-1}s^{-1}$.

Using the spectrophotometric method to obtain initial rate, the values obtained from the fit of eq 3-6 were $k_{01} = 7.5\ (\pm 0.7) \times 10^{-3}\ M^{-1}s^{-1}$ and $k_c = 0.48\ (\pm 0.08)\ M^{-1}s^{-1}$. These results were comparable to the ones obtained from the numerical fits of the ^1H NMR data. And as in the thiol oxidation, the second-order rate constant, k_c, for the peroxymonocarbonate oxidation was ~100-fold greater than hydrogen peroxide.

Methionine oxidation by *tert*-butylhydroperoxide was also investigated and compared to hydrogen peroxide and peroxymonocarbonate oxidation. The rate of methionine oxidation by *tert*-butylhydroperoxide (eq 3-7) was slower than the oxidation by hydrogen peroxide.

$$t\text{-BuOOH} + \text{RSMe} \rightarrow t\text{-BuOH} + \text{RSOMe} \qquad k_{tb} \qquad (3\text{-}7)$$

The calculated second-order rate constant, k_{tb} was $5.8\ (\pm 0.2) \times 10^{-4}\ M^{-1}s^{-1}$ (Figure 3-9), about an order of magnitude lower than k_{01}. This was consistent with the Brønsted analysis of the kinetics for heterolytic oxidants [83]. Addition of bicarbonate to the reaction mixture did not alter the rate of reaction further supporting the formation of HCO_4^- in the bicarbonate-catalyzed hydrogen peroxide oxidation of methionine. No such carboxy adduct was formed with *tert*-butylhydroperoxide as observed in ^{13}C NMR.

Unlike the thiol oxidation, variation of pH showed the rate of methionine oxidation to be independent of $[H_3O^+]$ in the pH range of 5 to 9 for both the uncatalyzed (Figure 3-10a) and catalyzed hydrogen peroxide oxidation (Figure 3-10b) and for the *tert*-butylhydroperoxide oxidation (Figure 3-10c).

Purification of α1-PI

The human α1-proteinase inhibitor is the major proteinase inhibitor in plasma (normal levels of 130 mg of α1-PI/100 mL plasma) [116] and acts on several serine

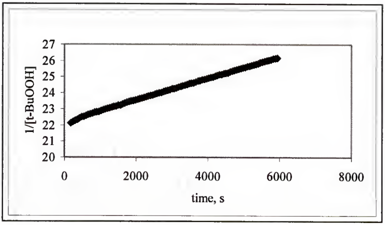

Figure 3-9. Plot of the reciprocal of [*t*-BuOOH] versus time for the oxidation of methionine to methionine sulfoxide by *tert*-butylhydroperoxide. The slope of the line gives the second order rate constant for the background reaction, k_{TB} = 5.75 (± 0.23) x 10^{-4} $M^{-1}s^{-1}$. Reaction conditions are: [RSMe] = [*t*-BuOOH] = 50 mM in 0.10 M HPO_4^- at 25°C.

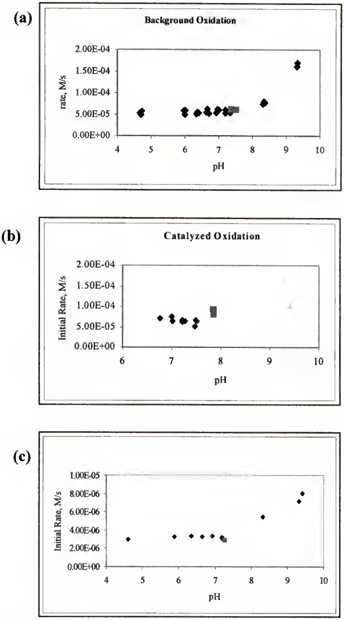

Figure 3-10. Dependence of the oxidation rate on pH. Plots show the independence of the rate of methionine oxidation on pH < 9 for (a) the uncatalyzed hydrogen peroxide oxidation, (b) the catalyzed hydrogen peroxide oxidation, and (c) the *tert*-butylhydroperoxide. Presence of a metal chelator DTPA does not alter the rate of oxidation.

proteases including neutrophil elastases. Human α1-PI is a glycoprotein containing 12% carbohydrate and an estimated MW ~ 52kDa [124]. Isolation of inhibitor is complicated by albumin and orosomucoid (α1-acid glycoprotein). Albumin is a major constituent of the plasma protein (> 50% of total plasma protein) and can interfere in the detection and assay of minor protein components [117]. Albumin (MW ~ 66 kDa) elutes at the same time as α1-PI in gel-exclusion chromatography. The ionic properties of albumin closely mimic that of the α1-PI rendering the two proteins irresolvable in ionic exchange chromatography.

The removal of albumin was based upon the ability of albumin to bind dyes very tightly and was accomplished by passage through a column of a sepharose-dye conjugate which selectively binds albumin [117]. Blue dextran (MW ~ 2 x 10^6) was chosen due to its ability to bind albumin regardless of the ionic strength [117]. From the SDS-PAGE (Figure 3-11), nearly all of the albumin component (initial sharp band seen in sample from Sigma) has been adsorbed in the SBD column along with other high MW proteins or lipoproteins. Incubation time for the elastase-α1-PI complex formation to attain maximum inhibitory activity was also shorter from one hour to five minutes after albumin removal.

Removal of other proteins was accomplished by a series of ion exchange chromatography. Transferrin or the apo-transferrin (MW ~ 76-81 kDa) was separated from α1-PI by running the crude fraction in a DEAE-cellulose column at pH 8.8. Transferrin or apo-transferrin eluted first before α1-PI [124]. Orosomucoid, (stains very weakly using conventional protein stains) was separated in the next run using a DEAE-cellulose

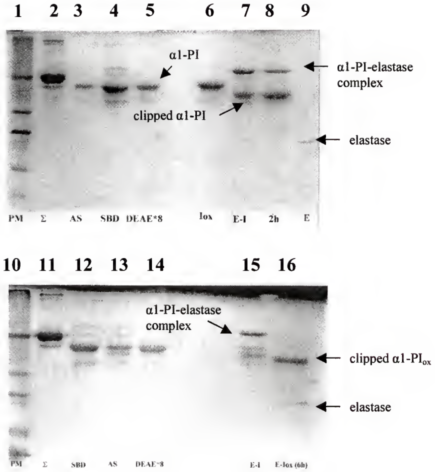

Figure 3-11. SDS-PAGE of α1-proteinase inhibitor in 12% gel and 0.1% SDS. Gels were stained with Coomassie brilliant blue G. Direction of migration is from top to bottom. Lanes 1 and 10 are protein markers, 2 and 11 are crude α1-PI from Sigma Chemicals (St. Louis, MO), 4 and 12 are the α1-PI after SBD column chromatography, 3 and 13 are α1-PI protein fractions after $(NH_4)_2SO_4$ fractionation, 5 and 14 are fractions after the DEAE column chromatography at pH 8.80, 6 is the oxidized α1-PI after 2 h of exposure to 0.10 M HCO_3^-/10 mM H_2O_2, 7 and 15 are the native α1-PI with elastase, 8 is the oxidized (for 2h) α1-PI with elastase, 16 is the oxidized (for 6h) α1-PI with elastase and 9 is the elastase obtained from Sigma Chemicals (St. Louis, MO).

column at pH 6.5. Pure α1-PI eluted in the first four hours before orosomucoid and other plasma proteins [124].

Oxidation of Methionines in α1-PI

As an example of methionine oxidation in proteins, the oxidation of α1-PI was investigated. Oxidation of Met358 in the reactive center loop has been implicated in the loss of the inhibitory activity of α1-PI [125-128]. This loss of the inhibitory activity to elastase was monitored by measuring the residual hydrolytic activity of elastase (Figure 3-2). Results for the oxidation of α1-PI are summarized in Figure 3-12. As the exposure time to the oxidant was lengthened, the inhibitory activity of α1-PI was reduced and the elastase activity was increased in agreement with previous studies [124-128]. With increasing [HCO_3^-] in the oxidation reaction mixture, the loss of inhibitory activity was also increased. This loss of inhibitory activity was attributed to the inability of α1-PI to form a complex with elastase when oxidized [124-126,128] as observed using an SDS-PAGE (Figure 3-12). The native α1-PI (MW ~ 52 kDa) was able to form a complex with elastase (MW ~ 25 kDa) (observed as the band higher than the inhibitor band in lanes 7 and 15 of Figure 3-11) even in the presence of 0.1 % SDS indicating that a tight complex was formed. Some complex dissociation was also observed in the presence of 0.1 % SDS. The dissociated α1-PI from the complex has a lower molecular weight than its native form indicating cleavage of a small peptide during complex formation. Studies have shown that the small peptide cleaved is the carboxy terminal of α1-PI containing Met358 [129]. After oxidation, the complex band disappeared and we observed two bands, the elastase and the clipped α1-PI. Elastase is then free to hydrolyze the substrate.

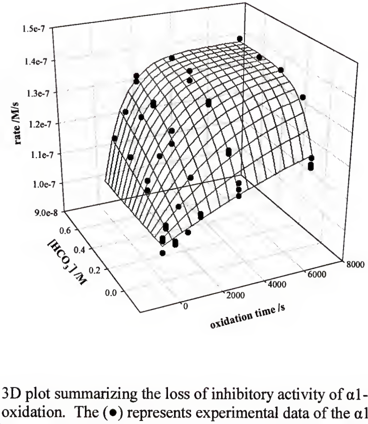

Figure 3-12. 3D plot summarizing the loss of inhibitory activity of α1-PI on elastase in the course of oxidation. The (●) represents experimental data of the α1-PI inhibitory activity and the mesh is the nonlinear fit to eq 3-18. Oxidation reaction conditions are: [α1-PI] ~ 13 μM, [H_2O_2] = 10 mM, [HCO_3^-] = 0 to 0.70 M at 25°C. For the assay conditions: [α1-PI]=[*E*]=0.10 μM, [*S*]= 0.33 mM at 25°C. All reactions are in 0.20 M TRIS-HCl buffer at pH 8.00.

A kinetic model describing the oxidation of the inhibitor was used to compare the kinetic parameters for the α1-PI oxidation to the oxidation of free methionine. The relevant reactions used to model the results are given in eqs 3-8 to 3-11 where E = elastase, S = Suc-$(Ala)_3$-Nan substrate, P = *p*-nitroaniline product, α1-PI = active form of the inhibitor, and α1-PI_{ox} = oxidized form of the inhibitor.

$$E + S \rightarrow P \qquad k_E = (k_{cat}/K_M)\,[S] \qquad (3\text{-}8)$$

$$\alpha 1\text{-PI} + E \rightarrow [E\text{-}\alpha 1\text{-PI}] \qquad \textit{irreversible} \qquad (3\text{-}9)$$

$$\alpha 1\text{-PI} + H_2O_2 \rightarrow \alpha 1\text{-PI}_{ox} + H_2O \qquad k_{01} \qquad (3\text{-}10)$$

$$\alpha 1\text{-PI} + HCO_4^- \rightarrow \alpha 1\text{-PI}_{ox} + HCO_3^- \qquad k_c \qquad (3\text{-}11)$$

Using Michaelis-Menten equation for enzyme kinetics (eq 3-12), the rate of product formation can be simplified to a *pseudo*-first order reaction under the conditions used since $[S] << K_M$ (Michaelis constant, K_M = 5.9 mM [130]). We can then write the rate equation as eq 3-13.

$$-\frac{d[P]}{dt} = \frac{k_{cat}[S][E]_o}{K_M + [S]} \qquad (3\text{-}12)$$

$$-\frac{d[P]}{dt} = k_E[E]_t \qquad (3\text{-}13)$$

The association rate constant for α1-PI to elastase is extremely large (~10^5 $M^{-1}s^{-1}$ [127]) and thus, the association can be considered irreversible [127]. Results and previous studies by Beatty and coworkers [127] have also shown that the oxidized α1-PI does not bind to elastase. The amount of the elastase-inhibitor complex can then be assumed to be equivalent to the amount of unoxidized α1-PI. Then at any time *t*, the amount of free elastase that can hydrolyze the substrate can be expressed as eqs 3-14 and 3-15.

$$[E]_t = [E]_o - [E\text{-}\alpha 1PI] \qquad (3\text{-}14)$$

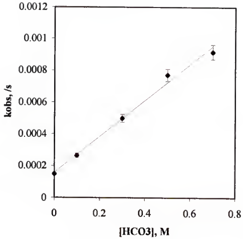

Figure 3-13. Plot of the dependence of k_{obs} on the $[HCO_3^-]$ indicating a first-order dependence (eq 3-18).

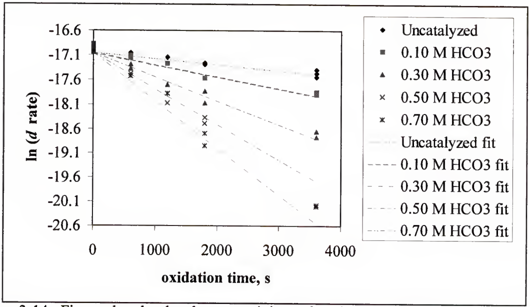

Figure 3-14. First-order plot the elastase activity as function of oxidation time from eq 3-19. As the exposure time to the oxidant increases, the rate of product formation (elastase activity) increases indicating a decreasing inhibitory activity for α1-PI. And as the $[HCO_3^-]$ in the oxidation reaction increases, elastase activity also increases.

$$[E]_t = [E]_o - [\alpha 1\text{-PI}]_t \qquad (3\text{-}15)$$

The amount of the unoxidized inhibitor can be related to the rate of its oxidation (eq 3-16).

$$-\frac{d[\alpha 1 - PI]}{dt} = \left(\frac{k_c K_{eq}[\mathrm{HCO_3^-}][\mathrm{H_2O_2}]}{1 + K_{eq}[\mathrm{H_2O_2}]} + k_{01}[\mathrm{H_2O_2}] \right)[\alpha 1 - \mathrm{PI}] \qquad (3\text{-}16)$$

Integration of eq 3-15 gives the concentration of the α1-PI at any time *t* (eq 3-17)

$$[\alpha 1\text{-PI}]_t = [\alpha 1\text{-PI}]_o \exp(-k_{obs}t) \qquad (3\text{-}17)$$

where k_{obs} is expressed as eq 3-17 (Figure 3-13).

$$k_{obs} = \frac{k_c K_{eq}[\mathrm{HCO_3^-}][\mathrm{H_2O_2}]}{1 + K_{eq}[\mathrm{H_2O_2}]} + k_{01}[\mathrm{H_2O_2}] \qquad (3\text{-}18)$$

We can then rewrite the rate law eq 3-13 as eq 3-19 using the relationships from eqs 3-15 and 3-17.

$$v = -d[P]/dt = k_E \{ [E]_o - ([\alpha 1\text{-PI}]_o \exp(-k_{obs}t)) \} \qquad (3\text{-}19)$$

A logarithmic form of 3-18 gives eq 3-19 which can be used to obtain a linear plot (Figure 3-14).

$$\ln(k_E[E]_o - v) = \ln(k_E[\alpha 1\text{-PI}]_o) - k_{obs}t \qquad (3\text{-}20)$$

From a nonlinear fit of eq 3-19 (Figure 3-12), we obtained the second-order rate constants $k_{01} = 0.014 \pm 0.003\ \mathrm{M^{-1}s^{-1}}$ and $k_c = 0.36 \pm 0.06\ \mathrm{M^{-1}s^{-1}}$. Results were close to the calculated second-order rate constants for the oxidation of free methionine. The acceleration in the rate of oxidation in the presence of bicarbonate was consistent with the formation of peroxymonocarbonate.

Methionine Sulfoxide Analysis

The presence of methionine sulfoxide was demonstrated by the simultaneous analysis for methionine and methionine sulfoxide by amino acid analysis of the purified native (Figure 3-15a) and oxidized protein (Figure 3-15b). Oxidation of other amino acids by hydrogen peroxide or by peroxymonocarbonate was also checked through amino acid analysis. Direct analysis of methionine sulfoxide in standard amino acid analysis has been reported to have considerable error. Acid hydrolysis partially decomposes methionine sulfoxide to methionine while alkaline hydrolysis results in low recoveries of methionine sulfoxide and decomposition of methionine [31,131]. Shechter and coworkers [91] first demonstrated the use of the cyanogen bromide procedure prior to acid hydrolysis for the simultaneous analysis of methionine and methionine sulfoxide. In the cyanogen bromide step, unoxidized methionines were converted to homoserines while methionine sulfoxides were left intact [91,93] (Figure 3-16). Dithiothreitol was added in the acid hydrolysis step to reduce the methionine sulfoxides back to methionines. The amount of methionine in the amino acid analysis corresponded to the amount of methionine sulfoxide residues in the oxidized inhibitor and the amount of homoserine in the amino acid analysis corresponded to the amount of unoxidized methionine residues (Figure 3-15).

Free amino acids are difficult to detect unless derivatized. Derivatization is automatically performed on the amino acid analyzer either prior to the separation (pre-column derivatization) or after HPLC separation (post-column separation). In this study, the pre-column derivatization using phenylisothiocyanate (PITC) was applied. Under basic conditions, the free amino acids were reacted with phenylisothiocyanate (PITC) to produce the phenylisothiocarbamate (PTC) derivatives (eq 3-21).

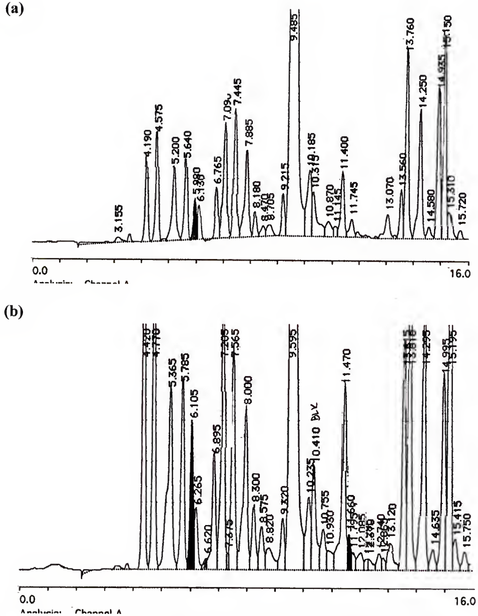

Figure 3-15. Amino acid analysis chromatogram of the (a) native α1-PI and the (b) oxidized α1-PI after 8 h of oxidation. A pre-column derivatization with PITC was performed in the hydrolyzed protein. Shaded peaks correspond to the PTC-derivative of homoserine (RT=6.0-6.1 min) and methionine (RT=11.6-11.7 min). The amount of homoserine corresponds to the amount of unoxidized methionine in the reaction and the amount of methionine corresponds to the methionine that has been oxidized to methionine sulfoxide. Native protein contains only homoserine and no methionine as expected. Oxidized proteins contain both, with the amount of methionine corresponding to the number of methionine residues oxidized. Differences in the heights of the two chromatograms are due to the difference in the attenuation.

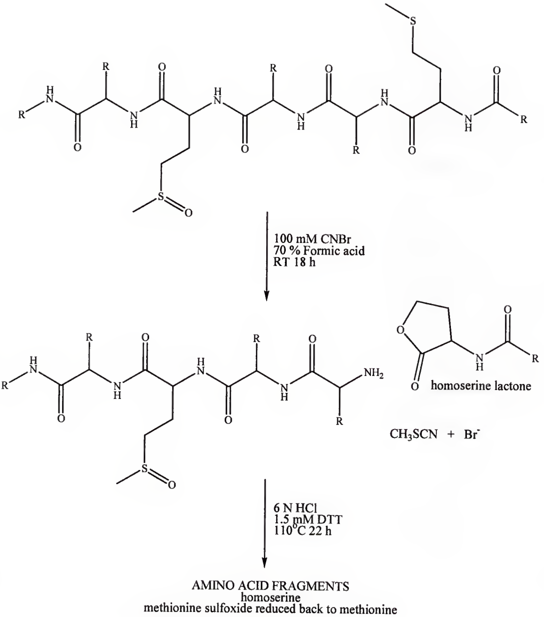

Figure 3-16. Schematic diagram for the simultaneous analysis of methionine and methionine sulfoxide. Treatment of the protein with cyanogen bromide in 70% formic acid converts methionines to homoserines leaving the methionine sulfoxides intact. The methionine sulfoxide is reduced back to methionine by DTT in the acid hydrolysis step. The amount of methionine corresponds to the amount of oxidized methionines in the protein and the amount of homoserine corresponds to the amount of unoxidized methionines in the protein.

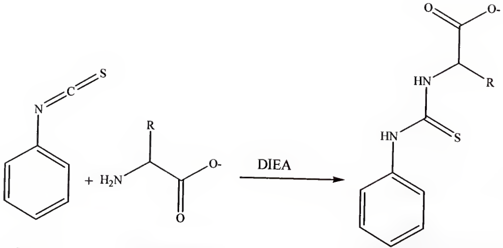

PITC amino acid PTC-amino acid derivative

(3-21)

A reverse phase column (C18) was then used to separate the derivatives and the PTC chromophores were detected at 254 nm (Figure 3-15). Some commons side reactions are written in eqs 3-22 to 3-24.

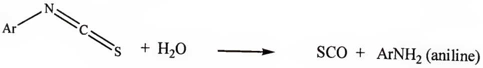

(3-22)

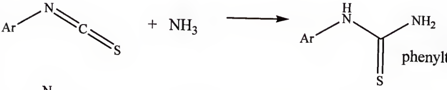

(3-23)

phenylthiourea (PTU)

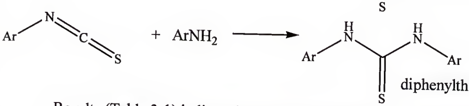

(3-24)

diphenylthiourea (DPTU)

Results (Table 3-1) indicated the oxidation of about one to two out of nine methionines in the uncatalyzed oxidation reaction of α1-PI. This value was consistent with the previous studies on the oxidation of two solvent-exposed methionines, Met 351 and Met 358 of the reactive center loop [122,125]. In the catalyzed oxidation of α1-PI,

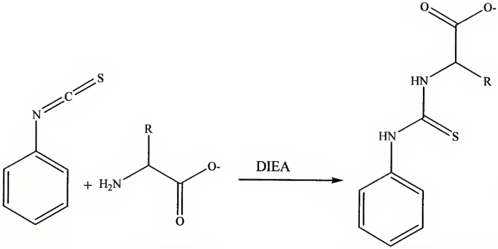

(3-21)

PITC amino acid PTC-amino acid derivative

A reverse phase column (C18) was then used to separate the derivatives and the PTC chromophores were detected at 254 nm (Figure 3-15). Some commons side reactions are written in eqs 3-22 to 3-24.

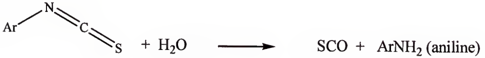

(3-22)

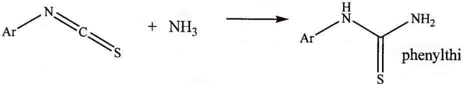

(3-23)

phenylthiourea (PTU)

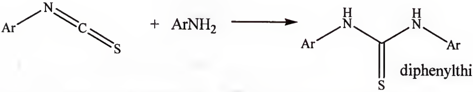

(3-24)

diphenylthiourea (DPTU)

Results (Table 3-1) indicated the oxidation of about one to two out of nine methionines in the uncatalyzed oxidation reaction of α1-PI. This value was consistent with the previous studies on the oxidation of two solvent-exposed methionines, Met 351 and Met 358 of the reactive center loop [122,125]. In the catalyzed oxidation of α1-PI,

Table 3-1. Comparative amino acid composition of native and oxidized α1-PI.

				oxidized α1-PI[c]	
RESIDUE	**theoretical[a]**	**Travis[b]**	**Native[c]**	**Uncatalyzed[c]**	**Catalyzed[c]**
Asx (D,N)	43	49 ± 1.6	35.0 ± 3.8	49.9 ± 4.3	43.6 ± 5.4
Glx (Q,)	50	54 ± 2.1	36.9 ± 3.4	49.9 ± 3.0	40.4 ± 3.3
Serine	21	23 ± 0.8	25.2 ± 0.9	29.6 ± 1.1	24.5 ± 1.8
Glycine	22	24 ± 1.1	24.9 ± 2.7	19.9 ± 1.4	21.9 ± 2.3
Homoserine	**9**	**8 ± 0.2**	**11.5 ± 3.7**	**6.5 ± 3.6**	**4.7 ± 3.0**
Histidine	13	13 ± 0.4	11.7 ± 2.5	7.5 ± 0.8	7.8 ± 4.1
Arginine	7	7 ± 0.2	7.6 ± 3.3	7.2 ± 0.9	7.6 ± 4.3
Threonine	30	25 ± 0.8	28.4 ± 2.9	32.2 ± 2.2	32.3 ± 1.6
Alanine	24	24 ± 0.6	29.8 ± 2.5	28.2 ± 4.1	25.9 ± 2.2
Proline	17	22 ± 0.1	18.4 ± 1.8	19.8 ± 4.9	16.3 ± 1.5
Tyrosine	6	6 ± 0.5	18.6 ± 4.9	3.1 ± 1.6	6.3 ± 1.7
Valine	24	27 ± 1.5	17.0 ± 1.9	20.9 ± 1.6	22.3 ± 3.9
Methionine	**0**	**0**	**0**	**0.9 ± 0.5**	**4.2 ± 0.7**
Cysteine	1	-	0.7 ± 0.6	0.6 ± 0.6	0.8 ± 0.6
Isoleucine	19	18 ± 1.4	11.2 ± 1.2	16.0 ± 0.9	18.8 ± 2.7
Leucine	45	50 ± 1.7	44.4 ± 2.8	46.8 ± 2.7	41.4 ± 1.7
Phenylalanine	27	28 ± 0.4	29.3 ± 2.4	28.6 ± 1.8	27.1 ± 3.0
Lysine	34	39 ± 1.1	33.2 ± 1.7	27.3 ± 2.9	32.2 ± 3.4

[a] Composition from the primary sequence of α1-PI and the crystallographic data work by Whisstock and coworkers [132].

[b] Composition of the native protein as reported by David Johnson and James Travis [125].

[c] Average of the analyses after cyanogen bromide and hydrochloric acid hydrolyses in the presence of 1.5 mM dithioerythritol. Errors are reported as standard deviations.

about three to four methionines were oxidized indicating that some unfolding may have occurred to expose the other two methionines. In both oxidation reactions, the amount of histidine was slightly lower indicating some oxidation may have occurred. The other two targets for oxidation in near neutral pH, tryptophan and cysteine, were inconclusive. Tryptophan is completely destroyed in the acid hydrolysis process while cysteine is oxidized to cysteic acid in the acid hydrolysis step. Other more specific analyses are needed to determine the oxidation of these two amino acids.

Peptide Mapping of the Oxidized α1-PI

In order to demonstrate the oxidation of the Met358 in the reactive center loop, a MS analysis of the peptide digest of the protein was performed (Figure 3-17). Endoproteinase Lys-C (Endo Lys-C) was used to cleave the protein at the C-side of the lysine [133]. The primary sequence of α1-PI containing 394 residues with 34 lysine residues is shown in Figure 3-18. We would expect 34 fragments (Table 3-2) from a completely perfect digestion by Endo Lys-C. However, we can expect more than 150 fragments from incomplete digestion. The possible combinations of the fragments at different charge states including possible cationic adducts such as $Na^+$and NH_4^+ were generated using the program FragESI developed by D. E. Richardson to aid in the MS peak identification (see Appendix A). Approximately 70% of the total ion charge-normalized intensities in the native and oxidized proteins have been assigned by using the FragESI program.

Analysis of the digest indicated that the methionines (Met 351 and Met 358) in the reactive center loop (ions containing fragment 30) were either singly or doubly oxidized (Figures 3-19 and 3-20) consistent with the loss of the inhibitory activity of α1-PI to elastase. This result was also expected as both methionines are solvent exposed

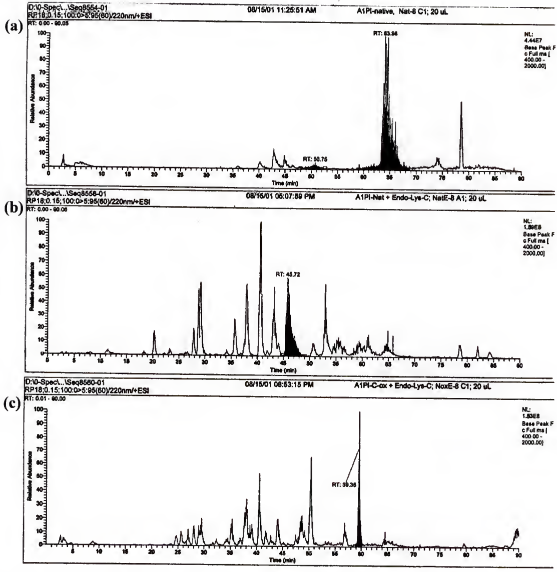

Figure 3-17. Full mass chromatograms of the native and oxidized α1-PI. (a) The mass chromatogram of the native α1-PI without Endo Lys-C (no digestion); (b) the mass chromatogram of an Endo Lys-C digest of the native α1-PI; and (c) the mass chromatogram of an Endo Lys-C digest of the oxidized α1-PI.

EDPQGDAAQ**K**$_{10}$ TDTSHHDQDH$_{20}$ PTFN**K**ITPNL$_{30}$ AEFAFSLYRQ$_{40}$
LAHQSNSTNI$_{50}$ FFSPVSIATA$_{60}$ FAMLSLGT**K**A$_{70}$ DTHDEILEGL$_{80}$ NFNLTEIPEA$_{90}$
QIHEGFQELL$_{100}$ RTLNQPDSQL$_{110}$ QLTTGNGLFL$_{120}$ SEGL**K**LVD**K**F$_{130}$
LEDV**KK**LYHS$_{140}$ EAFTVNFGDT$_{150}$ EEA**KK**QINDY$_{160}$ VE**K**GTQG**K**IV$_{170}$
DLV**K**ELDRDT$_{180}$ VFALVNYIFF$_{190}$ **K**G**K**WERPFEV$_{200}$ **K**DTEEEDFHV$_{210}$
DQVTTV**K**VPM$_{220}$ M**K**RLGMFNIQ$_{230}$ HC**KK**LSSWVL$_{240}$ LM**K**YLGNATA$_{250}$
IFFLPDEG**K**L$_{260}$ QHLENELTHD$_{270}$ IIT**K**FLENED$_{280}$ RRSASLHLP**K**$_{290}$
LSITGTYDL**K**$_{300}$ SVLGQLGIT**K**$_{310}$ VFSNGADLSG$_{320}$ VTEEAPL**K**LS$_{330}$
KAVH**K**AVLTI$_{340}$ DE**K**GTEAAGA$_{350}$ **M**FLEAIP**M**SI$_{360}$ PPEV**K**FN**K**PF$_{370}$
VFLMIEQNT**K**$_{380}$ SPLFMG**K**VVN$_{390}$ PTQ**K**

Figure 3-18. Primary sequence of α1-PI. Lysine (K) residues are in bold and underlined. Methionines (M) are underlined and the methionines in the reactive center loop (Met 351 and Met358) are in bold

Table 3-2. Predicted fragments for the native α1-PI digest by Endo Lys-C.

Frag. #[a]	**Start[b]**	**End[b]**	**m/z (+1)**	**max Z[c]**	**Met #**
1	1	10	1058.05	2	0
2	11	25	1779.8	5	0
3	26	69	4806.42	4	1
4	70	125	6249.78	5	0
5	126	129	473.56	2	0
6	130	135	749.85	2	0
7	136	136	146.19	2	0
8	137	154	2058.16	3	0
9	155	155	146.19	2	0
10	156	163	1008.09	2	0
11	164	168	489.52	2	0
12	169	174	685.85	2	0
13	175	191	2090.38	3	
14	192	193	203.23	2	0
15	194	201	1090.24	3	0
16	202	217	1891.96	3	0
17	218	222	604.83	2	2
18	223	233	1346.62	4	1
19	234	234	146.19	2	0
20	235	243	1076.35	2	1
21	244	259	1755.94	2	0
22	260	274	1804.02	4	0
23	275	290	1912.10	5	0
24	291	300	1110.24	2	0
25	301	310	1015.19	2	0
26	311	328	1833.97	2	0
27	329	331	346.42	2	0
28	332	335	453.54	3	0
29	336	343	888.01	2	0
30[d]	**344**	**365**	**2259.61**	**2**	**2**
31	366	368	407.47	2	0
32	369	380	1466.75	2	1
33	381	387	778.95	2	1
34	388	394	784.92	2	0

[a] Fragment number based on a completely digested protein.

[b] Numbers indicate the residue number in the primary sequence.

[c] Maximum charge based on the maximum charge from the number of the basic residues in that fragment.

[d] Fragment number containing methionines (Met351 and Met358) in the reactive center loop of the protein.

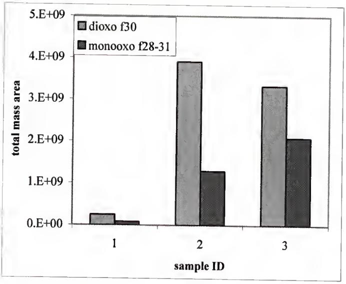

Figure 3-19. Relative abundance of the monooxidized fragment 28-31 and dioxidized fragment 30 of the reactive center loop. The total mass area is calculated from the sum of the mass chromatogram area of the specific m/z ion (f30 m/z = 1146 at +2 charge and f28-31 m/z = 1321 at +2 charge) and all the charge states (i.e. +1, +3). Sample ID **1** corresponds to the native α1-PI control protein with no oxidant, **2** for the oxidation of α1-PI in the uncatalyzed reaction, and **3** for the oxidation of α1-PI in the catalyzed reaction.

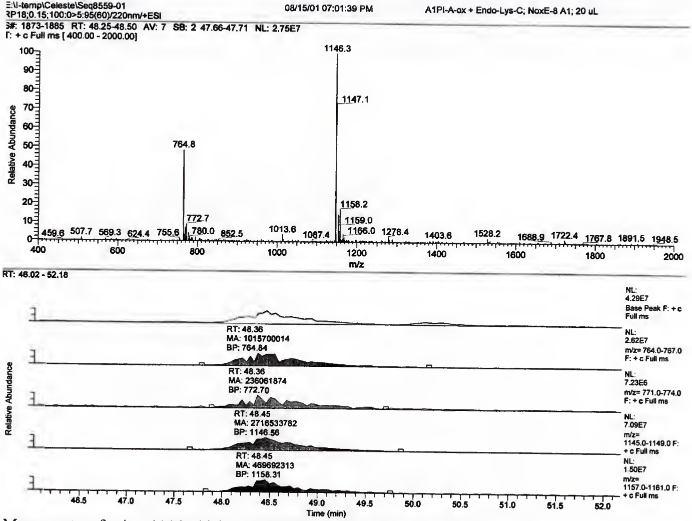

Figure 3-20. Mass spectra of m/z = 1146 which corresponds to the +2 charge state of the dioxidized species of fragment 30. The lower figure are the mass chromatograms of the different charge states of the dioxo species from which we can obtain the area for quantification.

(Figure 3-21). The native protein also showed some mild oxidation after eight hours exposure to air indicating that the reactive center is easily oxidized consistent with the decrease of inhibitory activity of the protein upon long exposure to air at room temperature.

Other possible substrates for oxidation are the partially accessible Met226 and Cys232 (Figure 3-22) both of which are contain in fragment 18. The MS analysis of the digest indicated that fragment 18 was also oxidized with one to two oxygens being added (Figures 3-22 and 3-23). Oxidation of Cys232 into the sulfenic acid form gives the same m/z ion as the oxidation of Met226 into methionine sulfoxide. Oxidation of both species produces a dioxidized fragment. Results indicated that the catalyzed oxidation reaction produced more of the oxidized both the mono- and dioxidized fragment 18 than the uncatalyzed reaction. From the previous chapter, we expected the cysteine oxidation to be faster than methionine oxidation. However, if that was to be the case we would expect the methionine count in the amino acid analysis to be of the same value for both the uncatalyzed and the catalyzed reaction (Table 3-1). The amino acid analysis indicated that another methionine was oxidized besides the two from the reactive center loop supporting the oxidation of Met226 in fragment 18. The cysteine residue then might be unionized and in a more protected environment than Met226.

Focusing on the other fragments containing methionines namely fragments 3 (Met61), 17 (Met220 and Met221), 20 (Met242), 32 (Met374), and 33 (Met385), results indicated no oxidation of these methionines. These methionines are well buried and unexposed (Figure 3-21) thus less likely to be oxidized unless the protein is first denatured.

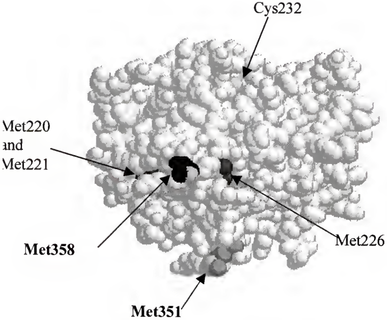

Figure 3-21. A space-filled model of α1-PI showing the exposed methionines and cysteine. This model is obtained from the RCSB Protein Data Bank code 1QLP. Methionines 351 and 358 are the methionines in the reactive center loop; Methionine 226 is only partially exposed along with Cys232. Both Met220 and Met221 are buried deep in the protein.

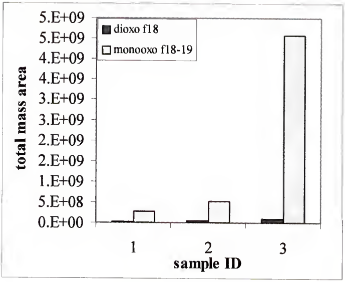

Figure 3-22. Relative abundance of the monooxidized fragment 18-19 and dioxidized fragment 18 of the reactive center loop. The total mass area is calculated from the sum of the mass chromatogram area of the specific m/z ion (f18 m/z = 692 at +2 charge and f18-19 m/z = 748 at +2 charge) and all the charge states (i.e. +1, +3). Sample ID **1** corresponds to the native α1-PI control protein with no oxidant, **2** for the oxidation of α1-PI in the uncatalyzed reaction, and **3** for the oxidation of α1-PI in the catalyzed reaction.

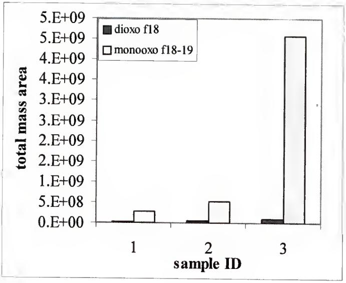

Figure 3-22. Relative abundance of the monooxidized fragment 18-19 and dioxidized fragment 18 of the reactive center loop. The total mass area is calculated from the sum of the mass chromatogram area of the specific m/z ion (f18 m/z = 692 at +2 charge and f18-19 m/z = 748 at +2 charge) and all the charge states (i.e. +1, +3). Sample ID **1** corresponds to the native α1-PI control protein with no oxidant, **2** for the oxidation of α1-PI in the uncatalyzed reaction, and **3** for the oxidation of α1-PI in the catalyzed reaction.

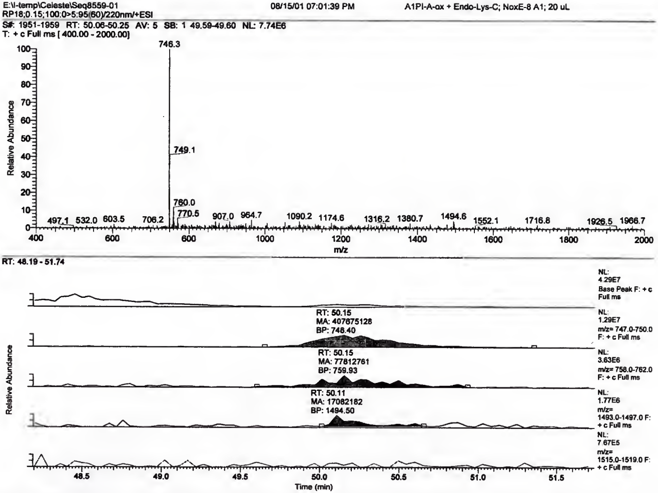

Figure 3-23. Mass spectra of m/z = 748 which corresponds to the +2 charge state of the monooxidized species of fragment 18-19. The lower figure are the mass chromatograms of the different charge states of the monooxo species from which we can obtain the area for quantification.

RNase A oxidation

Oxidation of RNase A was followed by monitoring the signal intensities of the native protein using the ESI/FTICR-MS. The most abundant and stable signal is the +8 charged state of RNase, $[M + 8H]^{8+}$ (m/z ~1711). At this charge state, addition of one oxygen by O-transfer to the protein will correspond to a $\delta m/z = 2$ (Figure 3-24). By monitoring the decrease in the signal intensity of m/z = 1711 or the increase in the signal intensity of m/z = 1713, we obtained the rate of oxidation on-line in 0.1 % acetic acid and 10 % methanol.

Using *pseudo*-first-order conditions, where [RNase] = 55 μM and $[H_2O_2]$=10 mM, the calculated second-order rate constant for hydrogen peroxide oxidation of RNase in 0.1 % acetic acid and 10% methanol was $k_{01} = 2.5 \times 10^{-3}\ M^{-1}s^{-1}$. This value was comparable to free methionine oxidation by hydrogen peroxide.

Using the same technique used in the oxidation of α1-PI, assay of the hydrolytic activity of RNase A during oxidation reaction was performed. Results showed that there was no change in the catalytic activity of RNase A upon oxidation (Figure 3-25). This was not surprising since no methionine is involved in the catalytic site or near the active site. A view of the protein shows a surfaced-exposed methionine far from the active site (Figure 3-26).

Conclusions

Kinetic parameters for the methionine oxidation by hydrogen peroxide in the absence and presence of bicarbonate are obtained. In the absence of bicarbonate, the second-order rate constant for the oxidation of methionine ($k_{01} = 0.0075\ M^{-1}s^{-1}$) by hydrogen peroxide is about ~10^3 times lower than that of thiols ($k_{01} = 17\ M^{-1}s^{-1}$). The presence of bicarbonate in the oxidation reaction accelerates the rate of oxidation by a

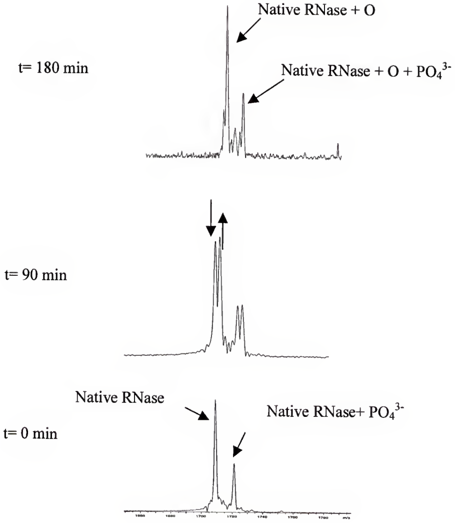

Figure 3-24. Profile for RNase oxidation by ESI/FTICR-MS. The peaks correspond to the 8+ charge state of the protein in the absence (left peak) and the presence (right peak) of bound phosphate. A $\delta m/z = 2$ change is observed for the oxidation reaction corresponding to the transfer of one oxygen (Z=16).

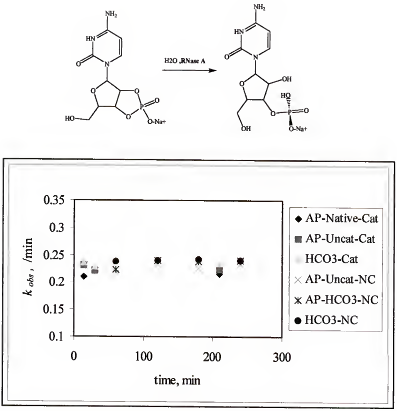

Figure 3-25. Assay of the hydrolytic activity of RNase A towards cytidine 2',3'-cyclic monophosphate (2',3'-cCMP) to yield cytidine 3'-monphosphate [118] (reaction above).

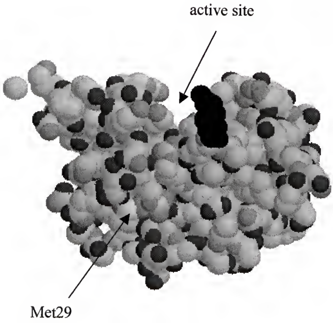

Figure 3-26. A space-filled model of ribonuclease A showing solvent-exposed Met29.

factor of 2, consistent with the acceleration observed from the thiol oxidations in the previous chapter. This result is also consistent with the equilibration reaction for the formation of peroxymonocarbonate. As with thiols, methionine, being a strong nucleophile, catalyzes the equilibration reaction for the formation of peroxymonocarbonate.

Oxidation of solvent-exposed methionine residues in proteins may or may not affect their biological activity and would depend upon the site of oxidation. Oxidation of α1-PI leads to the loss of its inhibitory activity towards proteases such as elastase. However, oxidation of RNase A does not destroy its hydrolytic activity towards cCMP.

Loss of the inhibitory activity of α1-PI upon oxidation is consistent with the oxidation of the crucial Met358 in the reactive center loop. Kinetic parameters obtained are comparable to the oxidation of free methionine and are consistent with the formation of peroxymonocarbonate.

CHAPTER 4
OXIDATION OF GUANOSINE MONOPHOSPHATE

Introduction

Nucleic acids are stable molecules but can undergo decomposition over time. and oxidative stress accelerates this decomposition process [134,135]. The reactive oxygen species can lead to nucleic acid damage by direct chemical attack on the nucleic acid [135,136] and by indirect mechanisms such as activation of Ca^{2+}-dependent endonucleases as a consequence of the increased level of intracellular Ca^{2+} or by interference with enzymes involved in the replication and repair of nucleic acids [135,137]. These oxidative damages to nucleic acids have been associated with mutagenesis, carcinogenesis, and aging [138-144].

The electron-rich nucleobases are prime targets for reaction with electrophiles such as alkylating agents, halogens and oxidizing agents (Figure 4-1) [136]. Oxidative modification of the nucleobases has been reported to be the major pathway for strand scission in both DNA and RNA via alkaline hydrolysis or enzymatic processes (Figure 4-2) [136,145]. Of the nucleobases, purines are more sensitive to deglycosylation via enzymatic process, acid hydrolysis or nucleophilic displacement since the purines (A,G) are more basic than pyrimidines (C,T,U) and thus make a better leaving group once protonated [146,147]. The depurination step is 500 times more rapid for the deoxyribonucleoside moiety than the ribonucleoside moiety [148].

Oxidative damage to the nucleic acid has been reported to be mediated by one-electron transfer between the oxidant and the base to produce the nucleobase radical

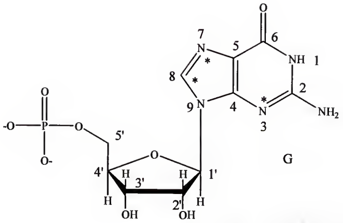

guanosine-5'-monophosphate

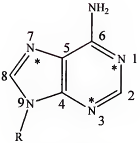

adenine (A)

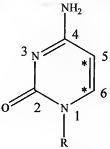

cytosine (C)

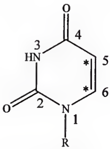

uracil (U)

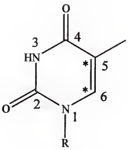

thymine (T)

Figure 4-1. Numbering scheme in nucleobases and nucleosides. The asterisks are the sites of nucleobase modification.

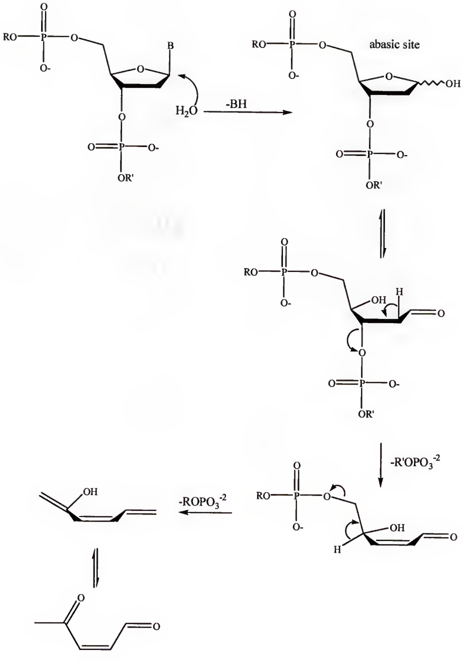

Figure 4-2. Schematic diagram of strand scission via deglycosylation of the nucleobase.

[136,149]. The one-electron reduction potentials of the different nucleobases have been recently by Steenken and Jovanovic [150] and are listed below in Table 4-1.

Table 4-1. One-electron reduction potentials for nucleobases.[a]

Species[b]	*E*° (vs. NHE), V	PH
rG	1.29	7
RA	1.42	7
DC	1.6	7
DT	1.7	7
r(8-oxoG)	0.58	8
r(8-oxoA)	0.92	8
r(5-OH-C)	0.62	8
r(5-OH-U)	0.64	8
Tryptophan	1.01	8
RS·[d]	0.75	8

[a] Data as reported by Steenken and Jovanovic [150].

[b] In the list, r denotes ribonucleoside and d denotes deoxyribonucleoside moiety.

Having the lowest reduction potential, guanine is the most oxidizable of the nucleobases and is therefore a main target of oxidants [136,145,150]. It has also been reported that the one-electron reduction potential of guanine in a DNA or RNA strand is lower than the value reported for the mononucleoside and is in the range of 1.10 to 1.24 V vs. NHE [136]. The reactivity of the guanine in a strand towards oxidants is sequence-dependent favoring guanines located at the 5' to another purine especially to another guanine [151-153]. Thus, the order of reactivity for the following sequence is GG > GA > GC ~ GT. Long-range electron transfer has also been observed by attaching an oxidant to one end of the oligonucleotide duplex and observing guanine oxidation at GGG and GG sites that are up to 11 nucleotides away [154].

Oxidation of guanine by hydroxyl radical that can be produced from γ radiolysis of water or from Fenton chemistry (Figure 1.2) produces three species of guanine radicals

1, **2**, and **3** (Figure 4-3) [136,155]. The guanine radicals **1** and **2** are believed to revert back to guanine. Deprotonation, hydration followed by another one-electron oxidation of the guanine radical **3** produces the 7,8-dihydro-8-oxoguanine (8-oxoG) derivative with a minor tautomer 7,8-dihydro-8-hydroxyguanine (8-hydroxyG) (Figure 4-3) [136].

Further oxidation of the 8-oxoG product is expected from the substantially lower reduction potential (Table 4-1). Some of the products of the oxidation of 8-oxoG are summarized in Figures 4-4 and 4.5. The initial product may be the 8-oxoG species which may or may not be detected due to its conversion into various oxidation products such as imidazolone and oxazolone.

In this chapter, oxidation of the mononucleotide guanosine-5'-monophosphate (GMP) by hydrogen peroxide in the presence and absence of bicarbonate is investigated. The oxidation reaction is studied using ^{1}H NMR, HPLC, and HPLC/ESI/QIT/MS.

Materials and Methods

Materials and Instrumentation

The sodium form of guanosine-5'-monophosphate (GMP) and thymidine were purchased from Acros (Atlanta, GA) and used as received. Adenosine 5'-triphosphate (ATP), and cytidine cyclic 2',3'-monophosphate (cCMP) were obtained from Sigma Chemicals (St. Louis, MO). Hydrogen peroxide (70%) was obtained from Solvay Interox (Houston, TX) and standardized iodometrically. Potassium persulfate (Oxone) was obtained from Aldrich (St. Louis, MO) and standardized iodometrically. Analytical grade ammonium hydrogen phosphate, ammonium dihydrogen phosphate and ammonium bicarbonate were obtained from Sigma Chemicals (St. Louis, MO) and used as received.

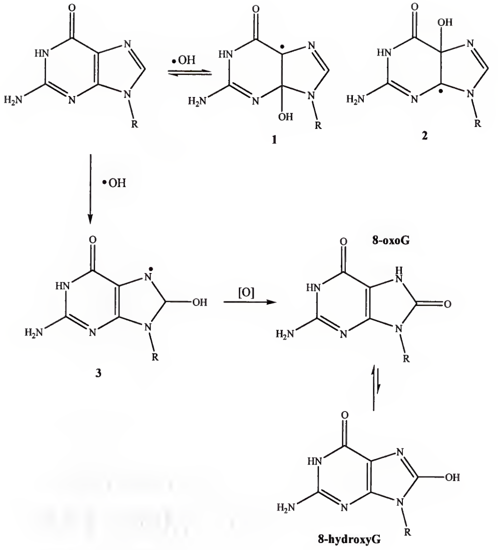

Figure 4-3. Reaction of hydroxyl radical to guanine [136].

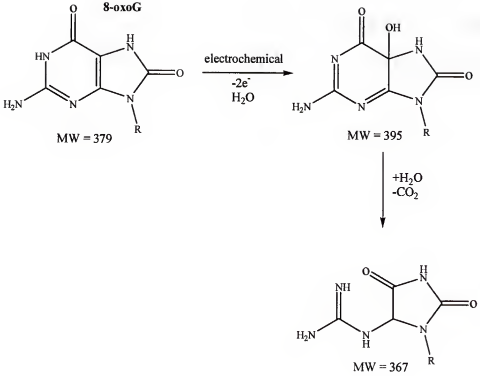

Figure 4-4. Electrochemical oxidation of 8-oxoG [136].

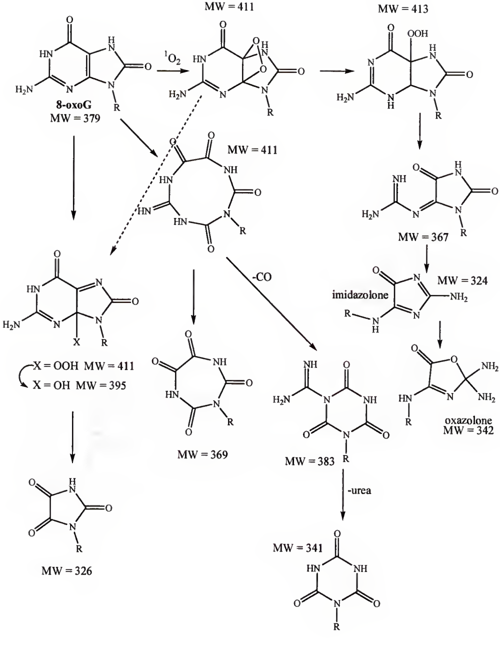

Figure 4-5. Oxidation pathway for 8-oxoG [136].

Diethylenetriaminepentaacetic acid (DTPA) was obtained from Sigma (St. Louis, MO). Water was purified using Barnstead E-Pure 3-Module Deionization System (water resistance $\geq$ 17 megohm-cm).

Proton NMR spectra were obtained on a Gemini 300 and QE 300 spectrometers. Chemical shifts are reported in parts per million. The residual solvent peak was used as an internal standard. Deuterated water (99.9%) used for the NMR experiments were obtained from Cambridge Isotope Laboratory Inc. (Andover, MA).

Spectral measurements were obtained on a Hewlett-Packard 8453 spectrophotometer using a 0.5 and 1.0 cm quartz cells from Starna Cells, Inc.

Oxidation of guanosine-5'-monphosphate (GMP)

The substrate GMP was dissolved in a solution of 0.50 M $(NH_4)_2HPO_4$ (pH ~ 8.0). Hydrogen peroxide (final concentration = 1.0 M) was added to the GMP solution and allowed to react at room temperature for 22 h before obtaining a ^{1}H NMR spectrum. Similar experiments in 1.0 M NH_4HCO_3 in the absence and presence of 1.0 mM diethylenetriaminepentaacetic acid (DTPA) were performed.

In a separate experiment, using the same reaction conditions as above, aliquots of the reaction mixture was taken at different time intervals and diluted by 10^6 before injecting to the HPLC. The GMP and the oxidation products were separated using a strong anion exchange column by Rainin (Hydropore AX 83-603-ETI 4.6 x 1.5 μm, 12 μm 300 Å) and detected at 254 and 280 nm using a UV-1 (Rainin) uv-vis spectrophotometer detector. Mobile phase was introduced using a Rainin HPXL binary pump system. The mobile phase A was 5.0 mM $NH_4H_2PO_4$ at pH 3.9 in a linear gradient elution with mobile phase B 750 mM $NH_4H_2PO_4$ pH 3.9 at 1.00 mL/min. All samples were eluted in 20 minutes.

An aliquot after 2 hours of reaction was taken and frozen to quench the reaction. The sample was then used in the MS experiments for the analysis of the products. The sample was run in an HPLC/ESI/QIT/MS with both spectrophotometric (Waters 486 Tuneable Absorbance Detector at λ= 254 nm) and mass spectrometric detection. The MS data were acquired using a ThermoFinnigan MAT LCQ (San Jose, CA) in electrospray ionization (ESI) mode. Mobile phase was introduced using a Beckman Instruments (Fullerton, CA) System Gold Model 126 pump. The separation was conducted under isocratic conditions of 0.5% acetic acid at 0.10 mL/min. Methanol was added post-column/post-UV at 0.10 mL/min to give a 50:50 MeOH:H_2O into the ESI source to enhance the ESI performance.

Results and Discussions

Proton NMR indicated that oxidation reaction only occurred in the presence of bicarbonate and absence of DTPA after 22 hours at high concentration of hydrogen peroxide (1.0 M) (Figure 4-6). The inability of hydrogen peroxide alone to react with GMP under the conditions used was in agreement with literature as it requires activation by either a metal ion or *uv* to form the hydroxyl radical [136,156]. A metal ion may also be implicated in the observed reaction for the bicarbonate-containing hydrogen peroxide oxidation since the presence of the metal chelator DTPA quenched the reaction.

Due to the poor quality of the spectra being obtained after the metal/bicarbonate-catalyzed oxidation, products have not been identified. An attempt to follow the bicarbonate-catalyzed oxidation reaction in the absence of DTPA by HPLC was made. Separation of the GMP from the products was observed (Figure 4-7) by using an anion exchange column. After only one hour of reaction, a peak was observed after the GMP peak. At least three additional peaks and some peaks which have low absorbance at the

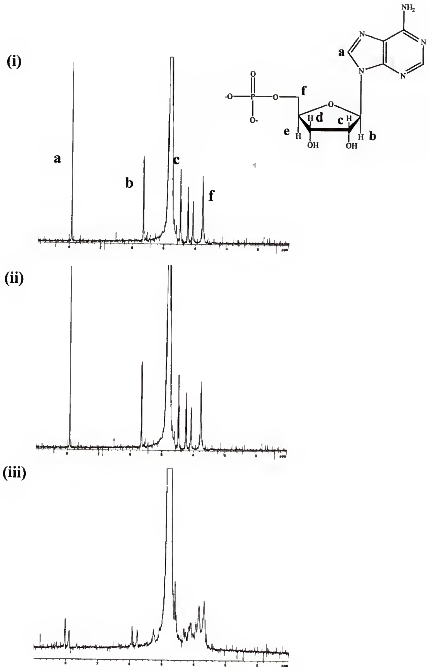

Figure 4.6. Proton NMR spectra of GMP and GMP reaction mixtures. (i) 0.10 M GMP in 0.50 M $(NH_4)_2HPO_4$ after 22.5 h; (ii) 0.10 M GMP in 0.50 M $(NH_4)_2HPO_4$ with 1.0 M H_2O_2 after 22.5 h of reaction; and (iii) 0.10 M GMP in 1.0 M NH_4HCO_3 with 1.0 M H_2O_2 after 22.5 h of reaction. In the absence of bicarbonate, no reaction is observed and the spectrum is unchanged. In the presence of bicarbonate, additional peaks are observed indicative of new species from products. In the presence of 1.0 mM DTPA, no reaction was observed even in the presence of bicarbonate in the reaction mixture.

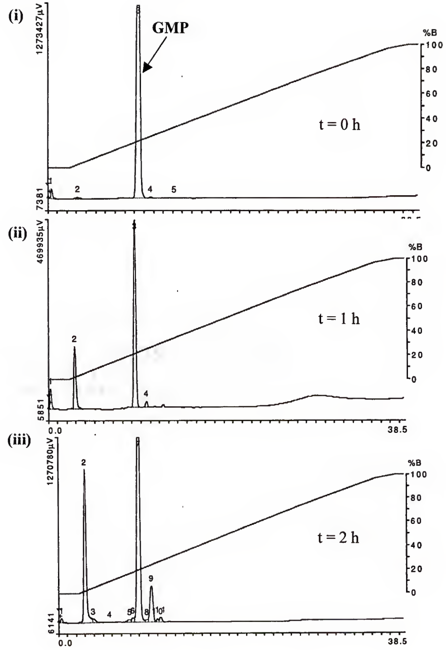

Figure 4-7. HPLC chromatograms of the GMP and the bicarbonate-containing oxidation reaction mixture using an anion exchange column. No DTPA was added to the reaction mixture. Reactant and products were detected spectrophotometrically at λ = 254 nm.

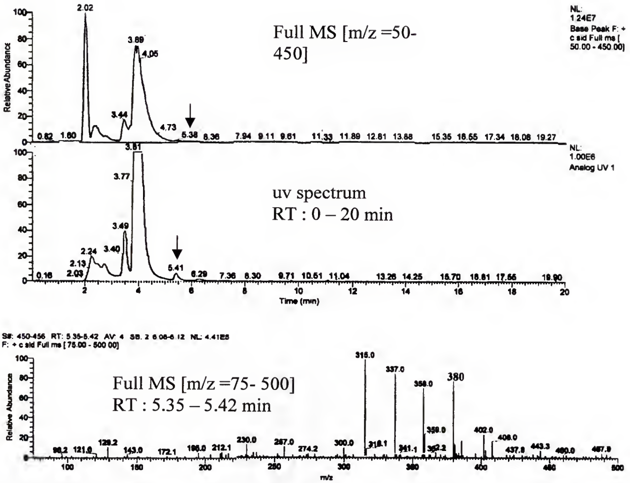

Figure 4-8. HPLC/ESI/QIT/MS of the oxidation reaction mixture. The top is the mass chromatogram of the sample (the mass spectrometer as detector), and the middle is the HPLC chromatogram with uv as the detector and the bottome represents the mass spectra at a particular point in the run i.e at RT = 5.35 – 5.42 min as indicated by the arrow in the top two spectra.

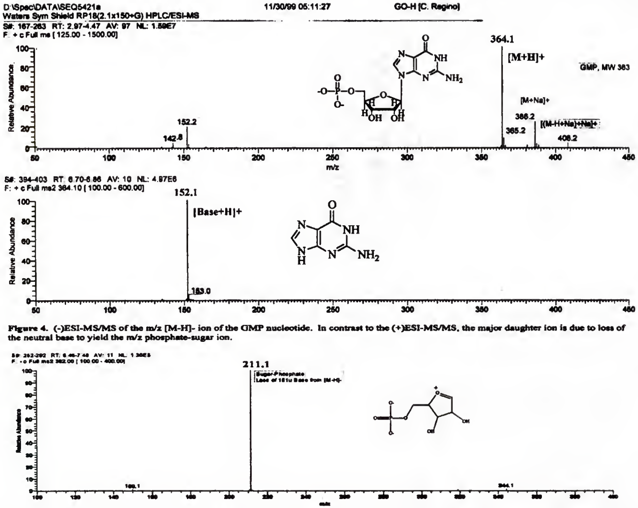

Figure 4. (-)ESI-MS/MS of the m/z [M-H]- ion of the GMP nucleotide. In contrast to the (+)ESI-MS/MS, the major daughter ion is due to loss of the neutral base to yield the m/z phosphate-sugar ion.

Figure 4.9. Mass spectra of GMP (m/z = 364) and MS/MS of GMP showing the intact nucleobase and sugar moieties.

Figure a (+)ESI-MS/MS of the m/z 380 ion-peak observed in Figure 1. Based upon the proposed structure of the MW 379 product and the MS/MS behavior of nucleotides, this is probably the proposed MW 379 product (or isomer).

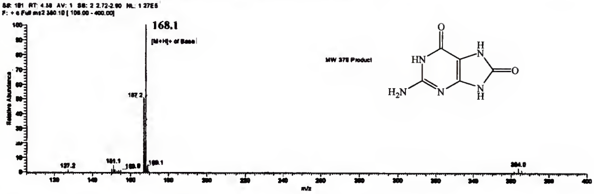

Figure b (-)ESI-MS/MS of the detected m/z 378 ion-peak. This confirms that the MW 379 component has a sugar-phosphate moiety and behaves as a nucleotide.

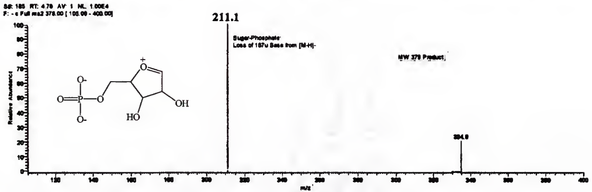

Figure 4.10. MS/MS of the m/z = 380 showing the modified guanine base, 8-oxoG species and the intact sugar moiety.

set wavelength (λ=254 nm), were observed after 18 hours of reaction. As with the ^{1}H NMR results, no new peaks were observed in the absence of bicarbonate in the hydrogen peroxide oxidation reaction.

Analysis of the oxidation reaction mixture by HPLC/ESI/QIT-MS has been attempted. Some of the ions that have been detected in the hydrogen peroxide reaction mixture in the presence of bicarbonate but absence of DTPA are listed in Table 4-2.

Table 4.2. Some m/z ions obtained from the HPLC/ESI/QIT/MS of the reaction mixture.

Species	**MW**	**ΔMW**[a]	**MS/MS**	**Other adduct**
GMP	363	-	(+1) 151, (-1) 211	386 (Na^+)
8-oxoG	379	+16	(+1) 167, (-1) 211	402 (Na^+)
	342	-22	(+1) 129, (+1) 213	359 (NH_4^+), 364 (Na^+)
	314	-49	(+1) 230, 212	337 (Na^+)
	330	-33		
	324	-39		
	358	-6	(+1) 300, 230	
	367	+4		
	383	+20		
	234	-129		
	385	+22	(+1) 257, 230	

[a]The numbers represent the difference between the MW of starting material GMP and the product.

Of the ions listed, only the starting GMP (m/z = 364) and the 8-oxoG (m/z = 380) can be confirmed by MS/MS (Figures 4-8 to 4-10). The formation of the 8-oxoG species indicates that the nucleobase guanine is susceptible to the bicarbonate-activated hydrogen peroxide oxidation. Other products may have been produced from further oxidation of 8-oxoG and other products as would be expected from the lower oxidation potential. With these other oxidation reactions going on, it is then difficult to determine the initial product of the bicarbonate-catalyzed hydrogen peroxide oxidation. The products of the oxidation are also more likely to be different since the mechanism of oxidation step is likely to be different from the radical process described in the literature.

CHAPTER 5
ANTIMICROBIAL ACTIVITY OF PEROXYMONOCARBONATE

Introduction

Polymorphonuclear leukocytes (also called neutrophils or granulocytes), the most prevalent form of white blood cells, are the primary cellular defense against pathogenic invasion [157]. Neutrophils are capable of producing a diverse set of both oxidative and non-oxidative microbial toxins which are contained in special granules that will be used later to kill ingested pathogens. Contents of these granules are also secreted to regulate various physiological and pathological processes, including inflammation [157-160] . Packed into these granules are digestive enzymes such as acid hydrolases, neutral proteases, alkaline phosphatase and lysozymes, cationic proteins that possess bactericidal properties, lipopolysaccharides, and two biopolymers, namely myeloperoxidase (MPO) and lactoferrin, that could be involved in oxidative microbicidal reactions [158,161].

Neutrophils migrate to sites of infection in response to chemotactic factors generated at those sites [157]. The sequences of events leading to phagocytosis are summarized as follows (Figure 5-1) [161,162]. Particles encountered as foreign bodies are "tagged" and bound to the plasma membrane of the neutrophils. The binding of the foreign bodies then activates a multimeric flavocytochrome called the NADPH oxidase, causing a marked enhancement of oxygen consumption called the respiratory burst. This respiratory burst generates superoxide that rapidly dismutates to hydrogen peroxide. Simultaneously, the bound particles are engulfed by membrane invagination leading to

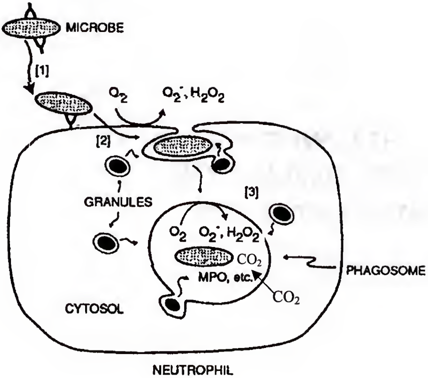

Figure 5-1. Schematic diagram of the phagocytic response of neutrophils. The process of the neutrophil microbicidal activity involves [1] the binding of the microbe eliciting a respiratory burst by NADPH oxidase, [2] the formation of the phagosome, and [3] the degranulation [161].

their isolation within sealed vacuoles called phagosomes. Because the membrane everts during phagocytosis, the NADPH oxidase is now oriented to generate the reactive oxygen species towards the phagosomal volume [161]. During and subsequent to these events, the granules migrate to the phagosome and discharge their contents into the phagosomal volume (degranulation).

Various oxidants that have been proposed as microbicidal agents formed during respiratory burst are presented in figure 5-2. The microbicidal properties of hydrogen peroxide, hypochlorous acid (HOCl) and *N*-chloramines have been demonstrated for centuries in their use in the treatment of topical wounds, the treatment of municipal sewage and other waste waters, and action of disinfectants. By itself, hydrogen peroxide is toxic to microbes at high concentrations [163]. Microbes are tolerant of lower levels of hydrogen peroxide, presumably due to endogenous catalases and peroxidases. This tolerance is most evident in aerobic microorganisms that produce H_2O_2 as their respiratory end product. However, the concentrations of H_2O_2 generated by phagocytes

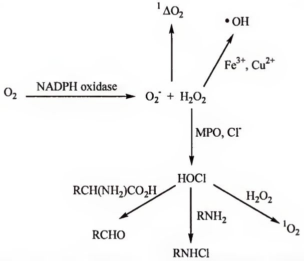

Figure 5-2. Various neutrophil-generated oxidative toxins that have been proposed and their pathways for formation [161]

are sublethal. Activation of hydrogen peroxide by MPO to produce HOCl or by metal ions to produce the hydroxyl radical increases its toxicity.

One of the components of the granules discharged into the phagosomal volume is myeloperoxidase. This enzyme myeloperoxidase catalyzes the two-electron oxidation of halides such as Cl^-, Br^-, I^- and pseudohalides by H_2O_2 [164]. The chloride is generally regarded as the physiological substrate for MPO because it is relatively abundant in intracellular fluids (~2 mM for humans) and extracellular fluids (~140 mM for humans) [164,165]. The HOCl toxicity, LD_{50} for *E.coli* in phosphate or succinate buffers at pH 7.4 has been determined to be about 10^8 molecules of HOCl per bacterium or equivalent to 10 to 50 μmol HOCl per gram dry weight of cells [166]. The microbicidal activity of *N*-chloramines generated from the reaction of HOCl with amines, on the other hand, varies depending on their solubility with lipophilic chloramines being toxic to cells [167].

Despite the impressive microbicidal activity of HOCl and other halogenic oxidants generated from it, a primary role for these agents in microbial defense has not been fully established. Mammalian neutrophils contain large amounts of the enzyme myeloperoxidase comprising about 1 to 5% of its dry weight; however avian neutrophils have no myeloperoxidase [161]. In humans, a congenital defect in the MPO characterized by the inability of the neutrophils and monocytes to produce the enzyme, does not have serious medical consequences aside from the susceptibility of some individuals to *Candida albicans* infections [168,169]. Considerably more damaging is the congenital defect known as chronic granulomatous disease (CGD) characterized by the inability of the individual to generate a respiratory burst which results in chronic and often fatal predisposition to bacterial and fungal infections [170]. These examples indicate the existence of other oxidative mechanisms in addition to the MPO-H_2O_2-halide system and non-oxidative ones in the cellular defense against invading pathogens.

Other oxidative toxins that have been proposed are singlet oxygen and the hydroxyl radical. Phagosomal singlet oxygen formation has been investigated and no compounds have been detected that could arise from $^1\Delta O_2$, thereby establishing that $^1\Delta O_2$ is not a major contributor to the phagosomal microbicidal agent [171-173]. On the other hand, hydroxyl radical formation requires exogenous, presumably bacterial, sources of iron or copper ions to effect microbicidal activity [161].

Peroxymonocarbonate is a proposed additional oxidative toxin that can be produce accompanying respiratory burst in the neutrophils. As the NADPH is the immediate source of reducing equivalents for the one-electron reduction of O_2 to superoxide [161,174], the enzyme is cyclically regenerated in the neutrophil cytosol through glucose oxidation by the hexose monophosphate pathway, the end product of which is CO_2 [161,174,175]. Thus, the respiratory burst is coupled to a CO_2 burst that could rise several-fold above its normal physiological level. The simultaneous burst in hydrogen peroxide and carbon dioxide can result in a sub-burst of peroxymonocarbonate prior to equilibration (eq 1-3). This sub-burst would result from a more rapid perhydration of CO_2 (left side of Figure 1-4) over the hydration reaction (right side of Figure 1-4). Kinetic evidence for such a sub-burst of HCO_4^- has been obtained in a pH shock experiments using CO_2/H_2O_2 solutions [176] (Figure 5-3).

Materials and Methods

Materials and Instrumentation

Escherichia coli MC 1061, *Staphylococcus aureus*, *Salmonella*, and *Candida albicans* were obtained from the Microbiology Laboratory of Shands Hospital

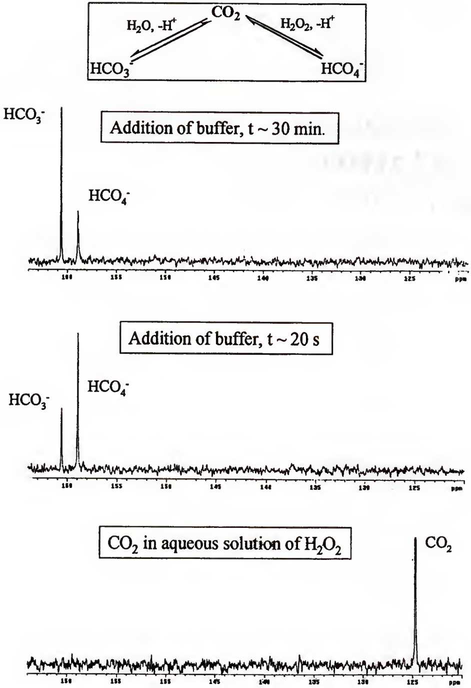

Figure 5-3. Carbon-13 NMR of pH shock experiments showing sub-burst formation of HCO_4^- [176]

(Gainesville, FL). *Streptococcus mutans* JH1140 were obtained from Dr. Jeffrey Hillman's labortaory (Oral Biology, University of Florida). Stock cultures were maintained in a 6% Todd-Hewitt broth (60 g/L) with 0.6 % yeast extract (6g/L) (THYex) agar plate.

Todd-Hewitt Broth (BBL dehydrated culture media), yeast extract and granulated agar used were obtained from Fisher (Atlanta, GA). Water used to make the media was doubly distilled using a Barnstead Mega-Pure Glass Still MP-1.

Sodium dihydrogen phosphate, sodium monohydrogen phosphate, sodium bicarbonate, sodium chloride, sodium hydroxide and hydrochloric acid were of analytical grade and were obtained from Fisher (Atlanta, GA). Diethylenetriaminepentaacetic acid (DTPA) was obtained from Sigma Chemicals (St. Louis, MO). Water used in the buffers was purified from a Barnstead E-Pure 3-Module Deionization System (water resistance $\geq$ 17 megohm-cm). Buffers were then run through a Chelex 100 50-100 μ (Sigma Chemicals from St. Louis, MO) column prior to use to remove adventitious ions. Sodium bicarbonate solutions used were freshly made. Hydrogen peroxide (70%) was obtained from Solvay Interox (Houston, TX) and standardized iodometrically.

Copper (II) sulfate pentahydrate was obtained from Fisher (Atlanta, GA) and used as received. Neocuproine (2,9-dimethyl-1,10-phenanthroline) was obtained from Acros (Atlanta, GA). Ethanol (190 proof) was obtained from AAPER Alcohol (Shelbyville, KY).

Sodium hypochlorite (5% active oxygen) was obtained from Acros (Atlanta, GA). Hypochlorous acid was purified according to the procedure by Albrich and Hurst [166] and Cady [177]. Briefly, the hypochlorite was acidified using hydrochloric acid to pH 5 and was then distilled under reduced pressure. The distilling fraction at 75-80°C was collected as hypochlorous acid solution. The amount of hypochlorous acid was quantified spectrophotometrically ($\varepsilon = 100\ M^{-1}cm^{-1}$ at λ=236 nm) [178]. The concentration was checked by iodometric titration. The presence of chloride ion was checked by adding a solution of silver nitrate to an aliquot of the fraction.

Turbidity Measurements

A 5.0 mL solution of THYex broth was inoculated with the microbe from the agar plate cultures. The microbe was then allowed to grow overnight at 37°C. A 50 μL aliquot of the inoculated broth was then used to inoculate a fresh 5.0 mL of THYex broth in a sealed test tube. The growth of the microbe was then monitored spectrophotometrically at 600 nm using a Spectronic 20D (Milton Ray Company).

Microbicidal Assay (Figure 5-4)

A 5.0 mL THYex broth was inoculated with the sample organism from the agar plate cultures. The microbe was then grown overnight (<15 h) at 37°C. A 50-μL aliquot of the broth culture was then used to inoculate a second 5.0 mL THYex broth. The sample was then grown at 37°C to mid-log phase as determined by turbidity measurements. For anaerobically-grown microbes, the microbes were grown in an anaerobic chamber supplied with carbon dioxide gas (99.9% and less than 10 ppm of O_2) just before harvesting in the next step. The microbes was then harvested by centrifugation and washed with cold 2x200 μL 0.15 M sodium phosphate buffer at pH 7.4 with 67 μM DTPA and by 2x200 μL 0.15 M sodium phosphate at pH 7.4. The pellet was then resuspended in 5.0 mL 0.15 M sodium phosphate buffer at pH 7.4. The suspension was then sampled and viable cell counts were determined as colony forming units (cfu) (~10^7 to 10^8 cells).

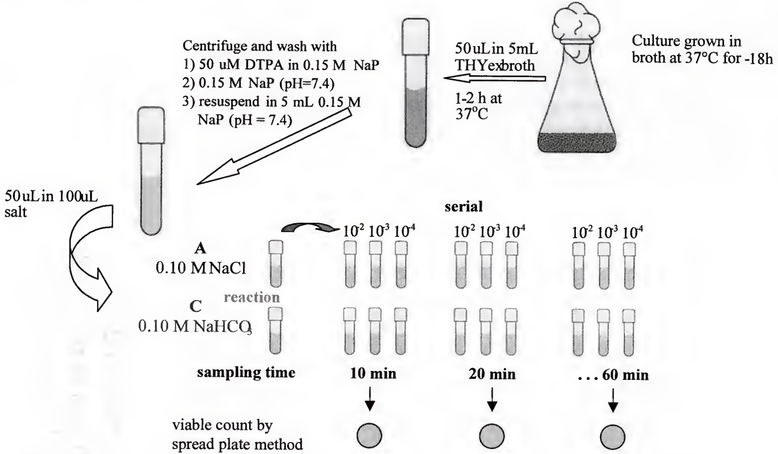

Figure 5-3. Schematic diagram of the procedure for themicrbicidal assay. NaP = sodium phosphate buffer at pH 7.4.

A 50 μL aliquot of the suspension was added to an Eppendorf tube with hydrogen peroxide solutions of either sodium chloride (0.10 M) or sodium bicarbonate (0.10 M). Controls wherein no oxidant was added were done. Aliquots (5.0 μL) of the reaction mixture were taken at different time intervals for viable cell counts using spread plate method. Colonies were counted after incubating anaerobically for ~18 to 24 hours at 37°C. All experiments were run at least in triplicate.

Similar procedures were used for different organisms and for hypochlorous acid oxidation. Oxidant activity was inactivated by addition of the aliquot to a solution of sodium thiosulfate (1.0 mM) before serial dilutions for viable cell count.

Hydrogen Peroxide Determination by CuDMP Method [179]

A stock solution of 2,9-dimethyl-1,10-phenanthroline (DMP) (also called neocuproine) (0.5 g in 50 mL ethanol ~ 0.48M) was prepared. A 10 mM stock solution of copper (II) solution was also prepared. A 100 μL of the stock copper (II) solution (final concentration is 1.0 mM) was added to 83.3 μL of the stock DMP solution (final concentration = 4.0 mM) and 100 μL of 0.10 M sodium phosphate buffer at pH 7.4. Various concentrations of hydrogen peroxide ranging from 0 to 50 μM in the presence of 0.10 M $NaHCO_3$ were added to the copper (II) solutions. Water was added to make a final volume of 1.0 mL. Absorbance of the solution was measured at 454 nm (Figure 5.4).

For the determination of hydrogen peroxide in the microbicidal assay, aliquots (10 μL) of the reaction mixture were used instead of the hydrogen peroxide solution. Only the hydrogen peroxide in the reaction mixtures with $NaHCO_3$ was measured since the presence of high concentrations of Cl^- interferes with the determination of hydrogen peroxide.

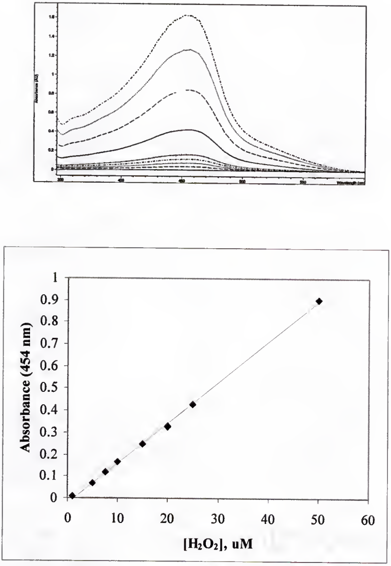

Figure 5-5. Calibration curve for $Cu(DMP)_2^+$ for H_2O_2 determination. The top portion illustrates the absorption spectrum of $Cu(DMP)_2^+$ in 10 mM sodium phosphate buffer at pH 7.4 and 1.0 mM $NaHCO_3$. The calculated molar absorptivity is ε =18312 ±123 $M^{-1}cm^{-1}$ at $\lambda = 454$ nm.

Results and Discussions

Cell Growth

Cell growth was monitored indirectly by use of turbidity measurements. A cell suspension looks cloudy to the eye as each cell scatters visible light. The more cells present in the material, the more the suspension scatters light and the more turbid it will be. As turbidity is measured in terms of absorbance, absorbance is then proportional to the cell number as well as cell mass. This is a simple, quick and easy method of determining rate of growth of the sample organism.

In the method described above, both the living and dead cells are counted. In our study, we are interested in counting only live cells after treatment (viable cells). For this reason, the viable count method was used.

Hydrogen Peroxide Toxicity

By varying the concentration of hydrogen peroxide and measuring the viability of the sample after one hour of exposure to the oxidant, we measured the susceptibility of each organism to hydrogen peroxide. Figures 5-6 and 5-7 summarize the results for the different organisms used. Results indicated that *Candida albicans*, a fungi, has the least tolerance to hydrogen peroxide and *E. coli* and *Salmonella* were more resistant to hydrogen peroxide. These results were consistent with previous studies wherein eukaryotic cells are less resistant to hydrogen peroxide-induced damage than bacteria [180]. Also aerobically-grown bacteria have a slightly higher tolerance for hydrogen peroxide than those grown anaerobically. This was expected as organisms that have been previously been exposed to oxygen and other oxidants have a more developed antioxidant defense system than those that have little or no exposure to oxygen.

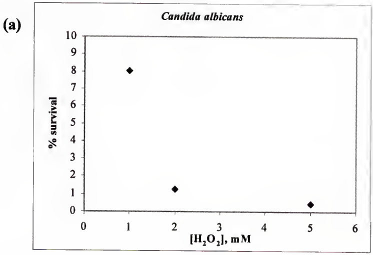

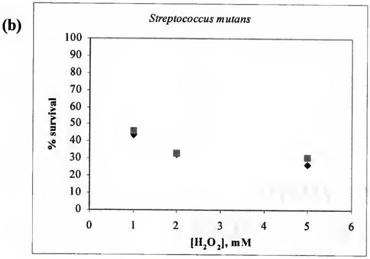

Figure 5-6. Hydrogen peroxide toxicity. Susceptibility of aerobically-grown *Candida albicans* and *Streptococcus mutans* to hydrogen peroxide after 30 minutes of exposure to hydrogen peroxide.

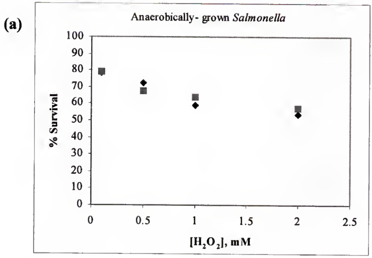

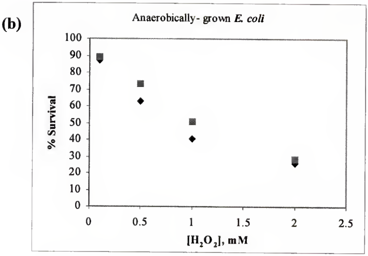

Figure 5-7. Hydrogen peroxide toxicity. Susceptibility of anaerobically-grown *Salmonella* and *Escherichia coli* to hydrogen peroxide after 30 minutes exposure to hydrogen peroxide.

Hydrogen peroxide concentration was also monitored to ensure that no decomposition was occurring during the assay. Results indicated that no apparent change in the concentration of hydrogen peroxide was occurring during the microbicidal assay (Figure 5-8).

Kinetics

The rate of cell death was measured by monitoring the number of viable cells remaining after treatment (%survival) with respect to control experiments with no oxidant (Figure 5-9). In the presence of bicarbonate, the antimicrobial properties of hydrogen peroxide were enhanced (Figures 5-10 and 5-11). The rate of cell death was doubled in the presence of 0.10 M $NaHCO_3$. The rate was also proportional to the amount of bicarbonate added and appeared to be first-order with respect to bicarbonate concentration (Figure 5-10). We can write an equation to estimate the rate of cell death as eq 5-1.

$$-\frac{d[\text{survivors}]}{dt} = k_{so}[\text{oxidant}][\text{initial\#cells}] \qquad (5\text{-}1)$$

Under the conditions used wherein the amount of oxidant was in excess to the amount of the oxidant over the "substrates", we can then rewrite eq 5-1 to eq 5-2

$$-\frac{d[\text{survivors}]}{dt} = k_{obs}[\text{initial\#cells}] \qquad (5\text{-}2)$$

wherein $k_{obs} = k_{so}$ [oxidant].

In terms of the fraction of surviving cells, *f*, where $f = \frac{\#\text{survivors}}{\text{initial\#cells}}$, eq 5-2 becomes eq 5-3.

$$\ln[f] = k_{obs}t \qquad (5\text{-}3)$$

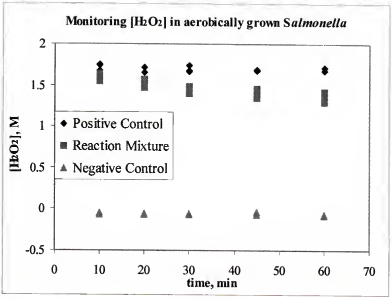

Figure 5-8. Monitoring the [H_2O_2] in the microbicidal assay for aerobically-grown *Salmonella.* Concentrations of hydrogen peroxide were measured using the CuDMP method (see text). Initial conditions for the assay (reaction mixture) are as follows: [H_2O_2] = 2.0 mM, [$NaHCO_3$] = 0.10 M and 50 mM sodium phosphate buffer at pH 7.4. The positive control (◆) does not contain the bacteria *Salmonella* but contains hydrogen peroxide, bicarbonate and phosphate buffers. Reaction mixture (■) is the microbicidal assay itself with the bacteria, hydrogen peroxide, bicarbonate and phosphate buffers. Negative control (▲) contains the bacteria, bicarbonate and phosphate buffers and no hydrogen peroxide. No apparent change in hydrogen peroxide is observed during the assay. Differences are negligible if errors are included (mostly volumetric).

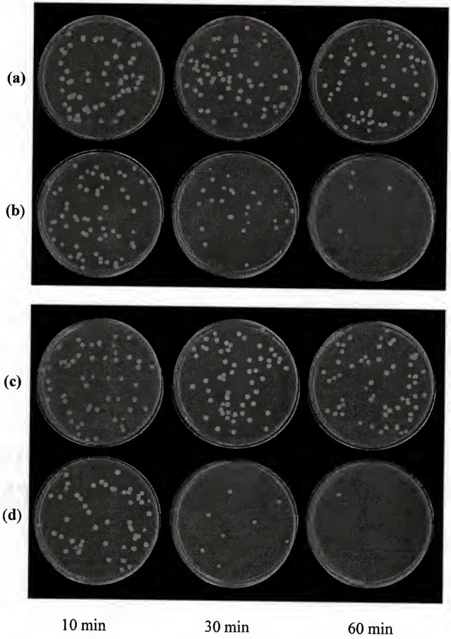

Figure 5-9. Viable cell count using spread plate method. Rows (a) and (c) are control experiments with no oxidant added in (a) 0.10 M NaCl and (c) 0.10 M $NaHCO_3$. Rows (b) and (d) are the plates for the hydrogen peroxide treated cells in (b) 0.10 M NaCl and (d) 0.10M $NaHCO_3$. The bacteria used is anaerobically-grown *E. coli.*

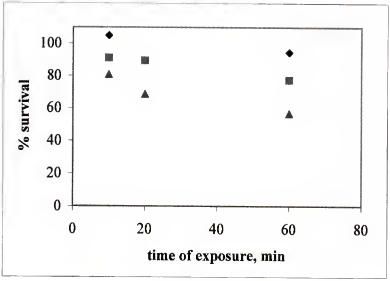

Figure 5-10. Viabilities of aerobically-grown *Streptococcus mutans* following exposure to 500 µM hydrogen peroxide. Assay conditions are as follows: 500 µM H_2O_2 with 50 mM sodium phosphate buffer at pH 7.4 in (♦) 0.10 M NaCl, (■) 0.050 M NaCl + 0.050 M $NaHCO_3$, and (▲) 0.10 M $NaHCO_3$.

From the slope of the plot of ln[*f*] versus time (Figure 5-11), we obtained the *pseudo*-first-order rate constant, k_{obs}, for the rate of cell death and calculated for the apparent second-order rate constant, k_{so}, for the different oxidants used.

Comparing the antimicrobial potency of hypochlorous acid over hydrogen peroxide (Figure 5-12), hypochlorous acid was about a 100-fold more potent than hydrogen peroxide alone by our kinetic calculations and was in agreement with literature estimates [166]. Replacement of the salt solution from NaCl to $NaHCO_3$ in the HOCl assay produced no change in the rate of cell death.

In the presence of bicarbonate, the oxidants were assumed to be the hydrogen peroxide and the peroxymonocarbonate formed from the equilibrium reaction between hydrogen peroxide and bicarbonate. The amount of peroxymonocarbonate according to its equilibrium formation (eq 1-3) was estimated to be $[HCO_4^-] \sim K_{eq}[HCO_3^-][H_2O_2]$ at low $[H_2O_2]$ concentrations. Calculations indicated that the peroxymonocarbonate is ~50 to 100-fold more potent than hydrogen peroxide (Table 5-1). This value was in agreement with the enhancement calculated from the peroxymonocarbonate oxidations of thiols and methionines. The results also indicated that hypochlorous acid and peroxymonocarbonate have comparable potency (Figure 5-12).

Conclusions

Hydrogen peroxide and hypochlorous acid have long been known to have antimicrobial properties. However, the effect of the presence of HCO_3^-/CO_2 in hydrogen peroxide solutions has not been previously studied. An increase in the antimicrobial properties of hydrogen peroxide has been observed in the presence of bicarbonate. Kinetic calculations indicate that the potency of peroxymonocarbonate as an antimicrobial is comparable to that of hypochlorous acid and is about 50 to 100-fold

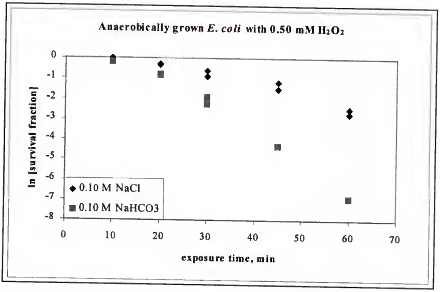

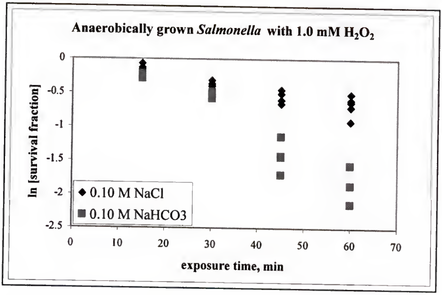

Figure 5-11. Plot of the ln[*f*] versus exposure time. From the slope of the line, the *pseudo*-first-order rate constant for the rate of cell death is obtained (eq 5-3).

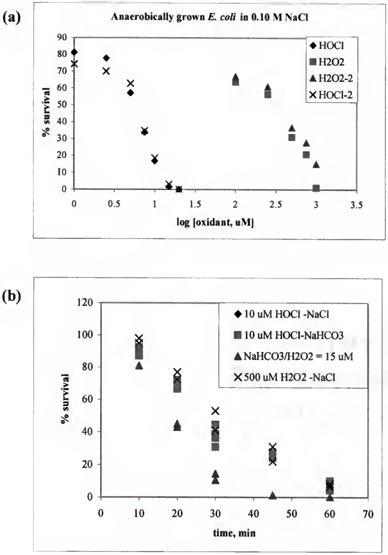

Figure 5-12. Comparison of the toxicities of hypochlorous acid, peroxymonocarbonate and hydrogen peroxide to anaerobically-grown *E. coli*. (a) Top graph compares hypochlorous acid (♦ and x) to hydrogen peroxide (■ and ▲) in terms of susceptibility. Hypochlorous acid is more potent than hydrogen peroxide by about 100-fold. (b) Bottom graph shows the survival rate of *E.coli* in (■ and ♦) 10 μM HOCl, in (**x**) 500 μM H_2O_2, and in (▲) 15 μM HCO_4^-.

Table 5-1. Rate constants for the different oxidants used in the microbicidal assay.

[Oxidant]	**$10^4 k_{obs}$, s^{-1}**	**k_{so}, $M^{-1}s^{-1}$ [a]**
For anaerobically-grown *E.coli*		
HOCl, 10 µM	8.3 ± 0.6	84 ± 6
H_2O_2, 500 µM	8.5 ± 1.3	1.7 ± 0.3
HCO_4^-, 15 µM	15.3 ± 2.6	102 ± 16
For anaerobically-grown *Salmonella*		
H_2O_2, 1000 µM	2.0 ± 0.6	0.2 ± 0.1
HCO_4^-, 30 µM	4.3 ± 1.3	14 ± 4
For aerobically-grown *Salmonella*		
H_2O_2, 2000 µM	2.5 ± 0.3	0.1 ± 0.1
HCO_4^-, 60 µM	3.2 ± 1.0	5.3 ± 1.7

[a] Note that the reported k_{so} for HCO_4^- have been corrected for the activity of hydrogen peroxide in the absence of bicarbonate.

greater than hydrogen peroxide alone. These results indicate that peroxymonocarbonate may be an important but overlooked oxidative toxin formed during respiratory burst. However, given the complexity of processes involved in the microbicidal activity of neutrophils, further evidence for the formation of peroxymonocarbonate *in vivo* is needed.

CHAPTER 6
GENERAL CONCLUSIONS

Peroxymonocarbonate has long been known and isolated. It is a moderately reactive heterolytic oxidant that can be classified as an anionic peracid [49], the structure of which represents that of a true peroxide ($HOOCO_2^-$) [50-52]. Formation of HCO_4^- from the equilibrium reaction of bicarbonate and hydrogen peroxide, both of which are ubiquitous in extracellular fluids, is rapid at near neutral pH and ambient temperature [49]. However, its reactivity towards biological targets had not been investigated. Our goal was to investigate the reactivity of peroxymonocarbonate as a possible reactive oxygen species. Reactivity towards biological targets of common reactive oxygen species was demonstrated.

Low molecular weight thiols and protein thiols are potential physiological targets for oxidation. Oxidations of cysteine, gluthathione and *N*-acetylcysteine using hydrogen peroxide in the absence and presence of bicarbonate have been investigated. Kinetic parameters that have been obtained from the thiol oxidations indicated that the thiols are more reactive when ionized as thiolates such that thiols with a lower pK_a are more reactive, such that cysteine ($pK_a = 8.3$, $k_{obs} = 5.6 \pm 0.1\ M^{-1}s^{-1}$) is more reactive than *N*-acetylcysteine ($pK_a = 9.5$, $k_{obs} = 0.5 \pm 0.1\ M^{-1}s^{-1}$). The calculated second-order rate constant for the reaction of the thiolate anion with hydrogen peroxide is $17 \pm 2\ M^{-1}s^{-1}$ for all three substrates. The presence of bicarbonate, through the formation of peroxymonocarbonate, catalyzes the reaction and at the least doubles the rate of oxidation. The calculated second-order rate constants for the direct reaction of the thiolate anions with peroxymonocarbonate fall within the range of 910-1990 $M^{-1}s^{-1}$. The rate enhancement observed is consistent with the formation of peroxymonocarbonate.

Further oxidation of thiols or disulfides to sulfonic acid is very slow. The product distributions vary depending on the conditions used. Thiosulfonate formation is favored under acidic conditions while sulfonic acid/sulfonate is favored at higher pH. The bicarbonate is believed to catalyze the first step of the disulfide oxidation reaction and can also be a good source of thiosulfonate at near neutral pH. This may have a potential application in organic chemistry as thiosulfonates are good sulfenylating agents [65]. It has also been used as a protecting group for protein thiols [181]. The unusual product distribution may also shed light into the investigations on thiol metabolism. Though higher *S*-oxidation products are naturally found, only few have been known and isolated [69].

Another target of biological oxidants is methionine. The presence of methionine sulfoxide in proteins has long been known and implicated in various diseases and the process of aging. As with thiol oxidations, in the presence of bicarbonate, the rate of hydrogen peroxide oxidation of methionine is at least doubled. In the absence of bicarbonate, the calculated second-order rate constant is $7.5\ (\pm\ 0.4) \times 10^{-3}\ M^{-1}s^{-1}$ which is about 2000-fold lower than thiol oxidation by hydrogen peroxide. For the bicarbonate-catalyzed oxidation, the calculated second-order rate constant is $0.5 \pm 0.1\ M^{-1}s^{-1}$. As with the thiol oxidation, the rate enhancement is consistent with the formation of peroxymonocarbonate as the active oxidant in the reaction.

Methionine oxidation can inactivate the biological activity of a protein such as α1-PI. The oxidation of α1-PI has been investigated and its significance in the control of elastase and other proteinases has been implicated in various diseases. Areas high in CO_2 concentration, such as the lungs, are potential sites for localized bursts of HCO_4^- prior to the equilibration of eq 1-3. And in such sites, the α1-PI oxidation is faster and may result in the development of emphysema, chronic bronchitis, and chronic obstructive pulmonary diseases. Oxidation of α1-PI has resulted in the loss of its inhibitory activity towards porcine pancreatic elastase. Kinetic parameters that have been obtained are comparable to the free methionine oxidation ($k_{01} = 0.014 \pm 0.003$ $M^{-1}s^{-1}$ and $k_c = 0.36 \pm 0.06$ $M^{-1}s^{-1}$).

Methionine oxidation may also result in no change in the protein activity. These methionines may then act as antioxidants and may be protecting important residues from oxidative damage. In the oxidation of RNase, no change in the hydrolytic activity is observed upon oxidation.

A direct method in monitoring the oxidation of proteins without proteolytic digest is through the use of ESI/FTICR-MS. This method is only applicable to low molecular weight molecules or proteins. The sensitivity of this method would depend upon the molecular weight and stable charge state of the protein.

The use of HPLC/MS in the analysis of proteolytic digest of the protein is also illustrated. Sites of modification can be identified and be correlated to amino acid analysis and assays of biological activity of the protein. In the oxidation of α1-PI, amino acid analysis of the oxidized protein confirms the oxidation of at least two methionines and possibly some histidines. The oxidation of vital Met358 in the reactive center loop has been identified by the analysis of the proteolytic digest using HPLC/MS. In the oxidation of RNase, the site of modification is not identified though the kinetic parameters obtained are comparable to free methionine oxidation. Further studies such as amino acid analysis and proteolytic digest are needed to be able to identify the modification site in the oxidation of RNase A.

Another marker in oxidative stress is the presence of 8-oxoguanosine in DNA. As a model for DNA oxidation, oxidation of 5'-guanosine monophosphate has been investigated using HPLC/MS and MS/MS. Only when bicarbonate is present at high concentration in the oxidation reaction solution with hydrogen peroxide that oxidation occurs. Addition of a metal chelator such as DTPA quenches the reaction. Trace metal ions contained in the salt may be involved in the formation of an active oxidant involving bicarbonate. Previous studies on DNA oxidation usually involving radical oxidants, photolysis, metal catalysis, extreme conditions, or very strong oxidants such as oxone, also yield the 8-oxoguanosine as an oxidation product. Other oxidation products, some presumably arising through further oxidation of the 8-oxoguanosine, have yet to be identified. Results from the MS/MS data also indicated that the oxidation occurs in the purine ring and not in the sugar moiety. The use of anion exchange HPLC (AX-HPLC) seems to be promising in being able to separate at least three products. Possibly a two-dimensional separation (AX-HPLC followed by RP HPLC) prior to MS to remove salt may be employed to separate and identify the products. A macroscale separation using Dowex or some other appropriate anion exchange columns may be used to be able to obtain a sample for NMR analysis.

As a model for oxidative stress *in vivo*, the effect of oxidants on microbes has been investigated. Though the antimicrobial properties of hydrogen peroxide are well-known, the effect of the presence of bicarbonate has not been investigated. Eukaryotic cells such as *Candida albicans* are more susceptible to hydrogen peroxide toxicity.

Anaerobically-grown microbes are more susceptible to oxidative stress due to the reduce antioxidant activity in their growth phase. The presence of bicarbonate in the hydrogen peroxide solution enhances the antimicrobial properties of hydrogen peroxide. In the presence of bicarbonate, it takes only half the time it to kill the microbes versus hydrogen peroxide alone. Comparative studies on the potency of hypochlorous acid (bleach) and hydrogen peroxide in the absence and presence of bicarbonate have also been investigated. Hypochlorous acid is about 100-fold more potent than hydrogen peroxide alone. In the presence of 0.10 M bicarbonate and calculating for the [HCO_4^-], results indicated that peroxymonocarbonate potency may be comparable to that of hypochlorous acid. The peroxymonocarbonate may have a contributory role in the oxidative killing of microbes in host cells. The mode of cell death has yet to be determined though it is suggested that it is due to cumulative factors.

Catalase has also been shown to decompose peroxymonocarbonate directly. Results indicate that catalase may serve as an endogenous antioxidant against both hydrogen peroxide and peroxymonocarbonate. Further investigations into the kinetics and mechanism of the catalase decomposition of peroxymonocarbonate are needed.

The results discussed above have demonstrated the reactivity of peroxymonocarbonate with biological targets *in vitro*. Kinetic and spectroscopic results also support the role of peroxymonocarbonate as the oxidant involved. *In vitro,* we have demonstrated that peroxymonocarbonate is a potent oxidant capable of oxidizing a wide variety of targets.

At typical bicarbonate concentrations in the blood (~0.025 M) about ~1% of the plasma hydrogen peroxide is estimated to be converted to peroxymonocarbonate based on the *in vitro* oxidation data. Even under these low concentrations, the rate of oxidation would be double over the peroxide-only rate. This enhancement is a substantial increase in the oxidizing ability of hydrogen peroxide. Simultaneous release of CO_2 and H_2O_2 by a cell, as in the case of an NADPH-mediated respiratory burst [161], could lead to a "sub-burst" of HCO_4^- prior to equilibration of eq 1-3. Kinetic evidence for such a "sub-burst" of HCO_4^- in pH shock experiments using CO_2/H_2O_2 solutions has been obtained [176]. The HCO_4^- formed then reacts with the most potent nucleophiles in the vicinity, such as thiols or methionines, and may cause cellular damage.

In comparison with peroxynitrite ($ONOO^-$) and its conjugate acid (ONOOH), HCO_4^- exhibits more stability. Carbon dioxide catalyzes the decomposition of peroxynitrite via the formation of the CO_2 adduct ($t_{1/2} \approx 1$ s for $ONO_2CO_2^-$ vs. $t_{1/2} \approx 600$ s for HCO_4^-) [49,182]. This $ONOOCO_2^-$ adduct has been implicated in the oxidation and nitration chemistry of peroxynitrite. The presence of CO_2/HCO_3^- significantly enhances the nitration of aromatics such as tyrosines, but inhibits the oxidation of thiols, dimethylsulfoxide, oxyhemoglobin and cytochrome c^{2+}, and totally inhibits the hydroxylation of benzoate [183,184]. The presence of CO_2 in the media also protects bacterial suspensions from ONO_2^- toxicity [184] due to the formation of the adduct $ONO_2CO_2^-$ that has a shorter half-life ($t_{1/2} \approx 9$ s for ONO_2^- vs. $t_{1/2} \approx 1$ s for $ONO_2CO_2^-$) [184,185]. Carbon dioxide may protect cells from peroxynitrite-mediated damage, however it may also contribute to cellular damage via the formation of peroxymonocarbonate.

The formation or existence of peroxymonocarbonate *in vivo* has yet to be investigated. The difficulty lies in the method of identification *in vivo*. Although we have shown catalysis by bicarbonate in the hydrogen peroxide oxidation of thiols and other substrates, it is not known to what extent this pathway contributes to the oxidative damage in tissues. Given the complexity of biochemical media, a more detailed examination of HCO_4^- formation under physiological conditions is needed. From previous studies [49,53], we have shown that the equilibration rate for eq 1-3 is affected by the type of solvent used, the presence of other nucleophiles and the presence of dehydration catalysts for HCO_3^-/CO_2 system.

CHAPTER 7
SYNTHESIS AND REACTIVITY OF BIOCONJUGATABLE COPPER (II) COMPLEXES

Introduction

Many enzymes catalyze reactions by working in association with a metal ion or ions. Simple models for these metalloenzymes are metal complexes having the same metal ion or a different metal ion but having reactivity similar to the enzyme. These model complexes contain ligand systems that modify the reactivity of the metal ion and contain unsaturated or weakly coordinated sites to enable substrate binding or interaction with the substrate to form one or more activated species [186].

While the ligand system on the metal complex model can be varied widely to control the stereoselectivity of the complex and the nature of the metal to ligand interaction, a polypeptide environment provides a larger diversity and greater control of metal-substrate interaction. In an enzyme active site, a far larger variety of functional groups with different sizes, shapes and properties are present that can direct the reaction. The presence of hydrophobic groups near the active site reduces the dielectric constant and the solvation surrounding the substrate, which can then affect the stability of the bound substrate, transition state or product [187,188].

To be able to incorporate the complexity of an enzyme, a ligand system as complex as the enzyme itself is presumably necessary. One approach to this problem is to start with a complex system and modify it to do catalysis. Jencks proposed the use of antibodies as precursors to an artificial enzyme [189]. A catalytic antibody can be produced by preparing an antibody to a haptenic group that resembles the transition state of a given reaction [190-193]. In an alternative approach, Schultz and coworkers (1989) demonstrated a method wherein cleavable affinity labels, that can later be modified, are introduced to the antibody combining sites [194]. These labels can then be used to further increase the rate enhancement of the reaction by incorporating catalytic groups, such as a metal complexes or organic catalysts, into the combining sites.

Although production of catalytic antibodies is a proven way to develop a synthetic protein-based catalyst, a limitation to this approach is that the specificity of the catalytic antibody is only as good as the transition state analog of the reaction. Synthesis of an appropriate transition state model can be difficult and can be a limiting factor in the catalytic antibody production.

Another approach for the development of a semi-synthetic catalyst is to modify a known protein or enzyme at a specific site with a synthetic catalyst such as a metal complex. This strategy takes advantage of the inherent specificity and binding interaction of the enzyme. This method hopes to expand the capability of the enzyme and at the same time, possibly, enhance the catalytic activity of the metal complex.

The goal of this study was to synthesize an active metal complex for incorporation to the enzyme of interest. A hydrolytic enzyme, ribonuclease A, has been chosen as the starting enzyme. Normally, ribonuclease A catalyzes the hydrolysis of RNA but not of DNA. Through the incorporation of a metal complex catalyst, hydrolyses of DNA and other phosphate esters are feasible. Hydrolyses of carboxylate esters, amides, and phosphate esters are of interest due to its potential application as artificial nucleases and proteases.

To develop a hydrolytic semi-synthetic enzyme, an appropriate metal complex is needed for incorporation. The diaquo-2,2'-dipyridylamine copper(II) complex (Cudpa^{2+}) (Figure 7-1) has been chosen for incorporation due to its ability to hydrolyze carboxylic esters and amides [195,196].

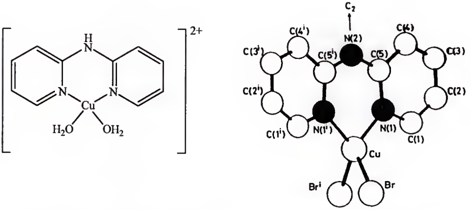

Figure 7-1. Diaquo-2,2'-dipyridylaminecopper (II), hydrolysis catalyst (Cudpa^{2+}). The right figure is the crystal structure of the dibromide salt of Cudpa (CudpaBr$_2$) as reported by [197]

The complex catalyzes both activated esters such as *p*-nitrophenyl acetate (pNPA) and unactivated esters such as methyl acetate (MeAc) with rate enhancement of 2.7 x 10^5 and 2.4 x 10^6, respectively [195]. It is interesting that this complex gives a greater rate enhancement for the unactivated ester than the activated one since many simple hydrolytic catalysts are more efficient with activated species [198,199]. Chin and coworkers have proposed that the mechanism for the promoted hydrolysis in the case of the unactivated ester involves activation of both substrates by the metal ion through coordination (Figure 7-2) [195]. Coordination of the oxygen of the carbonyl carbon increases the electrophilicity of the carbonyl carbon. Coordination of water to the metal ion increases the nucleophilicity of water through the formation of a bound hydroxide.

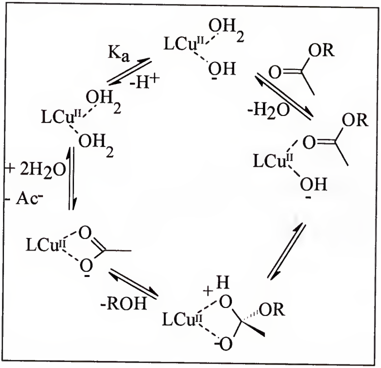

Figure 7-2. Proposed scheme for the catalyzed hydrolysis of methyl acetate by diaqua-2,2'-dipyridylaminecopper(II) [195].

The monohydroxo form of the complex is believed to be the active species of the complex, wherein the bound hydroxide acts as an internal nucleophile [195].

The ligand 2,2'-dipyridylamine (dpa) produces a stable complex with copper (II). It binds copper (II) ion more tightly than hydronium ion ($K_{\mathrm{CuL}} = 1.12 \times 10^8$ versus $K_{\mathrm{HL}}=1.38 \times 10^7$) [200] indicating that the metal ion does not dissociate from the ligand under physiological conditions (pH ~ 7). Another feature of this metal complex is that the pK_a of the coordinated water to give the bound hydroxide is near physiological pH implying that a significant concentration of the active species is available. These properties of the ligand and the reactivity of the corresponding copper (II) complex make it a desirable candidate for bioconjugation.

Before incorporation of 2,2'-dipyridylamine to the enzyme can be done, functionalization of the ligand is needed. This functionalization can be accomplished by alkylating the central nitrogen and incorporating a reactive functional group within the alkyl chain to serve as a point of attachment to the enzyme [201]. This linking arm would then allow the metal complex catalyst to be at close proximity to the active site of the enzyme.

A number of factors are considered in the functionalization of the ligand. The functional group in the linker must be capable of covalently binding to the enzyme under mild conditions, since most protein modification procedures are accomplished under mild conditions. It is preferable if the linker attaches at a position near the active site. The functional group must also be selective, reacting preferably with the target modification site. The linker must be stable under protein modification, purification and characterization, and catalytic reaction conditions. The length of the linking arm must easily be varied in order to optimize the position of the catalyst relative to the active site of the enzyme.

Two types of derivatives were used in this study to link the functionalized ligand to the enzyme. The first type used a *N*-hydroxysuccinimide ester of the ligand to take advantage of the nucleophilic amine already present in the enzyme to form an amide bond (Figure 7-3). This selectivity of *N*-hydroxysuccinimide esters for amino groups has been demonstrated by de Groot and coworkers [202] and by Lindsay and Shall [203]. Compared to acid anhydrides as acylating agents, *N*-hydroxysuccinimide esters are more reactive and selective at low concentrations and near neutral pH. Since the acid anhydrides undergo rapid hydrolysis at neutral pH [203], a large excess of the anhydride must be used to give an appreciable yield of the acylated protein.

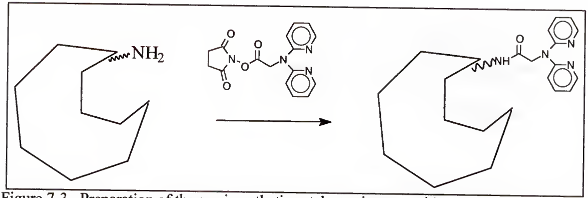

Figure 7-3. Preparation of the semi-synthetic catalyst using an amide group as the linking group.

The second type of derivative used a thiol group to form a disulfide bond to the enzyme. Since RNase A contains no free thiol group or an accessible disulfide group, chemical modification of the enzyme or mutagenesis would be needed before conjugation of the functionalized dipyridylamine can be achieved. A similar technique by Pollack and coworkers [194] was used in the modification of an antibody combining site. A thiol derivative of the dipyridylamine was chosen to selectively react with the modified enzyme via a disulfide exchange (Figure 7-4).

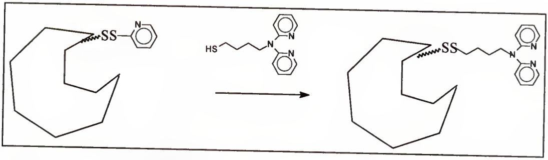

Figure 7.4. Preparation of the semi-synthetic catalyst using a disulfide as the linking group.

In the kinetic studies of this research, simple model complexes that resemble the immediate surroundings of the metal cofactor were used. The effect of alkylation of the central nitrogen and length of the alkyl chain on the catalytic activity of the functionalized dipyridylamine copper (II) complex were modeled using dipyridylamine derivatives containing varying chain length (ethyl, butyl, and octyl). The disulfide functionality that will be used to link the ligand to the enzyme was modeled using simple asymmetric disulfide derivatives. Other pyridine-based ligand systems such as 2,2'-bipyridine, 1,10-phenanthroline, and 2,2'-dipyridylketone were used to compare the reactivity of the original and functionalized dipyridylamine copper (II) complexes. Since the assumed active species of the metal complex is the monohydroxo form, the acid dissociation constants for the coordinated water of the copper (II) complexes need to be determined under the conditions that will be used in the study. Conditions for the hydrolysis of esters were initially chosen to be near physiological conditions when applicable.

Experimental Section

General Methods

Proton NMR spectra were obtained on a General Electric QE-300 spectrometer (300 MHz). Chemical shifts are reported in parts per million; the residual solvent peak was used as an internal standard. Elemental analyses were performed by the University of Florida Department of Chemistry Spectroscopic Services. All reagents were of analytical grade. All solvents used were purified and dried according to literature procedures. Deuterated solvents used for NMR were obtained from Cambridge Isotope Laboratory Inc.. Specialty chemicals used included: 2,2'-dipyridylamine (Pfaltz & Bauer) previously recrystallized from water; potassium *tert*-butoxide (Aldrich); ethyl bromoacetate (Acros) previously dried over anhydrous sodium sulfate and distilled under reduced pressure; *N,N*-dicyclohexylcarbodiimide, DCC (Acros); *N*-hydrosuccinimide (Aldrich) previously recrystallized from ethyl acetate-hexane; 1-bromo-4-chlorobutane, 97% (Acros); potassium *O*-ethyl xanthate (Aldrich); *p*-nitrophenyl acetate (Acros) and bis-(*p*-nitrophenyl)phosphoric acid (Acros) both previously recrystallized from ethanol-water; acid and sodium salt of HEPES buffer (Acros); *p*-nitrophenol (Aldrich) previously sublimed under reduced pressure; 2,2'-dipyridyl disulfide (Acros); diphenyl disulfide (Acros); bromoethane (Aldrich); bromobutane (Aldrich); chlorooctane (Aldrich); diethyl phosphochloridate (Acros), previously distilled under reduced pressure; copper (II) chloride (Fisher) previously dried *in vacuo* at 110°C overnight. Silica gel for column chromatography (70-230 mesh) obtained from Aldrich was deactivated to contain ~10% water by weight. Silica gel 60 TLC sheets were also obtained from Aldrich. All water used in the kinetics and potentiometric studies were purified using a Barnstead E-pure 3-Module Deionization System (water resistance of $\geq$ 17 megaohms-cm). Absorbance measurements were made on a Hewlett-Packard 8453 spectrophotometer. The pH of the solution was measured using an Orion Research Digital pH/Millivolt Meter Model 611.

Synthesis of *N*-Hydroxysuccinimidyl *N,N*-(2',2'-Dipyridyl)aminoacetate

Synthesis of ethyl *N,N*-(2',2'-dipyridyl)aminoacetate (2) [204,205]

To a Schlenk flask equipped with a magnetic stir bar, 2,2'-dipyidylamine (**1**) (1.71 g, 10 mmol) was added and sealed with a glass stopper. The flask was degassed for a few minutes before resealing with a septum. Tetrahydrofuran (30 mL) was added and the solution stirred for a few minutes. In another Schlenk flask, also with a magnetic stir bar, potassium tert-butoxide (1.12 g, 10 mmol) was added. The second Schlenk was placed in acetone/dry ice cold bath, degassed and stirred. The dipyridylamine solution was added slowly to the second Schlenk. The mixture was stirred for 30 minutes before the solvent was removed *in vacuo* to give the off-white dipyridylamide potassium salt. The amide was dissolved in dimethyl sulfoxide (30 mL). Ethyl bromoacetate (2.20 mL, 20 mmol) was added to the amide solution and stirred for 12 hours. Deionized water (20 mL) was added and the ester extracted using 4x15 mL of diethyl ether. The combined organic layer was re-extracted with 5% HCl. The combined acidic solution was neutralized to pH 7 with dilute NaOH and re-extracted with diethyl ether. The combined ether layer was washed with 3x10 mL deionized water and dried over anhydrous sodium sulfate. Solvent was then removed under reduced pressure to give **2** (1.36 g, 53%) as a yellow orange oil. ^{1}H NMR ($CDCl_3$): δ 8.35 (dd, J = 4.9, 2.3 Hz, 2H), 7.55 (dt, J = 8.2, 1.6 Hz, 2H), 7.25 (dd, J = 8.2, 1 Hz, 2H), 6.85 (dt, J = 6.5, 1 Hz, 2H), 4.85 (s, 2H), 4.2 (q, J = 5.8 Hz, 2H), 1.25 (t, J = 5.8 Hz, 3H)

Synthesis of *N,N*-(2',2'-dipyridyl)aminoacetic acid (3)

To a solution of 0.5 M H_2SO_4 (75 mL), ester **2** (0.76g, 3 mmol) was added and the mixture stirred for a week at room temperature. The acid solution was then neutralized to pH 6-7 using concentrated ammonia. Solvent was removed under reduced pressure to give an off-white solid. Recrystallization of the crude product in acetone yields **3** (0.34 g, 50%) as a light brown solid. ^{1}H NMR ($CDCl_3$) δ 8.25 (dd, J = 7.6, 2 Hz, 2H), 7.62 (dt, J = 8.6, 2 Hz, 2H), 7.22 (dd, J = 8.6, 2 Hz, 2H), 6.92 (dt, J = 7.6, 2 Hz, 2H), 4.75 (s, 2H). Melting Point: 228-230°C.

Synthesis of *N*-hydroxysuccinimidyl *N,N*-(2',2'-dipyridyl)aminoacetate (4) [203]

To a solution of acid **3** (0.33 g, 1.4 mmol) in dry dichloromethane (30 mL), was added a solution of *N*-hydroxysuccinimide (0.2137 g, 2.1 mmol) in anhydrous dioxane (10 mL). *N,N*-dicyclohexylcarbodiimide (0.2554 g, 1.68 mmol) was then added and the mixture stirred overnight at room temperature. The white precipitate, dicyclohexylurea (DCU), formed was filtered off and the filtrate concentrated under reduced pressure. Hot ethyl acetate was added until most of the precipitate was dissolved and filtered. The solution was concentrated under reduced pressure. Chloroform was added to precipitate a cream colored solid. For the filtrate, the solvent was removed to give **4** as a yellow oil. The cream-colored solid contains about 1:1 mixture of 4 and *N*-hydroxysuccinimide (yield ~ 25%). ^{1}H NMR of **3** ($CDCl_3$): δ 8.35 (dd , 2H), 7.65 (dt, 2H), 7.25 (dd, 2H), 7.05 (dt, 2H), 4.85 (s, 2H), 2.7 (s, 4H)

Synthesis of 4-Mercapto-*N,N*-(2',2'-dipyridyl)butanamine

Synthesis of *N*-(4-chloro)butyl-2,2'-dipyridylamine (5) [201,206]

To a stirred solution of 2,2'-dipyridylamine (1.71 g. 10 mmol) in dimethyl sulfoxide (15 mL), was added potassium hydroxide pellets (2.6 g, 46 mmol). The mixture was stirred for six hours at room temperature before adding 1-bromo-4-chlorobutane (1.40 mL, 15 mmol) and stirred for 12 hours more. Water (30 mL) was then added to the mixture and the mixture extracted with 4x25 mL of diethyl ether. The combined ether layer was re-extracted with 3x15 mL of 5% HCl to separate the product amine from the starting alkyl halide. The acidic solution was neutralized to pH 7 and extracted with 4x15 mL of diethyl ether. The combined ether layer washed with 3x10 mL water and dried over anhydrous magnesium sulfate. Solvent was removed under reduced pressure to give **5** (1.37 g, 52 %) as a red brown oil. ^{1}H NMR ($CDCl_3$): δ 8.35 (dd, J = 4.7, 1 Hz, 2H), 7.5 (dt, J = 7.1, 2.4 Hz, 2H), 7.1 (dd, J = 8.3, 1 Hz, 2H), 6.88 (dt, J = 7.1, 1 Hz, 2H), 4.25 (t, 2H), 3.6 (t, 2H), 1.85 (m, 4H)

Synthesis of *O*-ethyl *S*-4-(N,N-dipyridyl)aminobutylxanthate (6) [201,206]

To the stirred solution of 5 (2.25 g, 8.6 mmol) in dimethyl sulfoxide (30 mL), was added potassium O-ethylxanthate (2.25 g, 16 mmol). The solution was stirred for three days at room temperature. After three days, water (30 mL) was added and the pH adjusted to 7. The mixture was extracted with 4x20 mL of diethyl ether. The combined organic layer was dried over anhydrous magnesium sulfate. Solvent was removed under reduced pressure to give **6** (2.39 g, <80%) as a brown oil. ^{1}H NMR ($CDCl_3$): δ 8.35 (dd, J = 5.2, 2 Hz, 2H), 7.50 (dt, J = 8.3, 2 Hz, 2H), 7.05 (dd, J = 8.3, 2 Hz, 2H), 6.85 (dt, J = 6.2, 2 Hz, 2H), 4.62 (q, J = 6.7 Hz, 2H), 4.21 (t, J = 6.7 Hz, 2H), 3.15 (t, J = 6.7 Hz, 2H), 1.7 (m, 4H), 1.25 (t, J = 6.7 Hz, 3H).

Synthesis of 4-mercapto-*N*,*N*-(2',2'-dipyridyl)butanamine (7) [201,206]

To a stirred solution of **6** (2.39 g, 8.6 mmol) in methanol (50 mL), was added 20% (w/w) sodium hydroxide (25 mL). The mixture was stirred for about one hour at room temperature before adjusting the pH to 7. The neutralized mixture was extracted with

4x30 mL of diethyl ether. The combined ether layer was re-extracted with 4x20 mL of 10% NaOH. The basic solution was then neutralized to pH 7 and extracted with 4x20 mL of diethyl ether. The combined ether layer was washed with 3x15 mL of water and dried over anhydrous magnesium sulfate. Solvent was removed under reduced pressure to give **7** (1.9 g, 45%) as a red brown oil. ^{1}H NMR (CDCl3): δ 8.33 (dd, J = 5.9, 2 Hz, 2H), 7.46 (dt, J = 7.9, 2 Hz, 2H), 7.06 (dd, J = 8.9, 2 Hz, 2H), 6.82 (dt, J = 6.9, 2 Hz, 2H), 4.20 (t, J = 7.5 Hz, 2H), 2.57 (q, J = 7.5 Hz, 2H), 1.75 (m, 4H), 1.40 (t, J = 7.5, 1H), 1.25 (t, J = 7.5 Hz, 3H).

Synthesis of Disulfide Model Ligands

Synthesis of 4-*N,N*-(2'2'-dipyridyl)aminobutyl phenyl disulfide (8) [194]

To a stirred solution of phenyl disulfide (0.98 g, 4.5 mmol) in *N,N*-dimethylformamide (75 mL), a steady stream of nitrogen was bubbled through. A solution of **7** (0.78 g, 3 mmol) in *N,N*-dimethylformamide (50 mL) was added to the disulfide solution dropwise for a period of one hour. The mixture was then stirred at 40°C for two days. The solution was concentrated under reduced pressure before dissolving in 10% NaOH (30 mL). The basic solution was extracted with 4x15 mL of diethyl ether. The combined organic layer was re-extracted with 3x15 mL of 5% HCl to separate the phenyl disulfide from the products. The acidic solution was neutralized to pH 7 and extracted with 4x15 mL of diethyl ether. The combined ether layer was dried over anhydrous magnesium sulfate and the solvent removed under reduced pressure to give crude product **8** a yellow oil. Silica gel column chromatography with 1:1 chloroform:ethyl acetate as eluting solvent ($R_f = 0.73$) gives the pure product **8**. ^{1}H NMR ($CDCl_3$): δ 8.35 (dd, J = 4.8, 1.9 Hz, 2H), 7.5 (m, 4H), 7.27 (dt, J = 6.8, 2 Hz, 2H), 7.19

(dt, J = 6.8, 2 Hz, 1H), 7.05 (dd, J = 8.7, 1.9 Hz, 2H), 6.82 (dt, J = 5.8, 1.9 Hz, 2H), 4.20 (t, J = 6.7 Hz, 2H), 2.78 (t, J = 6.7 Hz, 2H), 1.78 (m, 4H).

Synthesis of 4-*N*,*N*-(2,2'-dipyridyl)aminobutyl pyridyl disulfide (9) [194]

Similar procedure as described above was employed in the synthesis of **9** except for the use of column chromatography. Purification of **9** was achieved through recrystallization of the 2,2-dipyridyl disulfide starting material in hexanes. The product **9** was obtained as a semi-crystalline yellow oil. ^{1}H NMR ($CDCl_3$): δ 8.45 (d, J = 5.2, 1H), 8.35 (dd, J = 4 Hz, 2H), 7.72 (d, J = 7.9 Hz, 1H), 7.62 (dt, J = 7.9, 2 Hz, 1H), 7.50 (dt, J = 7.9, 2 Hz, 2H), 7.05 (m, 3H), 6.85 (dt, J = 6.6, 2 Hz, 2H), 4.20 (t, J = 8.2 Hz, 2H), 2.85 (t, J = 8.2 Hz, 2H), 1.78 (m, 4H).

Syntheses of alkylated 2,2'dipyridylamine (11, 12, 13) [201,206]

The products **11**, **12**, and **13** are synthesized in the same manner as **5** using bromoethane, bromobutane, and chlorooctane, respectively. ^{1}H NMR ($CDCl_3$) of:

11 : δ 8.37 (dd, 2H), 7.52 (dt, 2H), 7.07 (dd, 2H), 6.82 (dt, 2H), 4.27 (q, 2H), 1.32 (t, 3H)

12: δ 8.35 (dd, 2H), 7.52 (dt, 2H), 7.07 (dd, 2H), 6.85 (dt, 2H), 4.18 (t, 2H), 1.65 (q5, 2H), 1.35 (q5, 2H), 0.92 (t, 3H)

13: δ 8.35 (dd, 2H), 7.52 (dt, 2H), 7.07 (dd, 2H), 6.85 (dt, 2H), 4.18 (t2H), 1.67 (m, 2H), 1.30 (m, 10H), 0.85 (t, 3H)

Syntheses of Dichloro Copper (II) Complexes [207]

All copper (II) complexes were synthesize according to Kirshcner [207]. Typically, to a stirred solution of 1.1 mmol of anhydrous copper(II) chloride in anhydrous methanol was added slowly a solution of 1 mmol of the ligand in anhydrous methanol. The resulting green solution was stirred for 12 hours and the green precipitate filtered, washed with cold methanol, and dried in a dessicator. The usual yield is about 80-95%. The complexes were analyzed by CHN for purity.

Cu(dpa)Cl_2 **14** : Analysis calculated for: $CuC_{10}H_9N_3Cl_2$: C, 39.296; H,2.968;, N, 13.745. Found: C, 39.146; H, 2.914; N, 13.549.

Cu(bpy)Cl_2 **15** : Analysis calculated for: $CuC_{10}H_8N_2Cl_2$: C, 41.326; H, 2.774; N, 9.639. Found: C, 41.047; H, 2.633; N, 9.364.

Cu(phen)Cl_2 **16** : Analysis calculated for: $CuC_{12}H_8N_2Cl_2$: C, 45.806; H, 2.563; N, 8.903. Found: C, 45.790; H, 2.403; N, 8.732.

Cu(dpk)Cl2 **17** : Analysis calculated for: $CuC_{10}H_8N_2Cl_2(CH_3OH)$: C, 41.100; H, 3.449; N, 7.988. Found: C, 41.309; H, 3.244; N, 7.890.

Cu(**11**)Cl_2 **18** : Analysis calculated for: $CuC_{12}H_{13}N_3Cl_2$: C, 43.191; H, 3.927; N, 12.592. Found: C, 43.132; H, 3.885; N, 12.353.

Cu(**12**)Cl_2 **19** : Analysis calculated for: $CuC_{14}H_{17}N_3Cl_2$: C, 46.482; H, 4.737; N, 11.615. Found: C, 46.176, H, 4.727; N, 11.503.

Cu(**13**)Cl_2 **20** : Analysis calculated for: $CuC_{18}H_{25}N_3Cl_2$: C, 51.738; H, 6.030; N, 10.056. Found: C, 51.396; H, 6.344; N, 10.012.

Cu(**8**)Cl_2 **21** : Analysis calculated for: $CuC_{20}H_{21}N_3S_2Cl_2$: C, 47.854; H, 4.217; N, 8.371. Found: C, 47.636; H, 3.918; N, 8.217.

Cu(**9**)Cl_2 **22** : Analysis calculated for: $CuC_{19}H_{20}N_4S_2Cl_2(1.5H_2O)$: C, 43.059; H, 4.374; N, 10.571. Found: C, 42.930; H, 4.150; N,10.573.

Cu(**10**)Cl_2 **23** : Analysis calculated for: $Cu_2C_{28}H_{32}N_6S_2Cl_4(H_2O)$: C, 41.847; H, 4.264; N, 10.457. Found: C, 41.796; H, 3.971; N, 10.145.

A crystal structure was obtained for the copper(II) complex **19**. The complex was crystallized form a solution of ethanol to give a monoclinic crystals, space group *P*2(1)/n with $a = 8.6359$, $b = 9.0949$, $c = 19.286$ Å, β= 93.074° (See Appendix).

Synthesis of Ethyl *p*-Nitrophenylphosphoric Acid (ENPP)

Synthesis of sodium *p*-nitrophenoxide (13) [208]

Sodium hydroxide (2.20 mL of 10 M solution) was added to a stirred suspension of 3.0 g p-nitrophenol in 14 mL of hot water. The suspension was stirred until it becomes clear orange. Another 2.0 mL of the sodium hydroxide solution was then added slowly to give yellow crystals. The mixture was allowed to cool at room temperature before placing in ice bath. The yellow crystals were filtered and washed with 3x3 mL of ice cold water in vacuo at 110°C overnight to give a red-orange anhydrous salt of **13** (3.2 g, 92%).

Synthesis of diethyl *p*-nitrophenylphosphate (14) [208-212]

To a stirred suspension of anhydrous sodium *p*-nitrophenoxide (3.22 g, 19.9 mmol) in benzene (70 mL) cooled in an ice bath was added slowly diethyl phosphochloridate (3.0 mL , 20.7 mmol). The mixture was refluxed in a Deanstark apparatus for two days then allowed to cool in an ice-bath. The precipitate of sodium chloride was filtered and washed with benzene. The benzene solution was washed with 3x10 mL of 0.1 M KOH and 3x10 mL of water until no yellow color is seen on the wash water. The organic layer was dried over anhydrous sodium sulfate and the solvent removed under reduced pressure to give a yellow oil (4.87 g, 88%). ^{1}H NMR ($CDCl_3$): δ 8.25 (dt, J = 9, 1.8 Hz, 2H), 7.40 (dd, J = 10.7, 2.7 Hz, 2H), 4.25 (q5, $J_{CH} = J_{PH} = 7.1$ Hz, 4H), 1.38 (t, J = 7.1 Hz, 6H).

Synthesis of ethyl *p*-nitrophenyl phosphoric acid (15) [208-212]

To a Schlenk equipped with a magnetic stir bar, was added anhydrous lithium chloride (0.31 g, 7 mmol). The Schlenk was flushed with nitrogen before the addition of anhydrous acetone (50 mL). A solution of **14** in dry acetone (20 mL) was added to the salt solution. Bubbling was observed for a few minutes. The mixture was refluxed for two days before allowing to cool to room temperature. A solvent mixture of 1:2 hexane:ether was added to aid in the precipitation of the lithium salt of **15** upon standing overnight. The white precipitate was filtered and dissolved in a few milliliters of concentrated HCl. The HCl solution was extracted with 4x10 mL of diethyl ether. The combined organic layer was dried over anhydrous sodium sulfate and solvent was removed under reduced pressure to give an oil. The oil was dissolved in a few mL of hot dry ether and addition of a few drops of dry hexanes give an off-white precipitate **15**. Melting point of the solid: 104-6°C (literature [212]: 102-3°C). ^{1}H NMR ($CDCl_3$): δ 8.25 (d, J = 10.7 Hz, 2H), 7.35 (d, J = 10.7, 2H), 4.25 (q5, J = 8 Hz, 2H), 1.38 (t, J = 8Hz, 3H).

Potentiometric Titrations [213]

A typical potentiometric determination of dissociation constant was done as follows: An aqueous solution (10 mL) of the acid form of the ligand (3-4 mM) in the absence of the metal ion (for the determination of the protonation constant of the ligand K_{HL}) or an aqueous solution of the complex (for the determination of the protonation constant of the Cu^{II}-bound hydroxide) (1 mM) in $\mu = 0.10$ in $NaNO_3$ at 25°C, was titrated with a dilute solution (0.1 to 0.2 M) of standardized NaOH. The titration data were treated using a FORTRAN program developed by Martell and Motekaitis [213]. This program is based upon mass balance method commonly used to evaluate the equilibrium constants [213]. The result for the pK_a value of the 2,2'-dipyridylamine ligand (7.075 +

0.018) is comparable to the reported pK_a value (7.14) [200]. All experiments were run at least in triplicate and the tabulated results (Table 7-1) represent the average of these experiments.

Molar Absorptivity of *p*-Nitrophenolate

Solutions of *p*-nitrophenolate in 10% acetonitrile at pH = 10 and $\mu = 0.10$ in $NaNO_3$ were prepared and the absorbance at 400 nm in a 1.0 cm path cell at the temperature used were determined. The molar extinction coefficient was then determined from the plot of the absorbance against concentration

Apparent Acid Dissociation Constant of *p*-Nitrophenol

Solutions of p-nitrophenol, $[p\mathrm{NPOH}]_t$, in 10% acetonitrile at pH = 7.00 and $\mu = 0.10$ in $NaNO_3$ were prepared and the absorbance at 400 nm in a 1.0 cm path cell were determined. Concentration of *p*-nitrophenolate, $[p\mathrm{NPO}\text{-}]_{eq}$, was calculated using Beer's law. The apparent acid dissociation constant, *K*a, is calculated from the eq 7-1.

$$K_a = \frac{[p\mathrm{NPO}^-]_{eq}[\mathrm{H}^+]}{[p\mathrm{NPOH}]_t - [p\mathrm{NPO}^-]_{eq}} \qquad (7\text{-}1)$$

Hydrolysis of *p*-nitrophenyl acetate (*p*NPA)

The initial rate of reaction was measured by following the absorption of the *p*-nitrophenolate ion at 400 nm ($\varepsilon = 19\,238\ \mathrm{M^{-1}cm^{-1}}$). The total amount of product formed was corrected for the degree of ionization of the *p*-nitrophenol at the reaction conditions (apparent $K_a = 5.07 \times 10^{-8}$). The reaction solution was maintained at 25 + 0.1°C and the ionic strength adjusted to 0.10 with $NaNO_3$. The pH of the solution was maintained and checked at 7.00 by using 50 mM HEPES. The substrate, *p*-nitrophenyl acetate, was dissolved in acetonitrile and added last to make a 10% in acetonitrile of reaction mixture.

The *pseudo*-first order rate constants (k_{obs}) were determined from the slopes of the linear plot of total amount of *p*-nitrophenol formed against time (Figure 7-5) and dividing by the initial amount of the substrate used. All experiments were run at least in triplicate and results representing the average of these experiments are tabulated in Table 7-2. The k_{obs} reported were corrected for the background hydrolysis by water (control). Standard errors were generally < 5%.

The second order rate constant, k_{cat}, was determine from the slope of the linear plot of the *pseudo*-first order rate constant, k_{obs}, against the concentration of the active form of the catalyst, $[LCu(OH)^+]_e$. This is assuming that the diaqua form, $[LCu(OH_2)^{2+}]$ does not contribute to catalysis.

Hydrolysis of bis-(*p*-nitrophenyl) phosphate (BNPP)

As with the hydrolysis of *p*NPA, the initial rate of reaction was measured by following the absorption of the *p*-nitrophenolate ion at 400 nm ($\varepsilon = 18\ 697$). The total amount of product formed was corrected for the degree of ionization of the *p*-nitrophenol at the reaction conditions ($K_a = 4.80 \times 10^{-7}$). The reaction solution was maintained at 75 ± 0.1° C and the ionic strength adjusted to 0.10 with $NaNO_3$. The pH of the solution was maintained by using 50 mM HEPES and checked at 75°C to be 6.50.

The *pseudo*-first order rate constants, k_{obs}, for the reaction were determined using the same method described above and the tabulated results (Table 7-3) represent the average from these experiments. Standard errors were generally < 5%. Reported k_{obs} were corrected for the background reaction with water using data obtained by Trogler and coworkers [214]. Compared to the catalyzed reaction, the background was too small and could be considered negligible.

Results and Discussions

Synthesis

Functionalization of the dipyridylamine ligand has been reported by Burkart and coworkers [201,206], Song and Trogler [204],and Addison and coworkers [205]. Their approach was to use an alkyl halide to functionalized the central nitrogen of the dipyridylamine. However, due to the delocalization of the electrons of the central nitrogen in the two pyridine rings, dipyridylamine is a poor nucleophile [201,204,205]. A strong base such as *tert*-butoxide or potassium hydroxide was used to deprotonate the central nitrogen, making it a better nucleophile towards the alkyl halide. The ease of this deprotonation is due to the presence of the electron-withdrawing pyridyl rings and the resonance-stabilized amide formed.

The ease of deprotonation of the central nitrogen is further supported by the observations made in the hydrolysis of **3**. The use of a strong base, even at dilute concentrations such as 2% KOH, cleaved not only the ester bond but also the C-N bond between the alkyl chain and the dipyridylamine. The use of strong acids such as 20% HCl or HBr also cleaved the dipyridylamine. These observations imply that the dipyridylamide is a weaker base compared to other amides and thus, the dipyridylamine makes a good leaving group.

The choice of counter-ion for the amide formation is critical, as has been reported by Burkart [201,206]. Using lithium di-isipropylamide to deprotonate the central nitrogen gives a lower yield by approximately 50%. This may be due to a stronger ion-pair formed between the lithium ion and the amide making the nitrogen less available for nucleophilic attack.

Synthesis of **4** (Figure 7-5) was modeled after the method of Lindsay and Shall [203] to form *N*-hydroxysuccinimidyl acetate. The carboxylic acid **3** is activated for esterification, under mild conditions, by the *N,N'*-dicyclohexylcarbodiimide through the formation of the highly reactive acylurea [215,216], (Figure 7-6). Nucleophilic attack by *N*- hydroxysuccinimide to the acylurea forms the ester **4**. The driving force of this reaction is the precipitation of dicylcohexylurea. Other synthetic routes were tried (Figure 7-7) but these routes failed to form **4**.

Synthesis of the thiol derivative (**7**) (Figure 7-8) was adapted from the methods of Burkart [201] and Richardson and coworkers [206]. In the formation of the thiol derivative of dipyridylamine, a dihalide, 1-bromo-4-chlorobutane, was used. The bromide, being a better leaving group, is displaced by the dipyridylamide to give **5**. To introduce the thiol functionality, **5** was reacted with the xanthate group. The chloride is displaced by the nucleophilic sulfur of the xanthate group to give **6** as the precursor to the thiol. The substituted xanthate is easily cleaved in basic solution to give the thiolate **8** and gaseous thio-carbon dioxide (SCO). The release of the gas provides the driving force for the formation of the thiolate ion.

Synthesis of the unsymmetric disulfide (Figure 7-9) was modeled after the method by Pollack and coworkers [190]. Attempts to synthesize unsymmetric disulfides with a short chain alkane failed. The formation of the symmetric disulfide **10** was more favored. However, reacting the thiol **8** with an aromatic disulfide to do the disulfide exchange gave quantitative amounts of the unsymmetric disulfides. Two aromatic disulfides were used. One contained a possible additional coordinating group, the pyridine ring (**9**). The pyridine ring, in a flexible chain, may bend around to coordinate

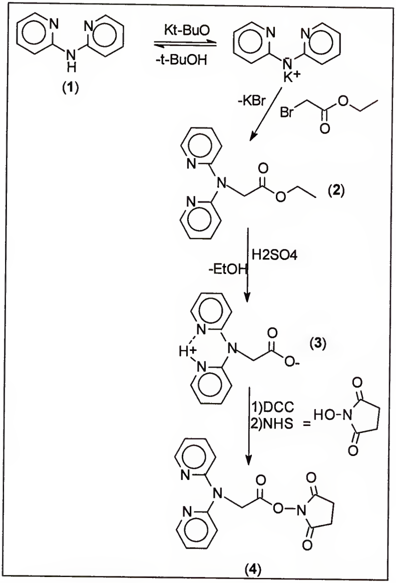

Figure 7-5. Preparation of the *N*-hydroxysuccinimidyl ester derivative of the dipyridylamine ligand

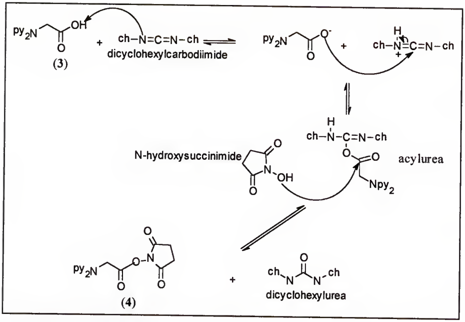

Figure 7-6.. Proposed mechanism for the formation of **4**.

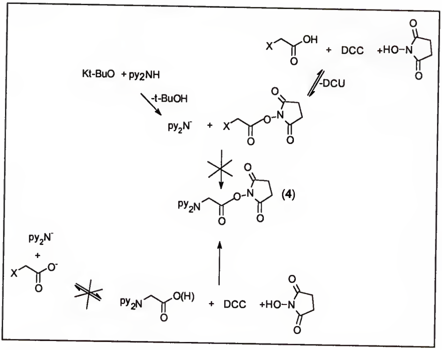

Figure 7-7. Other synthetic routes used to synthesize **4**.

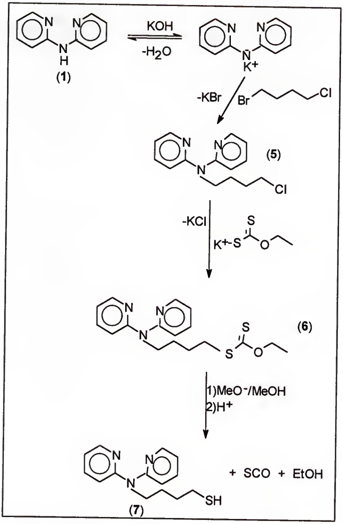

Figure 7-8. Preparation of the thiol derivative of 2,2'-dipyridylamine ligand

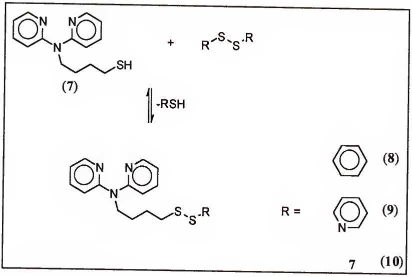

Figure 7-9. Preparation of a disulfide model.

to copper (II) of the same complex molecule or to a copper of another complex molecule. This extra coordination may then reduce the catalytic rate since this may block the coordination of the substrates. It may also act as a general base catalyst for ester hydrolysis that is independent from the catalysis due to the presence of the copper(II) complex. To compare and account for these possibilities, a phenyl group (**8**) was used instead of the pyridine in the unsymmetric disulfide. The phenyl disulfide derivative (**8**) gave a similar compound as that of the pyridine disulfide derivative but does not have the extra coordinating ability.

Ethyl *p*-nitrophenyl phosphoric acid was synthesized (Figure 7-10) as a substrate for a phosphodiester hydrolysis. Trogler and coworkers have synthesized the lithium salt [211], however, presumably the same salt that was synthesized in the lab proved to be hygroscopic and the stoichiometric ratio with the absorbed water was not constant. Synthesis of the acid form was favored since purity was assured although yield was lower.

Kinetics

The hydrolytic activities of the different copper (II) complexes (Figure 7-2) were evaluated by using esters such as *p*-nitrophenyl acetate and bis-(*p*-nitrophenyl)phosphate. Hydrolysis of both esters is slow, thus, the initial rate method was used. Data analysis was limited to within 10% of the extent of the reaction (initial rate method)

Catalyzed ester hydrolyses have been shown to be follow second order kinetics, first order in both the ester substrate and the catalyst concentrations [195]. This can be expressed as eq.7 2.

$$\upsilon = \frac{d[\mathrm{P}]}{dt} = k[\mathrm{ester}][\mathrm{catalyst}] \qquad (7\text{-}2)$$

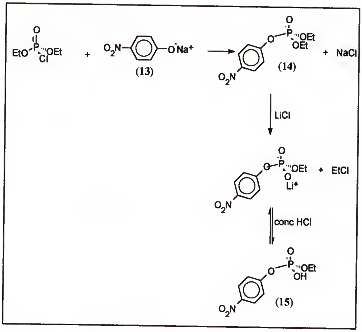

Figure 7-10. Preparation of ethyl p-nitrophenyl phosphoric acid (**15**).

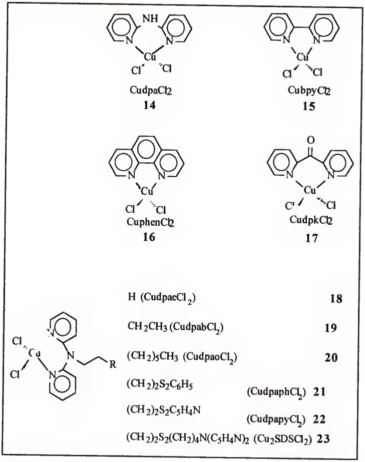
CudpaCl2
14
CubpyCl2
15
CuphenCl2
16
CudpkCl2
17
H (CudpaeCl$_2$) 18
CH$_2$CH$_3$ (CudpabCl$_2$) 19
(CH$_2$)$_5$CH$_3$ (CudpaoCl$_2$) 20
(CH$_2$)$_2$S$_2$C$_6$H$_5$ (CudpaphCl$_2$) 21
(CH$_2$)$_2$S$_2$C$_5$H$_4$N (CudpapyCl$_2$) 22
(CH$_2$)$_2$S$_2$(CH$_2$)$_4$N(C$_5$H$_4$N)$_2$ (Cu$_2$SDSCl$_2$) 23

Figure 7-11. Structures of the different copper (II) complexes synthesized and used.

This observed reaction rate is further divided into four components – catalysis due to hydroxide ions, protons, water, and monohydroxo form of the metal complex (eq.7-3).

$$v = k_{OH}[OH^-][ester] + k_H[H^+][ester] + k_{H2O}[ester] + k_{cat}[LCu(OH)^+][ester] \quad (7\text{-}3)$$

Equation 7-3 can be further simplified by assigning the background (bg) rate as the rate observed in the absence of the metal complex catalyst (eq. 7-4)

$$v = k_{bg}[ester] + k_{cat}[LCu(OH)^+][ester] \qquad (7\text{-}4)$$

where $k_{bg} = k_{OH}[OH^-] + k_H[H^+] + k_{H2O}$.

Since the copper (II) complex catalyst is assumed to be regenerated, the catalyst concentration remains constant. We can then simplify eq. 7-4 to eq. 7-5 and eq. 7-6.

$$v = k_{bg}[ester] + k'[ester] \qquad (7\text{-}5)$$

$$v = k_{obs}[ester] \qquad (7\text{-}6)$$

where $k' = k_{cat}[LCu(OH)^+]$ and $k_{obs} = k_{bg} + k'$. Subtraction of the background rate results in the rate solely due to the presence of the copper (II) complex catalyst. The second order rate constant, k_{cat}, can then be evaluated if the amount of the $LCu(OH)^+$ is known. This is assuming that the catalyst is solely the monohydroxo form, $LCu(OH)^+$, of the complex and the diaqua- form, $LCu(OH_2)^{2+}$, does not contribute to catalysis.

Given the total amount of the copper (II) complex and the acid dissociation constant of the metal complex (Table 7-1), we can then express the k_{cat} as (eq. 7-9)

$$[LCu]_T = [LCu^{2+}]_e + [LCu(OH)^+]_e \qquad (7\text{-}7)$$

$$[LCu(OH)^+]_e = \frac{[LCu]_T}{\frac{[H^+]}{K_a} + 1} \qquad (7\text{-}8)$$

$$k_{cat} = \frac{k'}{[LCu(OH)^+]_e} \qquad (7\text{-}9)$$

Table 7-1. Acid dissociation constants obtained using potentiometric titration and the FORTRAN-77 program by Martell and Motekaitis.

	$\mathrm{p}K_a$ exptl	$\mathrm{p}K_a$ lit
2,2'-dipyridylamine, **1**	7.075 ± 0.018	7.14[200]
12	8.665 ± 0.013	--
Cudpa^{2+}	7.097 ± 0.026	7.2[195]
Cubpy^{2+}	7.044 ± 0.023	7.1[211][i]
Cuphen^{2+}	7.043 ± 0.022	
p-nitrophenol (25°C)	7.087 ± 0.028	7.156[195][ii]
p-nitrophenol (75°C)	6.319 ± 0.048	6.670[211,214]
p-nitrophenol (37°C)	6.887 ± 0.006	

For the hydrolysis of *p*-nitrophenyl acetate (Figures 7-12 and 7-13 and Table 7-2), the observed catalytic rate constant for the original diaqua-2,2'-dipyridylamine copper (II) complex is 0.161 $M^{-1}\ s^{-1}$ using the acid dissociation constant obtained from the potentiometric data ($K_a = 7.998 \times 10^{-8}$). This is identical to the value obtained by Chin and coworkers (0.16 $M^{-1}s^{-1}$) [195].

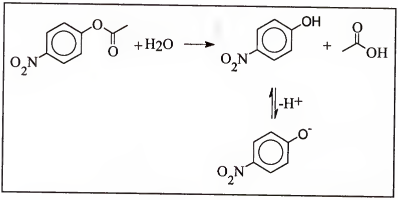

Figure 7-12. Hydrolysis of *p*-nitrophenyl acetate

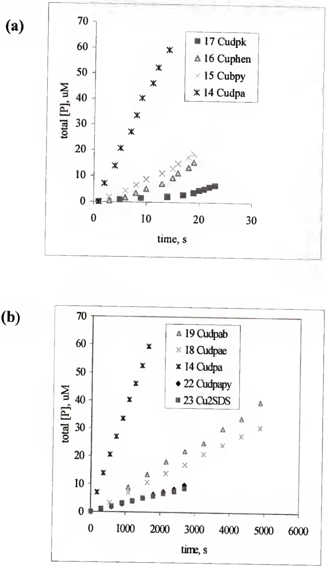

Figure 7-13. Catalyzed hydrolysis of *p*-nitrophenyl acetate by (a) similar pyridine-based copper(II) complexes, **14**, **15**, **16**, and **17**; and by (b) some derivatives of the dipyridylamine copper(II) complexes, **18**, **19**, **22** and **23**. See Table 7-2 for data.

Table 7-2. Catalyzed hydrolysis of *p*-nitrophenyl acetate

	$10^6 k_{obs}$, s^{-1}	k_{cat}, $M^{-1}s^{-1}$
uncatalyzed	2.029 ± 0.081	na
14, $Cudpa^{2+}$	35.871 ± 0.574	0.161
15, $Cubpy^{2+}$	5.100 ± 0.102	0.021
16, $Cuphen^{2+}$	4.021 ± 0.153	0.017
17, $Cudpk^{2+}$	0.614 ± 0.006	
18, $Cudpae^{2+}$	4.162 ± 0.067	
19, $Cudpab^{2+}$	5.460 ± 0.452	
22, $Cudpapy^{2+}$	1.516 ± 0.044	
23, Cu_2SDS^{2+}	1.195 ± 0.074	

Reaction Conditions are : $[LCu^{2+}]_T$= 0.50mM [pNPA] = 1.00 mM in 50 mM HEPES at pH 7.00, $\mu = 0.10$ $NaNO_3$ and 25°C;. Values for k_{obs} are corrected for background rate.

Alternatively, the second-order rate constant can be obtained from the slope of the plot of the *pseudo*-first-order rate constants, k_{obs}, against the concentration of the monohydroxo form of the complex $[LCu(OH)^+]$ (Figure 7-14). The calculated second-order rate constant for the range of 0.10 to 1.0 mM total [LCu] complex is 0.25 $M^{-1}s^{-1}$. As the plot would indicate, it is non-linear. Calculations can be improved if catalysis due to the diaqua form is considered or a possible second-order dependence on the catalyst concentration in the calculation.

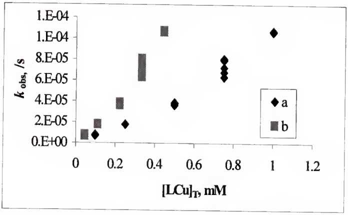

Figure 7-14. Dependence of the k_{obs} on the concentration of the catalyst. The plot of k_{obs} vs. (a) the total amount of [LCu] complex, (b) the amount of the monohydroxo form of the complex, $[LCu(OH)^+]_{eq}$ for the hydrolysis of *p*-nitrophenyl acetate using the original $Cudpa^{2+}$ complex.

Assuming that the catalysis is due to the presence of both the monohydroxo form and the diaqua form of the complex, the k_{obs} for the hydrolysis of *p*-nitrophenyl acetate is given by eq. 7-10.

$$k_{obs} = k_{bg} + k_1[LCu(OH_2)^{2+}] + k_2[LCu(OH)^{+}] \qquad (7\text{-}10)$$

Using equation 7-7, we can then express the k_{obs} in terms of the total amount of catalyst present as eq. 7-11.

$$k_{obs} = k_{bg} + \left(\frac{k_1[H^+] + k_2K_a}{[H^+] + K_a}\right)[LCu]_T \qquad (7\text{-}11)$$

The values for the second-order rate constants can be evaluated using a least square fit to the data. This will also give a kinetic p*K*a value that is expected to be near the experimental value of 7.097.

Using the same conditions, the model complexes were assessed for their catalytic activity. Table 7-2 summarizes the data for the hydrolysis of *p*-nitrophenyl acetate. From the results, under the conditions used, the original diaqua-2,2'-dipyridylamine copper (II) complex is the best hydrolytic catalyst among the copper (II) complexes tested. Changing the central nitrogen into a carbonyl group almost destroys its catalytic activity. Removing the central nitrogen decreases its catalytic activity by almost ten-fold. Alkylation of the central nitrogen, likewise decreases it catalytic activity. However, the length of alkyl chain does not seem to matter.

Preliminary results for the hydrolysis of bis-(*p*-nitrophenyl)phosphate (Figure 7-15 and Table 7-3) showed almost the same trend. The effectiveness of the original copper (II) dipyridylamine seems to lessen at higher temperature. This may be due to the stability of the copper (II) complex at higher temperature. The effectiveness of the original dipyridylamine copper (II) complex (1.0 mM) in the catalysis of the BNPP (0.50

mM) was tested at 25°C and was found to have a k_{obs} of 2.1353 (0.12) x 10^{-5} s^{-1} or an estimated k_{cat} of 0.048 $M^{-1}s^{-1}$.

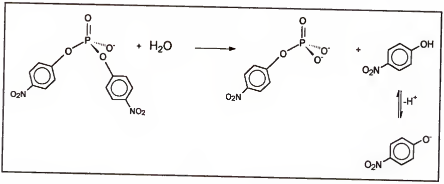

Figure 7-15. Hydrolysis of bis-(*p*-nitrophenyl)phosphate.

Table 7-3. Summary of the catalyzed hydrolysis of bis(*p*-nitrophenyl)phosphate.

	$10^5 k_{obs}$, s^{-1} [a]	est. 10^5 k_{cat}, $M^{-1}s^{-1}$ [b]
14, $Cudpa^{2+}$	4.883 ± 0.234	0.098
15, $Cubpy^{2+}$	1.589 ± 0.080	0.032
19, $Cudpab^{2+}$	2.223 ± 0.018	0.044
23, Cu_2SDS^{2+}	0.333 ± 0.014	0.007

Reaction conditions are as follows: 0.50 mM $[LCu]_T$., 0.50 mM BNPP in 50 mM HEPES at pH 6.5, $\mu = 0.10$ $NaNO_3$ and 75° C.

[a] Values for k_{obs} are corrected for background k_{bg} (0.002E-05 s^{-1})[18].

[b] Values for the k_{cat} are estimated by dividing the k_{obs} with the $[LCu^{2+}]_T$

There are various reasons that may cause this reduction in rate. One factor is the amount of the active species in solution under the reaction conditions. Assuming that the active species is the monohydroxo form of the complex ($LCu(OH)^+$), equilibrium reactions affecting the concentration of the active species affect the rate. The loss of a proton from the diaqua species $LCu(OH_2)_2^{2+}$ is expected to form the active monohydroxo $LCu(OH)^+$ (eq. 7-12), however, this species may then dimerize to form the inactive $(LCu(OH)_2)_2^{2+}$ species (eq. 7-13).

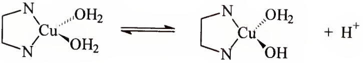

(7-12)

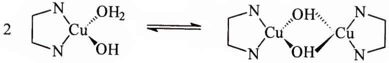

(7-13)

From the potentiometric data (Table 7-1), the acid dissociation constants of the different copper (II) complexes – Cudpa^{2+}, Cubpy^{2+}, Cuphen^{2+} -- do not vary much. Furthermore, the literature stability constant for the formation of the complex LCu^{2+} at 25°C of the Cudpa^{2+} ($pK_{CuL} = 8.05$) [200] does not differ much from that of Cubpy^{2+} ($pK_{CuL} = 8.10$) and Cuphen^{2+} ($pK_{CuL} = 9.00$) [217]. We then expect the difference in the activity for these complexes to be due to the propensity of the complex to form the inactive dimer, $(LCu(OH)_2.)_2$. An attempt to measure the pK_a of coordinated water from the butylated derivative of Cudpa under the same conditions failed to give an inflection point due to precipitation of the hydroxide or dimer form of the complex.

This propensity to form the dimer is further strengthened by the crystal structure obtained from one of the derivatized Cudpa (**19**) shown in Figure 7-16. Comparison of the structure of butylated-Cudpa to the Cudpa and Cubpy is summarized in Table 7-4. The crystal structure of a derivative of the Cudpa^{2+} is shown in Figure 7-16. Comparing the two crystal structures (Figure 7-1 and 7-16), the original copper (II) complex is a distorted tetrahedral [197] whereas the derivative is a distorted square planar. The N(1)-Cu-N(3) bite angle is considerably smaller, from Cudpa 94.8° to Cudpab 86.3°. This

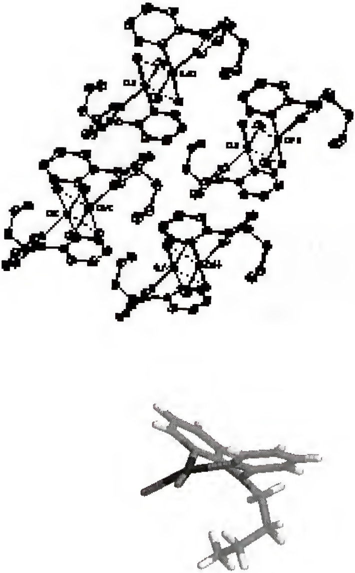

Figure 7-16. Crystal structure of butylated copper (II) dipyridylamine chloride.

can be expected from the nonplanarity of the two pyridine rings allowing the rings to be closer. This nonplanarity may be due to the steric presence of the alkyl chain at the central nitrogen. Also, intermolecular bond distances for the copper complexes are much smaller for the butylated derivative than the original Cudpa complex (2.86 Å vs. 5.09Å). Though these distances are for a solid-state structure, these may also be the case for the aqueous solutions of the complexes. Further proof of the dimer complex has yet to be obtained along with the stability constant for the butylated derivative.

Table 7-4. Selected bond angles and bond distances for copper (II) complexes.

	$CudpaCl_2$[a]	**$CudpabCl_2$**	**$CubpyCl_2$[b]**
Bond angles, °			
N_1-Cu-$N_{3(2)}$	94.8	86.2	80
N_1-Cu-Cl_1	100.1	90.1	93.8
N_1-Cu-Cl_2	133.8	172.7	172.6
C_1-N_2-C_6	134.6	120.4	na
C_1-N_3-C_{11}	Na	118.9	na
C_6-N_2-C_{11}	Na	117.7	na
Intermolecular distance for a dimmer, Å			
Cl_1-Cu-Cl_{2A}	5.091	2.864	3.106

[a]Data obtained from refs [197] and [218]
[b]Data obtained from ref [219].

Another factor to consider is the nucleophilicity of the bound water or hydroxide. It has been proposed by Jencks and coworkers [198,220], that the catalyzed hydrolysis of an activated ester such as *p*-nitrophenyl acetate proceeds through nucleophilic catalysis. Also, the hydrolysis of the bis-(*p*-nitrophenyl)phosphate is proposed to be catalyzed through the intramolecular attack of the bound hydroxide to the bound phosphate [221] (Figure 7-2). Results indicate that the ligand system seems to affects the nucleophilicity of the bound hydroxide.

Conclusions

Functionalization of the 2,2'-dipyridylamine for incorporation to an enzyme was accomplished through alkylation of the central nitrogen. Attachment of the derivatized ligand to the enzyme is possible by using disulfide exchange or an amide bond formation.

Preliminary results seem to suggest that the central nitrogen is important in the catalytic activity of the copper (II) complex. Removing, changing the central nitrogen into another group, or functionalizing it reduces the catalytic activity of the copper (II) complex under the conditions used. The reasons for the reduction in rate are still unknown. Functionalization of the ligand in a site other than the central nitrogen may give us some more insights on its importance. This strategy may also inhibit the dimerization of the hydroxo species.

Variations in the reaction conditions, such as temperature, pH, ionic strength, concentration of the reactant and catalyst species and type of electrolyte, still have to be tried. The pH dependence of the catalysts needs to be studied to be able to optimize the conditions and may prevent dimerization.

APPENDIX A
PROTEOLYTIC DIGEST OF α1-PI

Endoproteinase Lys-C is used for the proteolytic digest of the both native and oxidized α1-PI (see text for procedure). The analysis of the fragments obtained from the digest is accomplished by using the FragESI program to identify the fragments simultaneously with an Excel spreadsheet to help determine the charges (Figure A-1). FragESI program has been developed by Dr. David E. Richardson to help propagate the possible combinations of fragments that would be obtained from an imperfect digest (misses in the lysine cut). The program allows you to choose the maximum number of chains in a single fragment (i.e. how many misses) and allows you to have other counterions besides the proton (i.e., Na^+, NH_4^+) which may be encountered especially in a high-salt containing sample not dialyzed before injection into the HPLC/MS. A sample partial output for the di-oxidized species at fragment 30 (see Figure 3-17 and Table 3-2 in text) is illustrated in Table A-1, wherein two oxygens are added to the mass of fragment 30 corresponding to the oxidation of Met351 and Met358 to methionine sulfoxide. Table A-2 illustrates the data obtained from the HPLC/ESI/QIT-MS of the proteolytic digest for the hydrogen peroxide oxidation of α1-PI in the absence of bicarbonate. From the data in Table A-2, we can then choose a fragment and quantify it by looking at the total areas of the mass ion peak corresponding to that m/z ion and the related m/(z+n) ions.

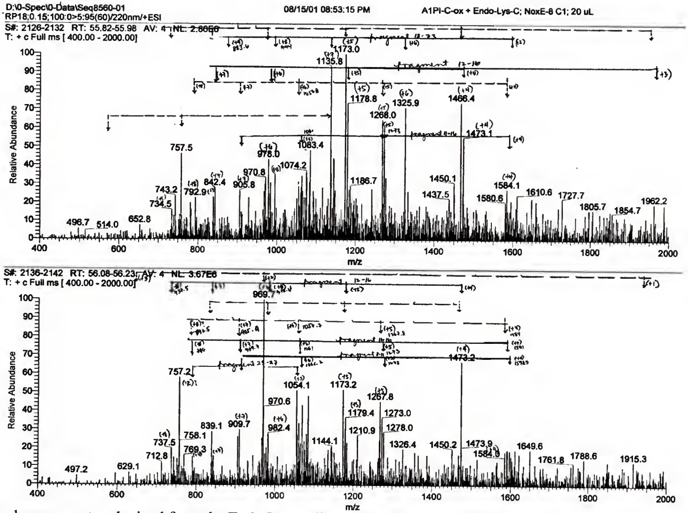

Figure A-1. A typical mass spectra obtained from the Endo Lys-C digest of the oxidized α1-PI. The horizontal lines correlates related m/z ions at different charge states. The solid horizontal lines are those m/z ions corresponding to fragments from α1-PI (unoxidized) and dash lines are "unknown" fragments which may be from impurities (can be checked by comparison with the native protein digest and controls) or a new species from the digest of oxidized α1-PI

Table A-1. Sample partial output from FragESI of a di-oxidized at fragment 30 α1-PI.

Fragment ion prediction for LysC Digest of A1PI di-oxidized M351 and Met358
File written by FragESI32, Version 1.11, D. E. Richardson, University of Florida
Date of file: 3/21/02 Time: 11:29:27 PM

Input Data
Number of input fragments = 34

Input Fragment #	Mass	Maximum charge
1	1058.05	2
2	1779.8	5
3	4806.42	4
4	6249.79	5
5	473.56	2
6	749.85	2
7	146.19	2
8	2058.16	3
9	146.19	2
10	1008.09	2
11	489.52	2
12	685.85	2
13	2090.38	3
14	203.23	2
15	1090.24	3
16	1891.96	3
17	604.83	2
18	1346.62	4
19	146.19	2
20	1076.35	2
21	1755.94	2
22	1804.02	4
23	1912.1	5
24	1110.24	2
25	1015.19	2
26	1833.97	2
27	346.42	2
28	453.54	3
29	888.01	2
30	**2291.61**	**2**
31	407.47	2
32	1466.75	2
33	778.95	2
34	784.92	2

Total number of predicted H+ fragments = 11811
Largest charge = 55
Maximum number of linked fragments in displayed results: 5
Predicted Fragment ions:

Fragment	Frag. m/Z	Charge (Z)	Sequence
1	74.103	2	7 to 7
2	74.103	2	9 to 9
3	74.103	2	19 to 19
4	102.623	2	14 to 14
5	147.198	1	19to 19
6	147.198	1	7 to 7
7	147.198	1	9 to 9
8	152.188	3	28 to 28
9	174.218	2	27 to 27
10	196.495	4	27 to 28
1057	748.001	27	4 to 20
1058	748.254	5	14 to 17
1059	748.871	6	11 to 15
1060	748.946	10	9 to 16
1061	748.990	9	16 to 21
4660	1146.154	12	13 to 23
4661	1146.755	21	12 to 32
4662	1146.813	2	30 to 30
4663	1146.845	29	2 to 24
4664	1147.025	17	14 to 30
4665	1147.367	21	10 to 31

Table A-2. Fragment identification for uncatalyzed hydrogen peroxide oxidized α1-PI.

SAMPLE ID: A1PI-A1-8-ox + Endo-Lys-C = NoxE-8 A1; 20 Ul		Date oxidized: 08/06/01
SEQ NO.: 8559-01	Filename: 8558-01	Date run: 08/15/01

Frag ID	Remarks	RT range	m/z	Z	others
5		4.72-4.88	**474.3**	1	
	blank		416.0		439
8-10			636.0	5	
29			889.5	1	
	blank	5.229-5.53	**416.9**		439
8-10			636.7	5	

(continued)

Frag ID	Remarks	RT range	m/z	Z	others	
32			732.8	2		
	blank	5.98-6.04	**416.9**		439	
8-10			636.6	5		
	blank		586.8			
11-14			684.2	5		
11		8.10-8.28	**489.9**			
	blank		416.8			
33-34			775.4	2		
23-24			501.0	6		
34		8.88-8.93	**785.4**	1		
	blank		587.3			
12			686.3	1		
5			473.3			
1		9.95-10.06	**529.9**	2	1058.4	
34			785.4	1		
	blank		587.3			
1		10.98-11.16	**530.0**	2	1058.4	541.8
31			408.1	1		
	blank	16.50-16.62	**502.0**	2	514.8	
	blank		813.0	2	542	
30	dioxo f30		1147.1	2		
	blank	17.43-17.49	**666.1**	2	444.6	
30-31	dioxo f30		1342.9			
15-20			1011.1	5		
	blank	17.83-17.89	**760.5**	4	1017.16	613.3
	blank		666.0	2	445	
11-13			1617.9	2		
31-32	mono f30		929.2			
5-8			842.8	4	1123.4	674.4
10		18.71-18.77	**505.6**	2	1012	
24-28			1172.6	4	935	
6-13			1210.6	6		
27-29			1651.0	1		
	blank	19.43-	**486.2**			

Frag ID	Remarks	RT range	m/z	Z	others		(continued)
10			505.8	2	1012		
6-9			611.1	5			
	blank		468.9	4	625		
5-7			667.5	2			
	blank	20.02-20.09	**599.3**	3	898		
			657.2	3	985		
			487.4	2	738		
			429.0				
10-15/8-11			914.6				
22		20.58-20.78	**600.8**	3	1831.1	900.7	451
			470.8	4	941	627	
			586.7	4	683	470.8	
17			604.8	1			
		21.29-21.48	**613.9**	3	770.6		
			618.6	2	1238	412.9	
8			688.5	3	516		
			470.9				
18-19		21.75-21.88	**739.4**	2	1480		
			428.1	6	513.9		
			520.8	2	1040.3		
			661.4				
		22.12-22.33	**520.9**	2	1040.4		
18-19			739.3	2	493	1480	
			428.9	4	536		
1-2			470.8	2	940.7		
28-29			661.3	2	441		
1-2			705.1	4	940.7		
5-9			1168.3	3	877		
20-24			1265.6	6			
			1616.3	4	1293		
			1553.3	8	1777		
		22.47-22.54	**436.9**				
1-2			470.9	2	941		
10-11			494.1				
11-13			646.5	5			
			543.9	2			
23			638.4	3	957	479	
12-13			921.1	3	1381	691	

Frag ID	Remarks	RT range	m/z	Z	others		(continued)
			797.5	3	1196		
28-30/15-17			713.8	5			
			1613.4				
			1444.2				
		22.71-22.82	**462.5**	2	923.2		
			463.4				
5			474.5				
		23.10-23.16	**691.9**	2	1383.4		
			692.7	4	1383.4	922	
1-2			566.1	5	705		
			463.2				
1-2		23.33-23.39	**566.1**	5	705		
12-13			692.0	2	1383	462	
31-32			619.0	3	928		
28-30			713.9	5			
10-12			1074.7	2			
6-7		23.58-23.65	**440.1**	2			
1-2			566.4	5	705		
			691.9	2			
11-13			646.5	5			
33-34			776.6	2			
		24.14-24.27	795.3	1			
6-7			410.4	2	880.4		
		24.98-25.42	**706.1**	2	1411.5	471.3	718 new
14-15		25.90-26.06	**638.6**	2	1276.2	426.4	
26-27			721.9	3	1082.4		
			721.9	2	481.7		
10		26.36-26.50	**505.0**	2	1008.3		
14-15			638.6	3	426.4		
			721.9	2	481.7		
12		27.48-27.84	**686.4**	1	708		
5			474.5				
			573.5				
			789.3				
29		28.48-	**888.4**	1			

28.74

Frag ID	Remarks	RT range	m/z	Z	others		(continued)
29			889.4	1	445.1	457	
			718.4				
			855.2				
			605.4				
23		29.10-29.24	**479.2**	2	638.4	957.1	
6			750.4	1			
			888.5	1	444.9		
27-29			551.8	3			
19-20/5-6			603.5				
			835.0				
23			956.5	2	1911.9		
6			751.1	1			
23			479.9	4			
23		29.37-29.83	**638.4**	2	956.8	479.2	
6			750.4	1			
			791.1				
			646.1				
		30.16-30.56	**863.1**	2	576		
			619.0				
6-8			729.9	4			
10-12			717.3	3	1075	538	
23			638.4	3	479.3		
16-20			714.0	7	830	630	
17	mono f17	30.84-31.17	**619.1**	1			
21-30	mono f30		653.1	6	559		
			511.0	3	765.9		
29			772.5	3	1158	580	
13			697.0	3			
			480.3				
7-9		31.58-31.88	**579.8**	4	772.4	1158.7	
11-12			579.8	2	1157.7		
			627.1				
			654.3	3	980.7	491.2	
			863.1				
			966.7				
18?		32.13-32.37	**677.2**	2	1354	452.1	

(continued)

Frag ID	Remarks	RT range	m/z	Z	others			
			619.1	2	1237.6			
7-9			579.7	4	1157.8	772.4		
		32.54-32.70	**619.1**	1				
7-9			772.1	3	1158.2	579.8		
			677.1	2	452			
			863.2	2	1725	575.9		
16			945.4	2	1887	630		
			964.5					
		33.46-33.93	**611.2**	2	1220.5	407.9		
			932.6					
			855.1					
7-9			772.3	3	1157.7	580		
		34.07-34.39	**855.1**	2	1709.6	570		
			611.1	2	1221.6			
			575.5	2	1149.5			
			932.7					
			866.9					
7-9			772.3	3	1158	280		
			501.1					
1-2			705.1	4				
		34.48-34.69	**855.3**	2	570			
			575.7	2	1149.4			
17-20			781.2	4	624.5			
			611.2					
8-9/7-8			729.7	3	1094	547.7		
7-9			772.0	3	1105	677		
			797.0					
			867.0					
			933.0	2	1865.7			
22		34.99-35.35	**902.8**	2	1804.8	602.4	452.2	914.6
8			685.1	3	1026.6			
			624.6					
			571.8					
		35.53-35.63	**991.4**					
22			602.5	3	902.8	452.5		
25			1015.2	1	508.4			
12			685.2	1				
17-20			781.5	4	1561.4	1041.1		

Frag ID	Remarks	RT range	m/z	Z	others	(continued)
		35.95-36.15	**991.4**			
			992.4			
			1005.3			
			1006.4			
22			902.9	2	603.1	452.1
			595.6			
8-9/7-8			729.8	3	1093.8	
17-20			781.4	4	1041.7	
12			685.0	1		
25			508.4	2	1015	
22		36.54-36.69	**602.6**	3	903.6	452
16			946.6	2	631	
17-20			781.0	4	1041.1	
7-9			772.4	3	1161	580
10-11			494.8	3	741.6	
19-20			1203.4	1		
16		36.64-37.01	**946.6**	2	631	958.5
10-11			494.9	3	741.5	1482
22			602.5	3		
5			474.1	1		
			869.2			
			788.2			
24		37.41-37.66	**556.1**	2	1110.4	557.1
			797.3			
25			508.6	2	1015	
25		37.85-38.06	**508.6**	2	1015.5	
24			556.0	2	1110.4	
			829.4			
25		38.37-38.51	**508.7**	2	1015.5	
24			556.1	2	1110	
16-21/5-30	mono f30		841.4	8	962.8	
			642.3			
			829.5			
		38.81-39.13	**731.6**	2	1461.4	
8-9/7-8			**731.6**	3	1096	539
15			547.1	2	1092.5	

(continued)

Frag ID	Remarks	RT range	m/z	Z	others	
			710.2	2	1418.6	
		39.31-39.69	**625.0**	3	1872.7	936.7
			731.6	2	1461.3	
			910.8			
15			547.0			
26		40.30-40.80	**917.7**	2	1833.8	
			718.1	2	1434.4	
			793.6			
25		41.59-41.83	**1013.3**	1	507.5	
22			909.2	2		
			749.1			
22		41.98-42.23	**909.2**	2		
			1013.4	1	507.6	
			749.3	3	1122.5	601.9
			793.9			
10-11		42.85-43.51	**742.2**	2	1482.4	496.7
			496.7	2	991.6	
26			918.2	2		
25			507.6	2	1013.9	
26		43.90-44.16	**918.2**	2	1834.6	
			496.6	2	991.6	
10-11			742.3	2	496.7	
			619.6			
			735.1			
		45.04-45.38	**595.7**	2	1189.8	
15-18	mono f18		1634.5	3	1226.2	
10-11			742.1	2	496.6	
			496.7	2	991.7	
17			606.6	1		
30-31	mono f30	45.92-46.25	**1334.2**	2		
			646.0	2	1292.6	
			496.7	2	991.6	
10-11			496.7	3	742.4	
2			595.7	3	893.9	447.1
			983.5	2	657	
15-18/30-33/17-21	mono		1628.8	3	1265	

Frag ID	Remarks	RT range	m/z	Z	others		(continued)	
31-32			1855.7	1	929			
			1154.8					
17-19	mono f18	46.65-46.76	**694.7**	3	1387.2			
17-19			1034.6	2	775			
			705.9	4	741	565		
30-31	mono f30		1334.3	2				
			983.4					
			828.4	3	1242			
10-14			735.0	6	882	630		
			1064.7					
			1121.9					
			595.6	3	893	447		
		47.41-47.61	**1023.2**	2	682.9			
			936.1	2	625			
			951.8	3	714			
			1035.1	4	828			
			596.0	3	893.3			
			742.1					
30	dioxo f30	48.16-48.29	**1146.3**	2	764.7	1158.4		
30	dioxo f30	48.41-48.80	**1146.4**	2	764.7	1158.9	1153.4	
25			1013.6	1	507.6			
30	dioxo f30	48.97-49.60	**1146.3**	2	764.8			
			863.2	2	1724.8			
			933.0					
			1099.1					
			1386.2					
18-19	mono f18	50.11-50.30	**748.2**	2	1494.5			
		50.87-51.13	**894.1**	3	1340.7	671		
22			902.0	2				
			1036.7					
18-19			748.1	2				
18-20	mono f18		851.9	3	1277			
			497.2	2	997			
14-19		52.87-53.10	**1299.1**	4	1731.8	1039.8	866.9	743.2
30-34	mono f30		1130.2	5	1411.6			
13-16			1306.2	4	1741	1045	871	745

Frag ID	Remarks	RT range	m/z	Z	others		(continued)			
13-16		53.37-53.65	**1306.2**	4	1741.7	1045.3	871.4	747.3		
14-19			1299.2	4	1732	1039.7	866.8	743		
30-34			1126.0	5	1406.9	936				
			1134.9	5	1408.2					
13-16		53.93-54.14	**1045.5**	5	1742	1306.7	871.4	747.8		
14-19			1299.0	5	1040	867	743			
13-15			838.0	4	1675.6	1116.9	670.9	559		
27-30/8-12	dioxo f30		1078.2	4	1437.1	862				
5-11			992.7	5	1241	827				
7-9			1158.1	2	772.7					
30-34			1407.2	4	1126	938				
			496.5	2	992.7					
			1367.0							
			596.0							
			1170.6							
30-32		54.34-54.68	**1025.3**	4	1366.5					
16-17			828.1	3	1241.6					
16-20/15-19n	mono f18		772.8	3	1158					
			1003.9	5	1306					
		54.98-55.40	**1267.5**	5	1584	1056.4	905.8	792.6	704.6	
11-16			1272.7	5	1591.5	1061	908	797	708.1	
			1173.2	5	1963	1465.9	977.9	838.4	734	652.6
12-16			1178.2	5	1472.1	982	843			
30-32			1366.9	3	1025					
			1072.3							
30-31			1325.6	2						
12-16			1179.2	5						
		55.40-55.70	**1173.2**	5	1954.4	1466.1	978	838.5	734	652.8
12-16			1473.0	4	1962	1178	982.7	842.5	736	655
			1267.5	5	1583.9	1056	905	792.9	704.8	
11-16			1273.2	5	1591.9	1061.1	908	797	708	
30-31			1325.5	2						
30-32			1367.0	3	1025					
5-9			1748.7	2						
12-16			1178.7	5	1964.1	1473.5	982.6	842.9	737.8	655
			1173.1	5	1954	1466.2	978.1	838	727	652

ID										
			1173.1	5	1954	1466.2	978.1	838	727	652
11-16			1273.1	5	1590.9	1061.8	909.9	796.1		
12-16		56.04-56.18	**1178.7**	5	1964.1	1473.5	982.6	842.9	737.8	655
11-16			1273.1	5	1590.9	1061.8	909.9	796.1	706	
			1173.1	5	1954	1466.2	978.1	838	733	652
			1267.3	5	1584	1056	906	792.6	733	
5-11			1656.2	3	1242	994				
			1069.2							
28-31	mono f30	56.46-56.78	**1321.3**	3	1981.1					
12-16			1178.9	5	1473.8	983.2	842.5			
11-16			1061.4	6	1591	1273	909			
			1267.6	5	1585	1056				
28-31	dioxo f30		1328.9	3						
27-29			1652.7	1						
29-33d/26-30m	f 30	57.57-57.81	**1437.9**	4	1916.3	1150.5				
11-16			1273.2	5	1591	1061	909.9	797	706	
			1267.9	5	1584	1056	907	838		
			1437.3							
32			1467.8	1						
20-21		58.26-58.46	**938.2**	3	1406.5					
17-18	mono f18		977.4	2	651.8					
11-16			1274.3	5	1591	1061				
29-33	mono f30		1437.8	4	1917	1150				
			1571.9	4	1258	1054.7				
			1267.0	5	1584	1056				
28-30			1188.9	3	1585	892				
30-32			1366.4	3	1026					
			529.2	4	706	424.1				
13		59.54-59.71	**1045.9**	2	697.7	1057.8				
12-13		60.27-60.64	**920.3**	3	1380	689.2				
24-28			1175.6	4	1567	941				
			1654.2	3	1240.8					
13			1045.9	2	698.2					
			1603.6							
			1418.4							
			1376.0							
21		62.61-62.88	**1757.5**	1						

(continued)

Frag ID	Remarks	RT range	m/z	Z	others	
10-13/20-21			1406.4	3 or 2		
			929.8	3	1379.4	692
20-29			1722.0	7	1523.3	
11-13			1617.4	3	1212	1079
15-16			1485.8	2		
			1289.5			
			1153.2			
			1048.4			
			1706.6			
13		63.39-63.66	**1045.5**	5	1307	871
			1692.0			
			1758.3	4	1406	1172
			1767.2			

APPENDIX B
^{1}H NMR SPECTRA OF DIPYRIDYLAMINE LIGANDS

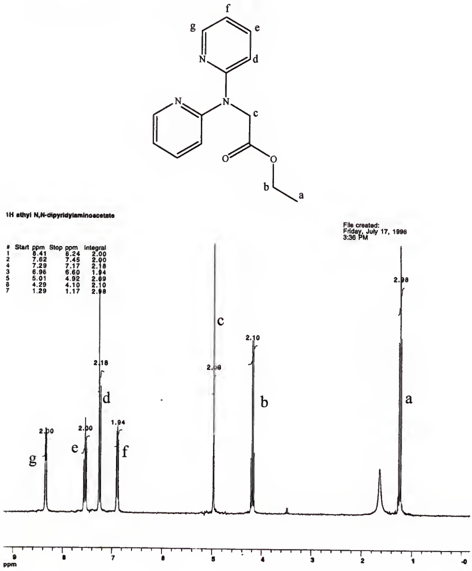

#	Start ppm	Stop ppm	Integral
1	8.41	8.24	2.00
2	7.62	7.45	2.00
4	7.29	7.17	2.18
3	6.96	6.60	1.94
5	5.01	4.92	2.09
6	4.29	4.10	2.10
7	1.29	1.17	2.98

Figure B-1. ^{1}H NMR of ethyl *N,N*-(2',2'-dipyridyl)aminoacetate (**2**).

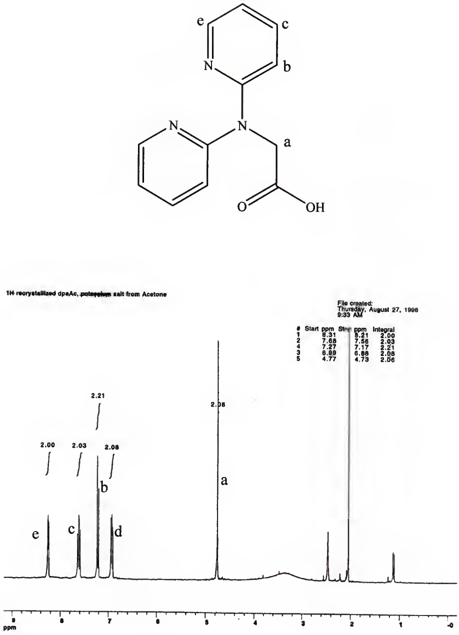

```
1H recrystallized dpaAc, ~~potassium~~ salt from Acetone

File created:
Thursday, August 27, 1998
9:33 AM

# Start ppm Stop ppm Integral
1       8.31     8.21     2.00
2       7.68     7.56     2.03
4       7.27     7.17     2.21
3       6.99     6.88     2.08
5       4.77     4.73     2.06
```

Figure B-2. ^{1}H NMR of *N,N*-(2',2'-dipyridyl)aminoacetic acid (**3**).

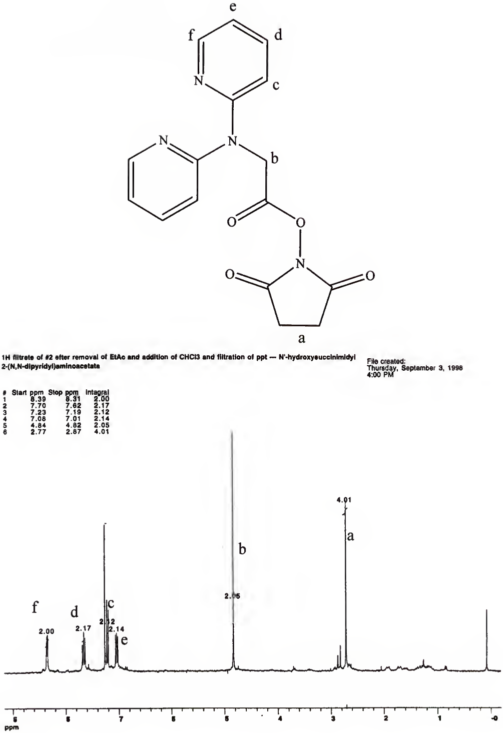

1H filtrate of #2 after removal of EtAc and addition of CHCl3 and filtration of ppt — N'-hydroxysuccinimidyl 2-(N,N-dipyridyl)aminoacetate

File created:
Thursday, September 3, 1998
4:00 PM

#	Start ppm	Stop ppm	Integral
1	8.39	8.31	2.00
2	7.70	7.62	2.17
3	7.23	7.19	2.12
4	7.08	7.01	2.14
5	4.84	4.82	2.05
6	2.77	2.87	4.01

Figure B-3. ^{1}H NMR of *N*-hydroxysuccinimidyl *N,N*-(2',2'-dipyridyl)aminoacetate (**4**).

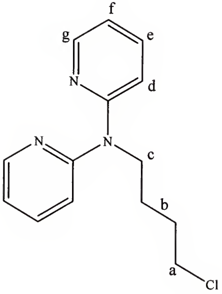

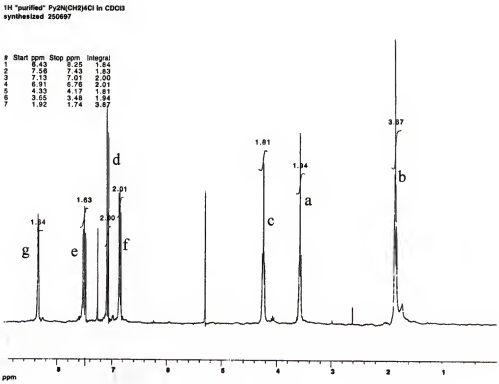

1H "purified" Py2N(CH2)4Cl in CDCl3
synthesized 250697

#	Start ppm	Stop ppm	Integral
1	8.43	8.25	1.84
2	7.56	7.43	1.83
3	7.13	7.01	2.00
4	6.91	6.76	2.01
5	4.33	4.17	1.81
6	3.65	3.48	1.94
7	1.92	1.74	3.87

Figure B-4. ^{1}H NMR of *N*-(4-chloro)butyl-2',2'-dipyridylamine (**5**).

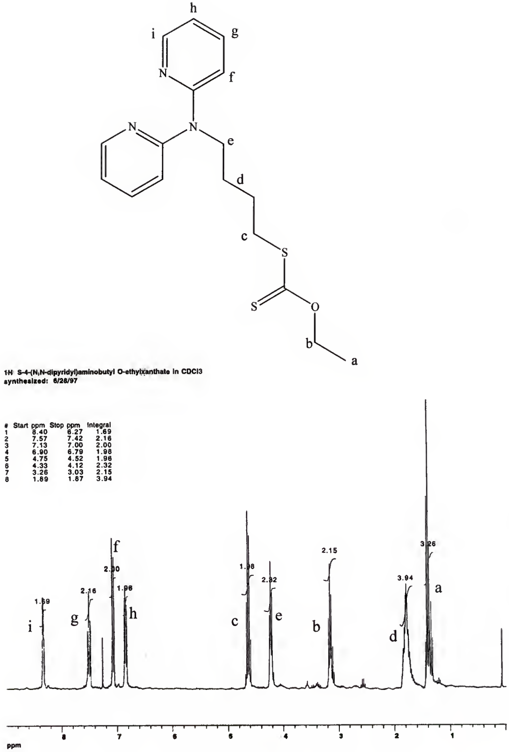

1H S-4-(N,N-dipyridyl)aminobutyl O-ethylxanthate in CDCl3
synthesized: 6/26/97

#	Start ppm	Stop ppm	Integral
1	8.40	8.27	1.69
2	7.57	7.42	2.16
3	7.13	7.00	2.00
4	6.90	6.79	1.98
5	4.75	4.52	1.96
6	4.33	4.12	2.32
7	3.26	3.03	2.15
8	1.89	1.87	3.94

Figure B-5. ^{1}H NMR of *O*-ethyl *S*-4-(*N,N*-2',2'-dipyridyl)aminobutylxanthate (**6**).

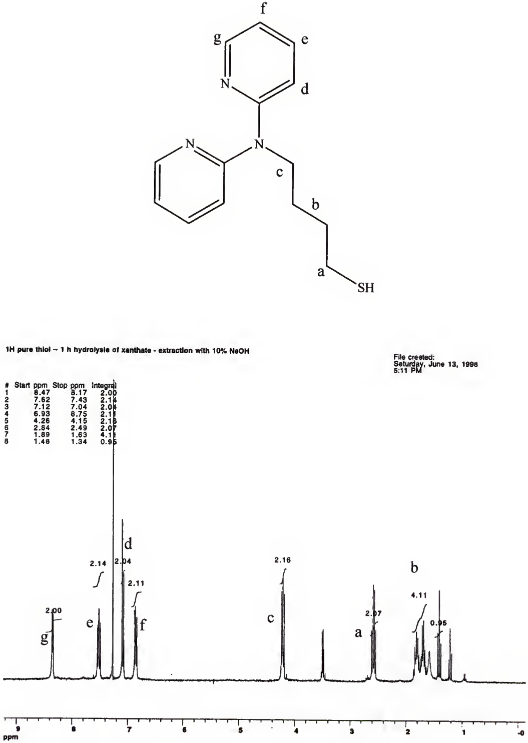

1H pure thiol -- 1 h hydrolysis of xanthate - extraction with 10% NaOH

File created:
Saturday, June 13, 1998
5:11 PM

#	Start ppm	Stop ppm	Integral
1	8.47	8.17	2.00
2	7.62	7.43	2.14
3	7.12	7.04	2.04
4	6.93	6.75	2.11
5	4.26	4.15	2.16
6	2.84	2.49	2.07
7	1.89	1.63	4.11
8	1.48	1.34	0.95

Figure B-6. ^{1}H NMR of 4-mercapto-*N,N*-(2',2'-dipyridyl)butanamine (**7**).

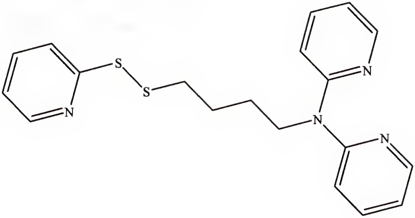

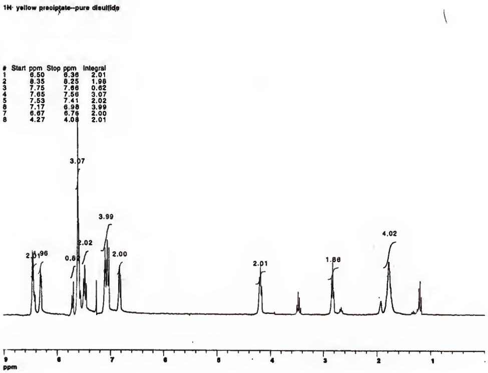
1H· yellow precipitate--pure disulfide

#	Start ppm	Stop ppm	Integral
1	8.50	8.36	2.01
2	8.35	8.25	1.96
3	7.75	7.66	0.62
4	7.65	7.56	3.07
5	7.53	7.41	2.02
6	7.17	6.98	3.99
7	6.87	6.76	2.00
8	4.27	4.08	2.01

Figure B-7. ^{1}H NMR of 4-*N*,*N*-(2’,2’-dipyridyl)aminobutyl pyridyl disulfide (**9**).

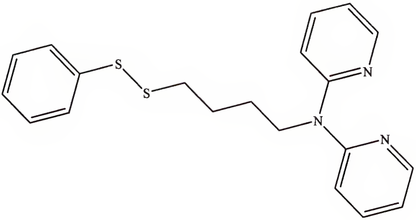

1H attempted purification of dpeph using deactivated silica (10% water)

File created:
Friday, October 2, 1998
4:11 PM

#	Start ppm	Stop ppm	Integral
1	8.38	8.29	1.75
2	7.54	7.47	2.88
4	7.47	7.44	0.48
3	7.34	7.24	1.75
7	7.23	7.15	0.83
5	7.08	7.00	1.82
6	6.89	6.79	1.75
8	4.22	4.15	2.00
9	2.82	2.74	1.92
10	1.84	1.68	4.03

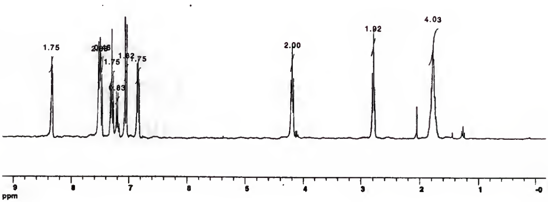

Figure B-8. ^{1}H NMR of 4-*N,N*-(2',2'-dipyridyl)aminobutyl phenyl disulfide (**8**).

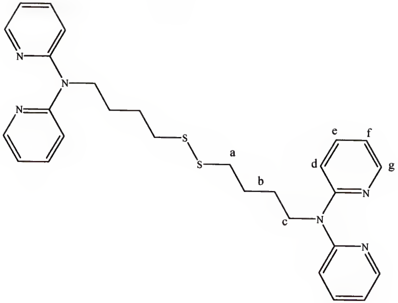

1H attempted purification of dpaph using deactivated silica (10% H2O) – slowest band (lowest Rf)

SYMMETRIC DISULFIDE

File created:
Friday, October 2, 1998
4:33 PM

#	Start ppm	Stop ppm	Integral
1	8.36	8.28	2.02
2	7.53	7.45	2.13
3	7.09	7.04	2.11
4	6.88	6.80	2.04
5	4.27	4.15	2.54
6	2.73	2.83	2.38
7	1.81	1.68	4.51

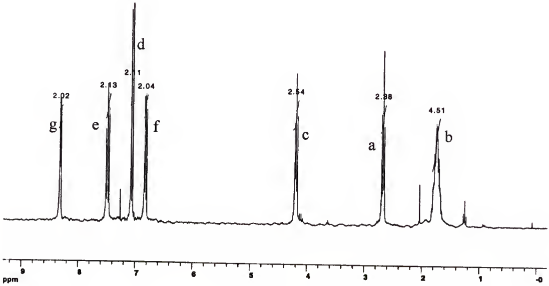

Figure B-9. ^{1}H NMR of 4-*N*,*N*-(2',2'-dipyridyl)aminobutyl disulfide.

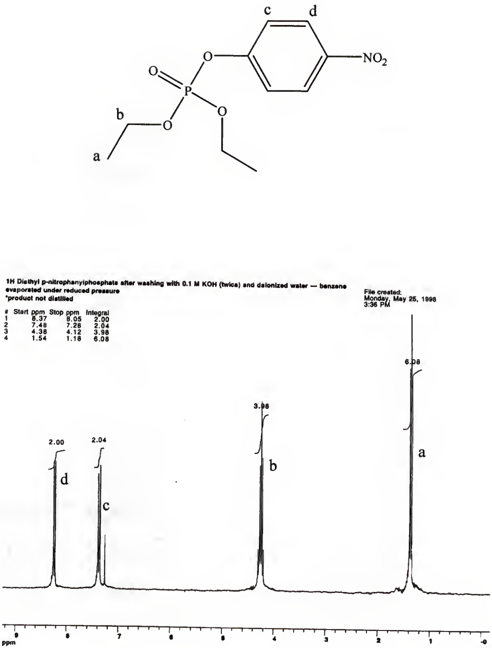

1H Diethyl p-nitrophenylphosphate after washing with 0.1 M KOH (twice) and deionized water — benzene evaporated under reduced pressure
*product not distilled

File created:
Monday, May 25, 1998
3:36 PM

#	Start ppm	Stop ppm	Integral
1	8.37	8.05	2.00
2	7.48	7.28	2.04
3	4.38	4.12	3.98
4	1.54	1.18	6.08

Figure B-10. ^{1}H NMR of diethyl *p*-nitrophenylphosphate (**14**).

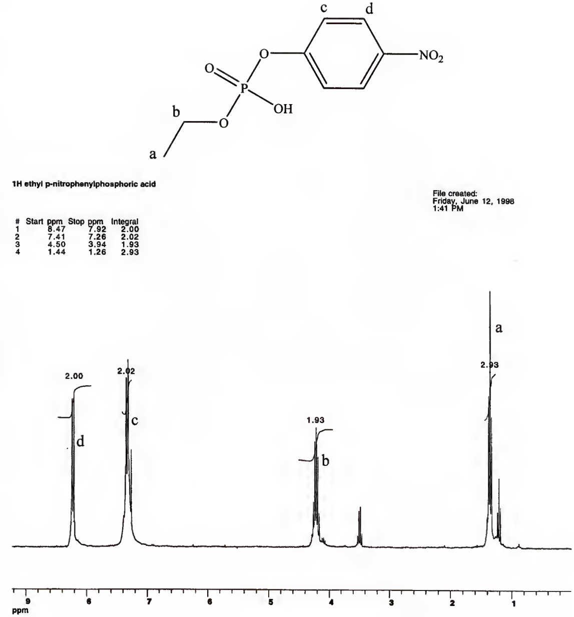

1H ethyl p-nitrophenylphosphoric acid

File created:
Friday, June 12, 1998
1:41 PM

#	Start ppm	Stop ppm	Integral
1	8.47	7.92	2.00
2	7.41	7.26	2.02
3	4.50	3.94	1.93
4	1.44	1.26	2.93

Figure B-11. ^{1}H NMR of ethyl *p*-nitrophenylphosphate (**15**)

APPENDIX C
CRYSTAL DATA FOR Cu(dpab)Cl_2 (19)

Table C-1. Crystal data and structure refinement for CudpabCl_2 (19).

Identification code	reg1	
Empirical formula	C14 H17 Cl2 Cu N3	
Formula weight	361.75	
Temperature	173(2) K	
Wavelength	0.71073 Å	
Crystal system	Monoclinic	
Space group	P2(1)/n	
Unit cell dimensions	a = 8.6359(5) Å	a= 90°.
	b = 9.0949(5) Å	b= 93.074(1)°.
	c = 19.286(1) Å	g = 90°.
Volume	1512.59(14) Å^3	
Z	4	
Density (calculated)	1.589 Mg/m^3	
Absorption coefficient	1.789 mm^{-1}	
F(000)	740	
Crystal size	0.06 x 0.12 x 0.32 mm^3	
Theta range for data collection	2.11 to 27.49°.	
Index ranges	-11<=h<=10, -11<=k<=11, -25<=l<=21	
Reflections collected	10854	
Independent reflections	3461 [R(int) = 0.0297]	
Completeness to theta = 27.49°	99.6 %	
Absorption correction	Integration	
Max. and min. transmission	0.8866 and 0.7166	
Refinement method	Full-matrix least-squares on F^2	
Data / restraints / parameters	3461 / 0 / 182	
Goodness-of-fit on F^2	1.015	
Final R indices [I>2sigma(I)]	R1 = 0.0236, wR2 = 0.0571 [2944]	
R indices (all data)	R1 = 0.0318, wR2 = 0.0606	
Extinction coefficient	0.0021(4)	
Largest diff. peak and hole	0.332 and -0.271 e.Å^{-3}	

Table C-2. Atomic coordinates (x 10^4) and equivalent isotropic displacement parameters (Å^{2}x 10^3) for reg1. U(eq) is defined as one third of the trace of the orthogonalized U^{ij} tensor.

	x	y	z	U(eq)
Cu	4720(1)	4152(1)	865(1)	20(1)
Cl1	3938(1)	5977(1)	1556(1)	34(1)
Cl2	6722(1)	5497(1)	498(1)	25(1)
N1	2839(2)	2992(2)	1065(1)	22(1)
C1	2941(2)	1741(2)	1431(1)	21(1)
C2	1613(2)	1083(2)	1680(1)	28(1)
C3	190(2)	1722(2)	1522(1)	32(1)
C4	80(2)	2981(2)	1120(1)	30(1)
C5	1428(2)	3586(2)	909(1)	26(1)
N3	5705(2)	2201(2)	638(1)	19(1)
C6	5449(2)	996(2)	1020(1)	20(1)
C7	6178(2)	-339(2)	893(1)	24(1)
C8	7178(2)	-429(2)	360(1)	27(1)
C9	7416(2)	809(2)	-45(1)	27(1)
C10	6649(2)	2078(2)	103(1)	23(1)
N2	4410(2)	1115(2)	1559(1)	22(1)
C11	4678(2)	148(2)	2174(1)	25(1)
C12	6271(2)	427(2)	2529(1)	28(1)
C13	6533(2)	2001(2)	2764(1)	38(1)
C14	5392(3)	2493(3)	3292(2)	57(1)

Table C-3. Bond lengths [Å] and angles [°] for reg1.

Cu-N1	1.9918(14)
Cu-N3	2.0256(14)
Cu-Cl1	2.2551(5)
Cu-Cl2	2.2627(5)
N1-C1	1.339(2)
N1-C5	1.352(2)
C1-N2	1.401(2)
C1-C2	1.402(2)
C2-C3	1.379(3)
C2-H2A	0.9500
C3-C4	1.383(3)
C3-H3A	0.9500
C4-C5	1.369(3)
C4-H4A	0.9500
C5-H5A	0.9500

Table C-3. Bond lengths [Å] and angles [°] for reg1 (continued).

N3-C6	1.345(2)
N3-C10	1.354(2)
C6-C7	1.396(2)
C6-N2	1.413(2)
C7-C8	1.379(3)
C7-H7A	0.9500
C8-C9	1.391(3)
C8-H8A	0.9500
C9-C10	1.368(2)
C9-H9A	0.9500
C10-H10A	0.9500
N2-C11	1.484(2)
C11-C12	1.525(3)
C11-H11A	0.9900
C11-H11B	0.9900
C12-C13	1.515(3)
C12-H12A	0.9900
C12-H12B	0.9900
C13-C14	1.521(3)
C13-H13A	0.9900
C13-H13B	0.9900
C14-H14A	0.9800
C14-H14B	0.9800
C14-H14C	0.9800
N1-Cu-N3	86.24(6)
N1-Cu-Cl1	90.11(4)
N3-Cu-Cl1	156.18(4)
N1-Cu-Cl2	172.69(5)
N3-Cu-Cl2	93.99(4)
Cl1-Cu-Cl2	92.569(18)
C1-N1-C5	119.35(15)
C1-N1-Cu	121.37(11)
C5-N1-Cu	118.66(12)
N1-C1-N2	118.17(15)
N1-C1-C2	120.77(16)
N2-C1-C2	121.05(16)
C3-C2-C1	118.68(18)
C3-C2-H2A	120.7
C1-C2-H2A	120.7
C2-C3-C4	120.45(17)
C2-C3-H3A	119.8
C4-C3-H3A	119.8
C5-C4-C3	117.77(18)

Table C-3. Bond lengths [Å] and angles [°] for reg1 (continued).

C5-C4-H4A	121.1
C3-C4-H4A	121.1
N1-C5-C4	122.91(18)
N1-C5-H5A	118.5
C4-C5-H5A	118.5
C6-N3-C10	118.33(15)
C6-N3-Cu	120.76(11)
C10-N3-Cu	120.90(12)
N3-C6-C7	121.50(15)
N3-C6-N2	118.10(15)
C7-C6-N2	120.41(15)
C8-C7-C6	119.29(17)
C8-C7-H7A	120.4
C6-C7-H7A	120.4
C7-C8-C9	119.14(16)
C7-C8-H8A	120.4
C9-C8-H8A	120.4
C10-C9-C8	118.60(16)
C10-C9-H9A	120.7
C8-C9-H9A	120.7
N3-C10-C9	123.07(17)
N3-C10-H10A	118.5
C9-C10-H10A	118.5
C1-N2-C6	120.39(14)
C1-N2-C11	118.86(14)
C6-N2-C11	117.70(14)
N2-C11-C12	110.96(14)
N2-C11-H11A	109.4
C12-C11-H11A	109.4
N2-C11-H11B	109.4
C12-C11-H11B	109.4
H11A-C11-H11B	108.0
C13-C12-C11	114.11(16)
C13-C12-H12A	108.7
C11-C12-H12A	108.7
C13-C12-H12B	108.7
C11-C12-H12B	108.7
H12A-C12-H12B	107.6
C12-C13-C14	112.79(18)
C12-C13-H13A	109.0
C14-C13-H13A	109.0
C12-C13-H13B	109.0
C14-C13-H13B	109.0

Table C-3. Bond lengths [Å] and angles [°] for regl (continued).

H13A-C13-H13B	107.8
C13-C14-H14A	109.5
C13-C14-H14B	109.5
H14A-C14-H14B	109.5
C13-C14-H14C	109.5
H14A-C14-H14C	109.5
H14B-C14-H14C	109.5

Symmetry transformations used to generate equivalent atoms:

Table C-4. Anisotropic displacement parameters ($Å^2$x 10^3)for regl. The anisotropic displacement factor exponent takes the form: $-2p^2[\ h^2a^{*2}U^{11} + ... + 2\ h\ k\ a^*\ b^*\ U^{12}\ ]$

	U^{11}	U^{22}	U^{33}	U^{23}	U^{13}	U^{12}
Cu	22(1)	17(1)	23(1)	1(1)	4(1)	-1(1)
Cl1	43(1)	28(1)	32(1)	-9(1)	13(1)	-3(1)
Cl2	24(1)	21(1)	29(1)	2(1)	3(1)	-4(1)
N1	20(1)	22(1)	24(1)	-1(1)	3(1)	0(1)
C1	21(1)	22(1)	19(1)	-3(1)	2(1)	-2(1)
C2	26(1)	28(1)	28(1)	-1(1)	5(1)	-7(1)
C3	21(1)	38(1)	39(1)	-7(1)	8(1)	-6(1)
C4	20(1)	39(1)	31(1)	-10(1)	1(1)	3(1)
C5	25(1)	28(1)	26(1)	-2(1)	1(1)	5(1)
N3	19(1)	18(1)	20(1)	0(1)	1(1)	-1(1)
C6	19(1)	21(1)	20(1)	-1(1)	-3(1)	-2(1)
C7	29(1)	18(1)	26(1)	1(1)	-3(1)	1(1)
C8	27(1)	24(1)	29(1)	-6(1)	-4(1)	5(1)
C9	26(1)	30(1)	25(1)	-7(1)	4(1)	-1(1)
C10	24(1)	24(1)	21(1)	-1(1)	2(1)	-4(1)
N2	22(1)	22(1)	21(1)	5(1)	2(1)	-2(1)
C11	31(1)	21(1)	23(1)	6(1)	2(1)	-5(1)
C12	30(1)	27(1)	26(1)	8(1)	-1(1)	0(1)
C13	40(1)	30(1)	44(1)	5(1)	-16(1)	-9(1)
C14	43(1)	36(1)	88(2)	-26(1)	-20(1)	9(1)

Table C-5. Hydrogen coordinates (x 10^4) and isotropic displacement parameters ($Å^2$x 10^3) for reg1.

	x	y	z	U(eq)
H2A	1691	214	1953	33
H3A	-721	1295	1690	39
H4A	-897	3411	995	36
H5A	1369	4463	641	32
H7A	5988	-1177	1170	29
H8A	7698	-1324	271	32
H9A	8095	773	-416	32
H10A	6786	2913	-184	27
H11A	4601	-894	2027	30
H11B	3867	333	2507	30
H12A	6406	-228	2937	33
H12B	7074	164	2203	33
H13A	6436	2658	2355	46
H13B	7601	2098	2972	46
H14A	5611	3515	3427	85
H14B	5498	1861	3703	85
H14C	4332	2422	3086	85

Table C-6. Torsion angles [°] for reg1.

N3-Cu-N1-C1	44.01(13)
Cl1-Cu-N1-C1	-112.44(13)
Cl2-Cu-N1-C1	136.0(3)
N3-Cu-N1-C5	-145.03(14)
Cl1-Cu-N1-C5	58.52(13)
Cl2-Cu-N1-C5	-53.0(4)
C5-N1-C1-N2	177.20(15)
Cu-N1-C1-N2	-11.9(2)
C5-N1-C1-C2	-3.0(3)
Cu-N1-C1-C2	167.90(13)
N1-C1-C2-C3	2.1(3)
N2-C1-C2-C3	-178.10(17)
C1-C2-C3-C4	0.5(3)
C2-C3-C4-C5	-2.2(3)
C1-N1-C5-C4	1.3(3)
Cu-N1-C5-C4	-169.85(14)
C3-C4-C5-N1	1.3(3)
N1-Cu-N3-C6	-39.27(13)
Cl1-Cu-N3-C6	42.44(19)

Table C-6. Torsion angles [°] for regl (continued).

Cl2-Cu-N3-C6	148.05(12)
N1-Cu-N3-C10	141.36(13)
Cl1-Cu-N3-C10	-136.92(11)
Cl2-Cu-N3-C10	-31.31(13)
C10-N3-C6-C7	2.6(2)
Cu-N3-C6-C7	-176.82(13)
C10-N3-C6-N2	-177.31(15)
Cu-N3-C6-N2	3.3(2)
N3-C6-C7-C8	-0.4(3)
N2-C6-C7-C8	179.50(16)
C6-C7-C8-C9	-1.1(3)
C7-C8-C9-C10	0.2(3)
C6-N3-C10-C9	-3.5(3)
Cu-N3-C10-C9	175.91(14)
C8-C9-C10-N3	2.1(3)
N1-C1-N2-C6	-45.2(2)
C2-C1-N2-C6	134.99(17)
N1-C1-N2-C11	154.95(15)
C2-C1-N2-C11	-24.8(2)
N3-C6-N2-C1	49.7(2)
C7-C6-N2-C1	-130.17(18)
N3-C6-N2-C11	-150.23(15)
C7-C6-N2-C11	29.9(2)
C1-N2-C11-C12	-139.91(16)
C6-N2-C11-C12	59.7(2)
N2-C11-C12-C13	58.0(2)
C11-C12-C13-C14	60.8(2)

Symmetry transformations used to generate equivalent atoms:

LIST OF REFERENCES

[1] Halliwell, B.; Gutterdige, J.M.C. *Oxygen is a toxic gas - an introduction to oxygen toxicity and reactive oxygen species.* In: *Free Radicals in Biology and Medicine.*; Oxford University Press: New York, 1999; pp 1-35.

[2] Halliwell, B. *Toxic effects of oxygen on plant tissues*. In: *Chloroplast Metabolism* ; Oxford University Press: New York, 1981; pp 179-205.

[3] Gilbert, D.L. *Oxygen and Living Processes: an Inter-disciplinary Approach*; Springer: New York, 1981;

[4] Davies, K.J. *IUBMB Life* **2000**, *50*, 279-289.

[5] Davies, K.J. *IUBMB Life* **2000**, *50*, 241-244.

[6] Halliwell, B.; Gutterdige, J.M.C. *Antioxidant defences*. In: *Free Radicals in Biology and Medicine*; Oxford University Press: New York, 1999; pp 105-245.

[7] Pacifici, R.E.; Davies, K.J.A. *Gerontology* **1991**, *37*, 166-180.

[8] Grune, T.; Reinheckel, T.; Davies, K.J.A. *FASEB J.* **1997**, *11*, 526-534.

[9] Knebel, A.; Rahmsdorf, J.; Ulrich, A.; Herrlich, P. *EMBO J.* **1996**, *15*, 5314-5325.

[10] Berlett, B.; Stadtman, E.R. *J.Biol.Chem.* **1997**, *272*, 20313-20316.

[11] Taylor, A.; Shang, F.; Obin, M. *Mol.Aspects Med.* **1997**, *18*, 305-414.

[12] Sitte, N.; Huber, M.; Grune, T.; Ladhoff, A.; Doecke, W.D.; von Zglinicki, T.; Davies, K.J.A. *FASEB J.* **2000**, *14*, 1490-1498.

[13] Wiese, A.G.; Pacifici, R.E.; Davies, K.J.A. *Arch.Biochem.Biophys.* **1995**, *318*, 231-240.

[14] Davies, K.J.A. *IUBMB Life* **1999**, *48*, 41-47.

[15] Ames, B.N.; Shigenaga, M.K.; Hagen, T.M. *Proc.Natl.Acad.Sci.USA* **1993**, *90*, 7915-7922.

[16] Ames, B.N.; Shigenaga, M.K. *Ann.N.Y.Acad.Sci.* **1992**, *663* , 85-96.

[17] Branda, R.F.; Sullivan, L.M.; O'Neill, J.P.; Falta, M.T.; Nicklas, J.A.; Hirsch, B.; Vasek, P.M. *Mutat.Res.* **1993**, *285*, 267-279.

[18] Grist, S.A.; McCarron, M.; Kutlaka, A.; Turner, D.R.; Morley, A.A. *Mutat.Res.* **1992** , *266*, 189-196.

[19] Oliver, C.N.; Ahn, B.W.; Stadtman, E.R.; Goldstein, S. *J.Biol.Chem.* **1987**, *262*, 5488-5491.

[20] Harman, D. *J.Gerontol.* **1956**, *11*, 298-300.

[21] Steinberg, D.; Parthasarathy, S.; Carew, T.E.; Khoo, J.C.; Witztum, J.L. *N.Engl.J.Med.* **1989**, *320*, 915-924.

[22] Regnstrom, J.; Nilsson, J.; Tornvall, P.; andou, C.; Hamsten, A. *Lancet* **1992**, *339*, 1182-1186.

[23] Adams Jr., J.D.; Odunze, I.N. *Free Radic.Biol.Med.* **1991**, *10*, 161-169.

[24] Jesberger, J.A.; Richardson, J.S. *Int.J.Neurosci.* **1991**, *57*, 1-17.

[25] Hauptmann, N.; Cadenas, E. *The oxygen paradox: Biochemistry of active oxygen.* In: *Oxidative Stress and the Molecular Biology of Antioxidant Defenses*; Scandalios, J.G. Ed. Cold Spring Harbor Laboratory Press: New York, 1997; pp 1-20.

[26] Halliwell, B.; Gutteridge, J.M.C. *Free Radicals in Biology and Medicine*; Oxford University Press Inc: New York, 1999;

[27] de Duve, C. *Harvey Lect.Ser.* **1965**, *59*, 48-87.

[28] Nicholls, P. *Biochim.Biophys.Acta* **1965**, *99*, 286-297.

[29] Dick, D.A.T. *J, Theoret.Biol.* **1964**, *7*, 504-531.

[30] Mlochowski, J.; Said, S.B. *Polish J.Chem.* **1997**, *71*, 149-169.

[31] Neumann, N.P.; Moore, S.; Stein, W.H. *Biochemistry* **1962**, *1*, 68-74.

[32] Brodie, A.E.; Reed, D.J. *Biochem.Biophys.Res.Commun.* **1987**, *148*, 120-125.

[33] Wang, S.-F.; Volini, M. *J.Biol.Chem.* **1968**, *243*, 5465-5470.

[34] Chao, C.C.; Ma, Y.S.; tadtman, E.R. *Proc.Natl.Acad.Sci.USA* **1997**, *94*, 2969-2974.

[35] Nakamura, H.; Nakamura, K.; Yodoi, J. *Annu.Rev.Immunol.* **1997**, *15*, 351-369.

[36] Zheng, M.; Aslund, F.; Storz, G. *Science* **1998**, *279*, 1718-1721.

[37] Stadtman, E.R.; Berlett, B.S. *J.Biol.Chem.* **1991**, *266*, 17201-17211.

[38] Drago, Russell S., Frank, Karen M., Yang, Y. C., and Wagner, George W. Proceedings of the 1997 ERDEC Scientific Conference on Chemical and Biological Defense Research. **1998**,

[39] Richardson, David E., Yao, Huirong, Xu, Cheng, Drago, Russell S., Frank, Karen M., Wagner, George W., and Yang, Y. C. Proceedings of the 1998 ERDEC Scientific Conference on Chemical and Biological Defense Research. **1999**,

[40] Xu, C. [Ph.D. Dissertation]. **1999**, University of Florida. Ph.D.

[41] Richardson, D.E.; Regino, C.A.S.; Yao, H. *Free Radical Biology & Medicine* **2002**, submitted

[42] Arnone, A.; Rogers, P.H.; Briley, P.D. *The binding of CO_2 to human deoxyhemoglobin: an X-ray study using low-salt crystals.* In: *Biophysics and Physiology of Carbon Dioxide*; Bauer, C.; Gros, G.; Bartels, H. Eds. Springer-Verlag: Berlin, 1980; pp 67-74.

[43] Perella, M.; Rossi-Benardi, L. *The determination of CO_2 bound to hemoglobin as carbamate*. In: *Biophysics and Physiology of Carbon Dioxide*; Bauer, C.; Gros, G.; Bartels, H. Eds. Springer-Verlag: Berlin, 1980; pp 75-83.

[44] Knoche, W. *Chemical reaction of CO_2 in water*. In: *Biophysics and Physiology of Carbon Dioxide*; Bauer, C.; Gros, G.; Bartels, H. Eds. Springer-Verlag: Berlin, 1980; pp 3-14.

[45] Breslow, R.; Berger, D.; Huang, D.L. *J.Am.Chem.Soc.* **1990**, *112*, 3686-3687.

[46] Liang, J.Y.; Lipscomb, W.N. *Proc.Natl.Acad.Sci.USA* **1990**, *87*, 3675-3679.

[47] Silverman, D.N.; Lindskog, S. *Acc.Chem.Res.* **1988**, *21*, 30-36.

[48] Montogomery, R.; Conway, T.W.; Spectro, A.A. *Blood, hemoglobin, and acid-base control*. In: *Biochemistry: A Case-Oriented Approach*; C.V. Mosby Company: St. Louis, 1990; pp 147-190.

[49] Richardson, D.E.; Yao, H.; Frank, K.M.; Bennett, D.A. *J.Am.Chem.Soc.* **2000**, *122*, 1729-1739.

[50] Adam, A.; Mehta, M. *Angew.Chem Int.Ed.* **1998**, *37*, 1387-1388.

[51] Flanagan, J.; Jones, D.P.; Griffith, W.P.; Skapski, A.C.; West, A.P. *J, Chem.Soc.Chem.Commun.* **1986**, *1986*, 21

[52] Jones, D.P.; Griffith, W.P. *J.Chem.Soc.Dalton* **1980**, *1980*, 2526-2532.

[53] Bennett, D.A.; Yao, H.; Richardson, D.E. *Inorg.Chem.* **2001**, *40*, 2996-3001.

[54] Esnouf, M.P.; Green, M.R.; Hill, H.A.O.; Irvine, G.B.; Walter, S.J. *Biochem.J.* **1978**, *174*, 345-348.

[55] Haliwell, B.; Gutterdige, J.M.C. *Oxidative stress and and antioxidant protection: some special cases.* In: *Free Radicals in Biology and Medicine*; Oxford University Press: New York, 1999; pp 485-543.

[56] Hutchison, K.A.; Matic, G.; Meshinchi, S.; Bresnick, E.H.; Pratt, W.B. *J.Biol.Chem.* **2002**, *266*, 10505-10509.

[57] Knoepfel, L.; Steinkühler, C.; Carri, M.T.; Rotilio, G. *Biochem.Biophys.Res.Commun.* **1994**, *201*, 871-877.

[58] Flohe, L.; Brigelius-Flohe, R.; Saliou, C.; Traber, M.; Packer, L. *Free Radic.Biol.Med.* **1997**, *22*, 1115-1126.

[59] Sen, C.K.; Packer, L. *FASEB J.* **1996**, *10*, 709-720.

[60] Shan, X.; Aw, T.Y.; ones, D.P. *Pharmacol.Ther.* **1990**, *47* , 61-71.

[61] Munday, R.; Winterbourne, C.C. *Biochem.Pharmacol.* **1989**, *38*, 4349-4352.

[62] Sullivan, S.G.; Chiu, D.T.; Errasfa, M.; Wang, J.M.; Qi, J.S.; Stern, A. *Free Radic.Biol.Med.* **1994**, *16*, 399-403.

[63] Schreck, R.; Rieber, P.; Baeurle, P.A. *EMBO J.* **1991**, *10* , 2247-2258.

[64] Allen, P.Jr.; Brook, J.W. *J.Org.Chem.* **1962**, *27*, 1019-1021.

[65] Wang, Y.; Espenson, J.H. *J.Org.Chem.* **2000**, *65*, 104-107.

[66] Bartlett, D.; Church, D.F.; Bounds, P.L.; ppenol, W.H. *Free Radic.Biol.Med.* **1995**, *18*, 85-92.

[67] *Organic Sulfur Chemistry: Structure and Mechanism*; Oae, S. Ed. CRC Press: Boca Raton, 1991; pp 213-216.

[68] Jocelyn, P.C. *Oxidation of thiols*. In: *Biochemistry of the SH Group*; Academic Press Inc.: London, 1972; pp 94-115.

[69] Block, E.; Bayer, T. *J.Am.Chem.Soc.* **1990**, *112*, 4584-4585.

[70] Freeman, F. *Chem.Rev.* **1984**, *84*, 117-135.

[71] Freeman, F.; Angeletakis, C.N. *J.Org.Chem.* **1985**, *50*, 793-798.

[72] Cavallini, D.; de Marco, C.; Scandurra, R.; Dupre, S.; Graziani, M.T. *J.Biol.Chem.* **1966**, *241*, 3189

[73] Cavallini, D.; Scandurr, R.; Monacell, F. *Biochem.Biophys.Res.Commun.* **1966**, *24*, 185

[74] Jocelyn, P.C. *The metabolism of thiols and disulphides*. In: *Biochemistry of the SH Group*; Academic Press Inc.: London, 1972; pp 163-189.

[75] Koechlin, B.A. *Proc.Natl.Acad.Sci.USA* **1954**, *40*, 60-65.

[76] Bersin, T. *Adv.Enzymol.Rel.S.Bi.* **1950**, *10*, 223-323.

[77] Riddles, P.W.; Blakeley, R.L.; Zerner, B. *Anal.Biochem.* **1979**, *94*, 75-81.

[78] Riddles, P.W.; Blakeley, R.L.; Zerner, B. *Methods Enzymol.* **1983**, *91*, 49-60.

[79] Ogura, Y. *Arch.Biochem.Biophys.* **1955**, *57*, 288-300.

[80] Barton, J.P.; Packer, J.E.; Sims, R.J. *J.Chem.Soc.Perkin II* **1973**, 1547-1549.

[81] Winterbourne, C.C.; Metodiewa, D. *Free Radic.Biol.Med.* **1999**, *27*, 322-328.

[82] Dennard, A.E.; Williams, R.J. *J.Chem.Soc.A* **1966**, *7*, 812-813.

[83] Edwards, J.O. *Peroxide Reaction Mechanisms*; Interscience: New York, 1962; pp 67-106.

[84] Toennies, G.; Callan, T.P. *J.Biol.Chem.* **1939**, *129*, 481

[85] Caldwell, K.A.; Tappel, A.L. *Biochemistry* **1964**, *3*, 1643

[86] Neumann, N.P. *Methods Enzymol.* **1977**, *25*, 393-400.

[87] Hachimori, Y.; Horinishi, H.; Kurihara, K.; Shibata, K. *Biochim.Biophys.Acta* **1964**, *93*, 346-350.

[88] Clamp, J.R.; Hough, L. *Biochem.J.* **1965**, *94*, 17-24.

[89] Knowles, J.R. *Biochem.J.* **1965**, *95*, 180-184.

[90] Atassi, M.Z. *Biochem.J.* **1967**, *102*, 478-484.

[91] Shechter, Y.; Burstein, Y.; Patchornik, A. *Biochemistry* **1975**, *14*, 4497-4503.

[92] Brot, N.; Weissbach, H. *Arch.Biochem.Biophys.* **1983**, *223* , 271-281.

[93] Shechter, Y. *J.Biol.Chem.* **1986**, *261*, 66-70.

[94] Vogt, W. *Free Radic.Biol.Med.* **1995**, *18*, 93-105.

[95] Gellman, S.H. *Biochemistry* **1991**, *30*, 6633-6636.

[96] Levine, R.L.; Moskovitz, J.; Stadtman, E.R. *IUBMB Life* **2000**, *50*, 301-307.

[97] Hershko, A.; Heller, H.; Eytan, E.; Reiss, Y. *J.Biol.Chem.* **1986**, *261*, 11992-11999.

[98] Levine, R.L.; Mosoni, L.; Berlett, B.S.; Stadtman, E.R. *Proc.Natl.Acad.Sci.USA* **1996**, *93*, 15036-15040.

[99] Ciorba, M.A.; Heinemann, S.H.; Weissbach, H.; Brot, N.; Hoshi, T. *FEBS Lett.* **1999**, *442*, 48-52.

[100] Gao, J.; Yin, D.; Yao, Y.; Williams, T.D.; Squier, T.C. *Biochemistry* **1998**, *37*, 9536-9548.

[101] Sun, H.; Gao, J.; Ferrington, D.A.; Biesiada, H.; Williams, T.D.; Squier, T.C. *Biochemistry* **1999**, *38*, 105-112.

[102] Swaim, M.W.; Pizzo, S.V. *J.Leuko.Biol.* **1988**, *43*, 365-379.

[103] Reddy, V.Y.; Pizzo, S.V.; Weiss, S.J. *J.Biol.Chem.* **1989**, *264*, 13801-13809.

[104] Reddy, V.Y.; Desrochers, P.E.; Pizzo, S.V.; Gonias, S.L.; Sahakian, J.A.; Levine, R.L.; Weiss, S.J. *J.Biol.Chem.* **1994**, *269*, 4683-4691.

[105] Almassy, R.J.; Janson, C.A.; Hamlin, R.; Xuong, N.H.; Eisenberg, D. *Nature* **1986**, *323*, 304-309.

[106] Clark, R.A.; Klebanoff, S.J. *J.Clin.Inves.* **1979**, *64*, 913-920.

[107] Clark, R.A.; Szot, S.; Venkatasubramanian, K.; Schiffmann, E. *J.Immunol.* **1980**, *124*, 2020-2026.

[108] Clark, R.A. *J.Immunol.* **1982**, *129*, 1507-1513.

[109] Clark, R.A.; Szot, S. *J.Immunol.* **1982**, *128*, 1507-1513.

[110] Schiffmann, E.; Corcoran, B.A.; Wahl, S.M. *Proc.Natl.Acad.Sci.USA* **1975**, *72*, 1059-1062.

[111] Brot, N.; Weissbach, H. *Mol.Cell Biochem.* **1981**, *36*, 47-63.

[112] Truscott, R.J.W.; Augusteyn, R.C. *Biochim.Biophys.Acta* **1977**, *492*, 43-52.

[113] Ellman, G.L. *Arch.Biochem.Biophys.* **1959**, *82*, 70-77.

[114] Garner, M.H.; Spector, A. *Proc.Natl.Acad.Sci.USA* **1980**, *77*, 1274-1277.

[115] Horstmann, H.J.; Rohen, J.W.; Sames, K. *Mech.Ageing Dev* **1983**, *21*, 121-136.

[116] Pannell, R.; Johnson, D.; Travis, J. *Biochemistry* **1974**, *13*, 5439-5445.

[117] Travis, J.; Pannell, R. *Clinica Chimica Acta* **1973**, *49*, 49-52.

[118] Crestfield, A.M.; Stein, W.H.; Moore, S. *J.Biol.Chem.* **1963**, *238*, 618-621.

[119] Méndez, T.J. [Ph.D. Dissertation]. **1999**, University of Florida. Ph.D.

[120] Morrison, H.M.; Burnett, D.; Stockley, R.A. *Biol.Chem.Hoppe-Seyler* **1986**, *367*, 371-378.

[121] Cuatrecasas, P. *J.Biol.Chem.* **1970**, *245*, 3059-3065.

[122] Taggart, C.; Cervantes-Laurean, D.; Kim, G.; McElvaney, N.G.; Wehr, N.; Moss, J.; Levine, R.L. *J.Biol.Chem.* **2000**, *275*, 27258-27265.

[123] Peskin, A.V.; Winterbourn, C.C. *Free Radic.Biol.Med.* **2001**, *30*, 572-579.

[124] Travis, J.; Johnson, D. *Methods Enzymol.* **1981**, *80*, 754-765.

[125] Johnson, D.; Travis, J. *J.Biol.Chem.* **1979**, *254*, 4022-4026.

[126] Matheson, N.R.; Wong, P.S.; Travis, J. *Biochem.Biophys.Res.Commun.* **1979**, *88*, 402-409.

[127] Beatty, K.; Bieth, J.; Travis, J. *J.Biol.Chem.* **1980**, *255*, 3931-3934.

[128] Rapala-Kozik, M.; Potempa, J.; Nelson, D.; Kozik, A.; Travis, J. *Biol.Chem.* **1999**, *380*, 1211-1216.

[129] Travis, J.; Salvesen, G.S. *Ann.Rev.Biochem.* **1983**, *52*, 655-709.

[130] Nakajima, K.; Powers, J.C.; Ashe, B.M.; Zimmerman, M. *J.Biol.Chem.* **1979**, *254*, 4027-4032.

[131] Maier, K.L.; Lenz, A.-G.; Beck-Speier, I.; Costabel, U. *Methods in Enzymology* **1995**, *251*, 455-460.

[132] Whisstock, J.C.; Skinner, R.; Carell, R.W.; Lesk, A.M. *J.Mol.Biol.* **2000**, *295*, 651-665.

[133] Perides, G.; Kuhn, S.; Scherbarth, A.; Traub, P. *Eur.J.Cell Biol.* **1987**, *43*, 450-458.

[134] Lindahl, T. *J.Cell Sci.* **1995**, *Suppl. 19*, 73-77.

[135] Lindahl, T.; Wood, R.D. *Science* **1999**, *286*, 1897-1905.

[136] Burrows, C.J.; Muller, J.G. *Chem.Rev.* **1998**, *98*, 1109-1151.

[137] Halliwell, B.; Gutteridge, J.M.C. *Oxidative stress: adaptation, damage, repair and death.* In: Halliwell, B. Ed. Oxford University Press: Oxford, 1998; pp 246-350.

[138] Holliday, R. Azzi, A. and Packer Lester editors. DNA damage and epigenetic mechanism of aging. **1995**, pp. 63-67.

[139] Hirano, T.; Homma, Y.; Kasai, H. Azzi, A. and Packer, L. editors. Formation of 8-hydroxyguanine in DNA by aging and oxidative stress. **1995**, pp. 69-76.

[140] Michael, R.; Hudson, E.; Bohr, V. *FASEB J.* **2000**, *14*, 355-360.

[141] Barja, G.; Herrero, A. *FASEB J.* **2000**, *14*, 318

[142] Bohr, V.A.; Taffe, B.G.; Larminat, F. Azzi, A. and Packer, L. editors. DNA repair, oxidative stress and aging. **1995**, pp. 89-100.

[143] Randerath, K.; Chang, J.; Randerath, E. Azzi, A. and Packer, L. editors. Age-dependent DNA modifications (I-compounds): Effects of carcinogenesis and oxidative stress. **1995**, pp. 77-88.

[144] Wallace, S.S. Scandalios, J. G. editor. Oxidative damage to DNA and its repair. **1997**, 34. pp. 49-90.

[145] Vialas, C.; Claparols, C.; Pratviel, G.; Meunier, B. *J.Am.Chem.Soc* **2000**, *122*, 2157-2167.

[146] Shapiro, R.; Kang, S. *Biochemistry* **1969**, *5*, 1806-1810.

[147] Shapiro, R.; Danzig, M. *Biochemistry* **1972**, *11*, 23-29.

[148] Zoltewic, J.A.; Clark, D.F.; Sharpless, T.W.; Grahe, G. *J.Am.Chem.Soc* **1970**, *92*, 1741-1750.

[149] Cullis, P.M.; Malone, M.E.; Merson-Davies, L.A. *J.Am.Chem.Soc* **1996**, *118*, 2775-2781.

[150] Steenken, S.; Jovanovic, S.V. *J.Am.Chem.Soc* **1997**, *119*, 617-618.

[151] Budowsky, E.I.; Kovalsky, O.I.; Yakovlev, D.Y.; Simukova, N.A.; Rubin, L.B. *FEBS Lett.* **1985**, *188*, 155-158.

[152] Kino, K.; Saito, I. *J.Am.Chem.Soc.* **1998**, *120*, 7373-7374.

[153] Kovalsky, O.I.; Panutin, I.G.; Budowsky, E.I. *Photobiol.* **1990**, *52*, 509-517.

[154] Hall, D.B.; Holmlin, R.E.; Barton, J.K. *Nature* **1996**, *382*, 731-735.

[155] Doddridge, Z.A.; Cullis, P.M.; ones, G.D.D.; alone, M.E. *J.Am.Chem.Soc* **1998**, *120*, 10998-10999.

[156] Uppu, R.M.; Cueto, R.; Squadrito, G.L.; Salgo, M.G.; Pryor, W.A. *Free Rad.Biol.Med.* **1996**, *21*, 407-411.

[157] Reynolds, H.Y. *Am.Rev.Respir.Dis.* **1983**, *127*, S16-S25

[158] Cohen, A.B.; Rossi, M. *Am.Rev.Respir.Dis.* **1983**, *127*, S3-S9

[159] Tegner, H.; Fryksmark, U.; Ohlsson, K. *Eur.J.Respir.Dis.* **1985**, *66*, 62-65.

[160] Janoff, A.; Carp, H.; Laurent, P.; Raju, L. *Am.Rev.Respir.Dis.* **1983**, *127*, S31-S38

[161] Hurst, J.K.; Barrette Jr., W.C. *Crit.Rev.Biochem.Mol.Biol.* **1989**, *24*, 271-328.

[162] Segal, A.W. *Medical Biology* **1984**, *62*, 81-84.

[163] Halliwell, B.; Clement, M.V.; Ramalingan, J.; Long, L.H. *IUBMB Life* **2000**, *50*, 251-257.

[164] Hurst, J.K.; Barrette Jr., W.C.; Michel, B.R.; Rosen, H. *European Journal of Biochemistry* **1991**, *202*, 1275-1282.

[165] Kleinman, L.I.; Lorenz, J.M. *Physiology and pathophysiology of body water and electrolytes*. In: *Clinical Chemistry*; Kaplan, L.A.; Pesce, A.J. Eds. CV Mosby Company: St. Louis, 1984; pp 363-386.

[166] Albrich, J.M.; Hurst, J.K. *FEBS Letters* **1982**, *144*, 157-161.

[167] Thomas, E.L. *Infection and Immunity* **1979**, *25*, 110-116.

[168] Nauseef, W.M.; Root, R.K.; Malech, H.L. *J.Clin.Inves.* **1983**, *71*, 1297-1300.

[169] Lehrer, R.I.; Cline, M.J. *J.Clin.Inves.* **1969**, *48*, 1478-1481.

[170] Johnson, R.B.; Newman, S.L. *Ped.Clin.North Am.* **1977**, *24*, 365-376.

[171] Kanofsky, J.R.; Wright, J.; Miles-RIchardson, G.E.; Tauber, A.I. *J.Clin.Inves.* **1984**, *74*, 1489-1492.

[172] Kanofsky, J.R.; Wright, J.; Tauber, A.I. *FEBS Lett.* **1985**, *187*, 299-302.

[173] Botsivali, M.; Evans, D.F. *J.Chem.Soc.Chem.Commun.* **1979**, *1979*, 1114-1115.

[174] Segal, A.W.; Shatwell, K.P. *Ann.N.Y.Acad.Sci.* **2001**, 215-222.

[175] Hurst, J.K.; Lymar, S.V. *Acc.Chem.Res.* **1999**, *32*, 520-528.

[176] Yao, H.; Richardson, D.E. 2002; manuscript in preparation.

[177] Cady, G. *Inorganic Syntheses*; McGraw-Hill Co.: New York, 1957; pp 156-165.

[178] Adam, L.C.; Fábián, I.; Suzuki, K.; Gordon, G. *Inorg.Chem.* **1992**, *31*, 3534-3541.

[179] Baga, A.N.; Johnson, G.R.A.; Nazhat, N.B.; Saadalla-Nazhat, R.A. *Anal.Chim.Acta* **1988**, *204*, 349-353.

[180] Hyslop, P.A.; Hinslaw, D.B.; Hyslop, P.A.; Spragg, R.G.; Cochrane, C.G. *J.Clin.Inves.* **1986**, *77*, 1312-1320.

[181] Trost, B.M. *Chem.Rev.* **1978**, *78*, 8-18.

[182] Lymar, S.V.; Hurst, J.K. *Inorg.Chem.* **1998**, *37*, 294-301.

[183] Denicola, A.; Freeman, B.; Trujillo, M.; Radi, R. *Arch.Biochem.Biophys.* **1996**, *333*, 49-58.

[184] Lymar, S.V.; Hurst, J.K. *Chem.Res.Toxicol.* **1996**, *9*, 845-850.

[185] Goldstein, S.; Czapski, G. *Inorg.Chem.* **1997**, *36*, 5113-5117.

[186] Martell, A.E. . Metal ions in biological systems. **1973**, 2. pp. 207-268.

[187] Fraústo da Silva, J.J.R.; Williams, J.P. *The principles of the uptake and chemical speciation of the elements in biology*. In: *The Biological Chemistry of the Elements: The Inorganic Chemistry of Life*; Oxford University Press: Oxford, 1991; pp 23-68.

[188] Hatano, M.; Nozawa, T. . **1976**, 5. pp. 245-277.

[189] Jencks, W.P. *Strain, distortion, and conformational change*. In: *Catalysis in Chemistry and Enzymology*; Dover Publications, Inc.: New York, 1986; pp 282-321.

[190] Schultz, P.G.; Pollack, S.J.; Nakayama, G.R. *Science* **1988**, *242*, 103-1040.

[191] Cochran, A.; Sugasawara, R.; Schultz, P.G. *J.Am.Chem.Soc.* **1988**, *110*, 7888-7890.

[192] Shokat, K.; Leumann, C.; Sugasawara, R.; Schultz, P.G. *Nature* **1989**, *338*, 269-270.

[193] Iverson, B.L.; Lerner, R.A. *Science* **1989**, *243*, 1184-1188.

[194] Pollack, S.J.; Nakayama, G.R.; Schultz, P.G. *Methods Enzymol.* **1989**, *178*, 551-568.

[195] Chin, J.; Juian, V. *J.Chem.Soc.Commun.* **1989**, *1989*, 841

[196] Chin, J.; Jubian, V.; Mrejen, K. *J.Chem.Soc.Commun.* **1990**, *1990*, 1326-1328.

[197] Ray, N.; Tyagi, S.; Hathaway, B. *J.Chem.Soc.Dalton* **1982**, *1982*, 143-146.

[198] Jencks, W.P. *J.Am.Chem.Soc.* **1964**, *86*, 837-846.

[199] Menger, F.M.; Ladika, M. *J.Am.Chem.Soc.* **1987**, *109*, 3145-3146.

[200] Andregg, G. *Helv.Chim.Acta* **1971**, *54*, 509-511.

[201] Burkart, M.A. [Dissertation]. **1995**, University of Florida. Ph.D.

[202] de Groot, N.; Lapidot, Y.; Panet, A.; Wolman, Y. *Biochem.Biophys.Res.Commun.* **1966**, *25*, 17-22.

[203] Lindsay, D.G.; Shall, S. *Biochem.J.* **1971**, *121*, 737-745.

[204] Song, L.; Trogler, W. *J.Organomet.Chem.* **1993**, *452*, 271-275.

[205] Addison, A.W.; McDevitt, M.R.; Ru, Y. *Transition Met.Chem.* **1993**, *18*, 197-204.

[206] Richardson, D.E.; Zheng, T. 2000; unpublished work.

[207] Kirschner, S. . **1957**, 5. pp. 14-16.

[208] Khorana, G.H.; Mofatt, J.G. *J.Am.Chem.Soc.* **1957**, *79*, 3741-3746.

[209] Kirby, A.J.; Younas, M. *J.Chem.Soc.B* **1970**, *1970*, 1165-1172.

[210] de Roos, A.M.; Toet, H.J. *Recl.Trav.Chim.Pays-Bas.* **1958**, *77*, 946-955.

[211] Morrow, J.R.; Trogler, W.C. *Inorg.Chem.* **1988**, *27*, 3387-3394.

[212] Hendry, P.; Sarsegon, A.M. *J.Am.Chem.Soc.* **1989**, *111*, 2521-2527.

[213] Martell, A.E.; Motekaitis, R.J. *Determination and Use of Stability Constants*; VCH Publishing Co.: New York, 1992;

[214] de Rosch, M.A.; Trogler, W.C. *Inorg.Chem.* **1990**, *29*, 2409-2416.

[215] Khorana, G.H. *Chem.and Ind.* **1955**, *1955*, 1087-1088.

[216] Khorana, G.H. *Chem.Rev.* **1953**, *53*, 145-166.

[217] Perrin, D.D.; Sharma, V.S. *J.Inorg.Nucl.Chem.* **1966**, *28* , 1271-1278.

[218] Spodine, E.; Atria, A.M.; Baggio, R.; Garland, M.T. *Acta Crystallogr.Sect.C* **1996**, *52*, 1407-1410.

[219] Garland, M.T.; Grandjean, D.; Spodine, E.; Atria, A.M.; Manzur, J. *Acta Crystallogr.Sect.C* **1988**, *44*, 1209-1212.

[220] Jencks, W.P.; Gilchrist, M. *J.Am.Chem.Soc.* **1968**, *90*, 2622-2637.

[221] Hendry, P.; Sarsegon, A.M. . Progress in Inorganic Chemistry: Bioinorganic Chemistry. **1990**, 38. pp. 201-258.

BIOGRAPHICAL SKETCH

Celeste Aida Servando Regino was born on the 17th of December 1973 in Dagupan City, Pangasinan, Philippines, as the youngest of the six children of Teodoro and Aida Regino. Her interest in science started in the third grade and further developed when she went to study in Philippine Science High School at Quezon City on 1986 as a Department of Science and Technology (DOST) scholar. It was during her high school years that her interest in chemistry developed.

Upon graduating in 1990, she attended college at the University of the Phillipines-Diliman (UPD) at Quezon City. During her college years, she joined the UP Chemical Society and the Philippine Association of Chemistry Students and served as the head of the membership committee of both organizations. She did her undergraduate research under the direction of Dr. Titos Anacleto O. Quibuyen on the heavy metal content of volcanic ash and of plants grown in ash-contaminated soil. She earned her Bachelor of Science in chemistry from the UPD in 1994.

After receiving her degree, she joined the Institute of Chemistry of UPD as an instructor before leaving to pursue her graduate studies in 1996. She began her graduate work in bioinorganic chemistry at the University of Florida under the supervision of Dr. David E. Richardson. Upon completion of her doctoral studies, she will begin her postdoctoral studies with Dr. Martin Brechbiel at the National Cancer Institute in Bethesda, Maryland.

I certify that I have read this study and that in my opinion it conforms to acceptable standards of scholarly presentation and is fully adequate, in scope and quality, as a thesis for the degree of Doctor of Philosophy.

David E. Richardson, Chairman
Professor of Chemistry

I certify that I have read this study and that in my opinion it conforms to acceptable standards of scholarly presentation and is fully adequate, in scope and quality, as a thesis for the degree of Doctor of Philosophy.

James M. Boncella
Professor of Chemistry

I certify that I have read this study and that in my opinion it conforms to acceptable standards of scholarly presentation and is fully adequate, in scope and quality, as a thesis for the degree of Doctor of Philosophy.

Brian D. Cain
Professor of Biochemistry & Molecular Biology

I certify that I have read this study and that in my opinion it conforms to acceptable standards of scholarly presentation and is fully adequate, in scope and quality, as a thesis for the degree of Doctor of Philosophy.

John R. Eyler
Professor of Chemistry

I certify that I have read this study and that in my opinion it conforms to acceptable standards of scholarly presentation and is fully adequate, in scope and quality, as a thesis for the degree of Doctor of Philosophy.

Benjamin A. Horenstein
Associate Professor of Chemistry

This thesis was submitted to the Graduate Faculty of the Department of Chemistry in the College of Liberal Arts and Sciences and to the Graduate School and was accepted as partial fulfillment of the requirements for the degree of Doctor of Philosophy

May 2002

Dean, Graduate School